No. 340
April 1999

Mooring Design Based on Catastrophes of Slow Dynamics

Michael M. Bernitsas
Luis O. Garza-Rios
Boo-Ki Kim

Department of Naval Architecture
and Marine Engineering

MOORING DESIGN BASED ON CATASTROPHES OF SLOW DYNAMICS

by

Michael M. Bernitsas, Ph.D.
Professor

Luis O. Garza-Rios, Ph.D.
Research Associate

Boo-Ki Kim
Research Assistant

Presented at the 8th Offshore Symposium
ENHANCING VALUE IN DEEPWATER DEVELOPMENTS
of the Texas Section of the Society of Naval Architects and Marine Engineers

February 25-26, 1999, Houston, TX

Department of Naval Architecture and Marine Engineering, University of Michigan
2600 Draper, Ann Arbor, MI 48109-2145

ABSTRACT

The design of mooring systems presently requires numerous trial and error iterations due to the high number of design variables involved such as positioning of the moored vessel, number and properties of mooring lines, length and arrangement of lines, orientation and pretension of lines, location and pretension of riser. Then, for a given configuration and environment, numerous simulations of the nonlinear mathematical model are performed which cannot reveal the complete picture of the system dynamics. This paper summarizes a methodology for assessment and design of mooring systems developed for the University of Michigan Offshore Industry Consortium in the past sixteen years, which virtually eliminates trial and error in design and the need for simulations. It is based on calculation of catastrophes and sequences of bifurcations and definition of the associated morphogeneses which define regions of qualitatively different dynamics in a design space, thus making direct selection of values of design variables possible. Sensitivity of catastrophes and morphogeneses on excitation, modeling, design and operational parameters makes it possible to assess their effect on design without simulations. Results show dynamic behavior contrary to practical design guidelines, explain observed nonlinear behavior, and reveal new phenomena related to slowly-varying wave drift.

ACKNOWLEDGMENTS

TABLE OF CONTENTS

LIST OF FIGURES

NOMENCLATURE

ABS	Average Breaking Strength
AC	Anchored Catenary
AE	Alternate Equilibrium
A-M	Abkowitz maneuvering Model
API	American Petroleum Institute
B	beam of vessel
BDL	Boundary of Dynamic Loss of stability
BSC	Buoy-supported catenary
BSL	Boundary of Static Loss of stability
CG	center of gravity of vessel (vessel and turret in TMS)
CG_B	center of gravity of supporting buoy
CG_T	center of gravity of turret
D_B	buoy diameter
D_{CG}	distance from center of gravity of the system to center of gravity of turret
DICAS	Differentiated Compliance Anchoring System
E_I	initial strain (synthetic fiber rope)
h	water depth
$H_{1/3}$	significant wave height
L	length of vessel
L_r	length of riser
ℓ_B	position of the buoy along the chain with respect to the vessel
ℓ_w	length of mooring line
n	number of mooring lines
n_B	number of buoys
O-M	Obokata maneuvering Model
PE	Principal Equilibrium
P_{RT}	horizontal pretension (chain)
T_P	total pretension (chain)
R	vessel resistance
SC	Suspended Catenary
SMS	Spread Mooring System
SPM	Single Point Mooring

SFR	synthetic fiber rope
SW-M	Short Wing maneuvering Model
t	time
T	mooring line tension
$T_{1/3}$	significant wave period
T-M	Takashina maneuvering Model
TMS	Turret Mooring System
TPM	Two Point Mooring
U	current speed
(x, y, z)	inertial reference frame fixed to mooring terminal 1
(X, Y, Z)	body-fixed reference frame with origin located at CG
(X', Y', Z')	body-fixed reference frame with origin located at CG_T
(X_B, Y_B, Z_B)	body-fixed reference frame with origin located at CG_B
(x_m, y_m, z_m)	mooring line coordinates on the mooring terminal
(x_p, y_p)	mooring line fairlead
x_r	location of top of the riser forward of CG
α	current angle with respect to (x, y)
Δ	initial riser offset
ϕ	angle of external excitation with respect to (x, y)
ψ	vessel drift (yaw) angle
ψ_T	absolute yaw angle of turret
λ_i, σ_i	i-th eigenvalue
$\theta = \alpha - \psi$	incident angle of relative flow
θ_d	wave drift angle with respect to (x, y)
θ_w	wind angle with respect to (x, y)
τ	moment friction coefficient between turret and vessel
Ω	absolute angle of aperture between X-axis and mooring line
$\overline{(\bullet)}$	equilibrium of $(\bullet)$

1. INTRODUCTION

In the past twenty years, significant research effort has been devoted to the development of station-keeping systems for Floating, Production, Storage and Offloading (FPSO) facilities. Mooring, dynamic positioning or hybrid systems are being designed and developed for depths up to 3,000 m. Mooring systems configurations include Single Point Mooring (SPM), Two Point Mooring (TPM), Spread Mooring System (SMS), Differentiated Compliance Anchoring System (DICAS), and Turret Mooring System (TMS). Environmental conditions such as direction and intensity of excitation, water depth, and duration of drilling or production operations, are dominant factors in selecting the mooring concept. Selection of configuration particulars for a given mooring concept largely depends on experience and extensive trial and error due to the high number of design parameters involved, as well as limitations in the state of art in modeling of excitation on the floating vessel, the mooring lines and the riser(s). Assessment of a selected configuration is achieved by systematic nonlinear time simulations which can reveal only a partial picture of the mooring system dynamics. Trial and error in design along with simulations for analysis are time consuming and cannot be conclusive [26].

The methodology presented in this paper considers the slow and intermediate frequency scales of the dynamics of a mooring system as the basis for modeling since they are the scales affecting positioning. For brevity, these two frequency scales corresponding to maneuvering and slow-drift will be referred to as slow motion in the horizontal plane. This is the dynamics that can be restrained by mooring and/or dynamic positioning. In addition, the slow underlying dynamics is required for calculation of fast (wave frequency) dynamics needed in prediction of extreme loads and motions. The methodology developed at the University of Michigan (UM) since 1983 assesses mooring system dynamics by calculating global properties as opposed to instantaneous response predicted by simulations. Such properties include system equilibria, sequences of bifurcations, catastrophe sets, singularities of bifurcations, and morphogeneses. The information contained in these global properties is adequate to infer the qualitative behavior of the system dynamics without simulations [26, 40, 59]. Presentation of such information in design spaces makes it possible to select values of design variables directly without trial and error. At the same time, it becomes possible to assess new designs and mooring concepts, to assess the range of validity of practical design guidelines, to compare mathematical models, and as in the case of slow-varying drift, reveal that resonance to mooring is only one of several possible associated phenomena [9].

The material in this paper is structured as follows: In the next chapter, background information with literature review is presented. In Chapter 3, the problem of design of mooring systems is described.

1

In Chapter 4, the mathematical model is summarized including two different schools of maneuvering models; quasistatic mooring line models, including synthetic fiber, steel cable, and chain with touchdown, drag and supporting buoys; marine riser - in three dimensional large quasistatic deformation; steady external excitation due to current, wind and mean wave drift forces; and intermediate scale hydrodynamic forces including memory effect and slowly-varying wave drift. In Chapter 5, the richness of nonlinear mooring dynamics is revealed using only a limited number of simulations selected properly based on the UM design methodology for mooring systems. Concepts of global stability analysis and bifurcation sequences of nonlinear mooring dynamics are introduced in Chapter 6 to explain the process of developing analytical physics-based expressions for the bifurcation sequences and linking them to specific morphogeneses. This leads to the outline of the UM methodology in Chapter 7. Of interest to the practitioner as well as the researcher are the results presented in Chapters 8, 9 and 10 where the effects of modeling issues, environmental excitation, and design parameters that can be adjusted during deployment and operation are assessed using catastrophe sets in the design space. Probably, most notable among these are the assessment of the Abkowitz, Takashina, Obokata and Short-Wing maneuvering models; and the phenomena of interaction between slowly-varying drift forces and system frequencies. Closing remarks discuss conclusions and future direction of the UM methodology for assessment and design of mooring systems.

2. BACKGROUND

The problems of towing, mooring, and anchoring are related in the sense that forces are applied by lines to a vessel in slow motion with respect to water. Dynamic positioning via automatic control of an array of thrusters [19] or combination of the above complete the spectrum of methods commonly used for station-keeping. The common thread among all these problems is that a floating vessel is moving slowly in surge, sway, and yaw and such motion can be restrained to achieve a desired positioning of the vessel. The wave frequency motions - referred to as fast motions - are not controllable. Fast vessel response is most important in the other three degrees of freedom - heave, roll, pitch - where restoring forces exist. Intermediate frequency motions, which are due to interactions between fast and slow motions (memory effect), and slowly-varying drift are controllable and should be included in modeling of mooring system dynamics.

Research in explaining a series of phenomena and field observations have instigated and fueled this effort at the University of Michigan. These phenomena which have been explained by the methodology presented in this paper are described below.

(i) In the decades of the 1950's, 1960's, and 1970's extensive research was conducted to explain the following contradiction: In 1950, Strandhagen et al. [64] modeled towing using maneuvering equations and an inextensible towline and performed basic stability analysis. He concluded that shorter towline improves stability. In 1955, Benford observed that towing of Canadian barges becomes more stable by increasing the towline length [4]. In 1971, Brix [13] arrived at the same conclusion using model tests. This contradiction was explained by Bernitsas and Kekridis in 1985 [8].

(ii) In the decades of the 1970's and 1980's jack knifing and fishtailing motions of moored tankers were observed [63]. The former is a slow periodic surge motion. Fishtailing is a slow periodic motion in coupled yaw and sway. These phenomena were attributed to the time dependence of environmental excitation [63]. In 1988 it was proven by Bernitsas and Papoulias [10, 59] that these periodic slow motions are due to Hopf bifurcations, that is, dynamic loss of stability.

(iii) In the decades of the 1980's and 1990's, several mooring patterns have been developed and recommended by API [3]. These are effective patterns but the dominant tool for analysis of mooring systems remains extensive nonlinear time simulations. The design approach is still dominated by trial and error. The method summarized in this paper provides an alternative

3

approach to design of mooring systems by calculating global (time independent) system properties.

(iv) Still in the decades of the 1980's and 1990's several design guidelines (rules of thumb) have been proposed and practiced to reduce the trial and error cycle in design. It has been shown that in general the bifurcation sequences in catastrophe sets do not have simple geometries, thus, making it practically impossible to develop simple design guidelines [6, 7, 27-29, 33]. Even basic guidelines such as that reversal of propeller or increased mooring line pretension have been proven by the UM methodology not to be always correct [5, 38]. Actually, such actions may instigate chaos in the system dynamics [11].

(v) In the decade of the 1980's, it has been shown that slowly-varying drift forces may resonate with the natural frequencies of mooring systems [23]. It was shown recently by Bernitsas and Kim [9] that the interaction between slowly-varying drift forces and mooring system dynamics is much richer in nonlinear phenomena. Specifically, wave drift may cause resonance, may render a stable Principal Equilibrium (PE) unstable resulting in trajectories attracted by Alternate Equilibrium (AE), may render an unstable PE stable, or may eliminate a limit cycle and the associated periodic motion.

(vi) In 1996, the UM methodology made it possible to distinguish between slow periodic motions instigated by Hopf bifurcations and quasiperiodic motions caused by inappropriate distribution of mooring lines [5, 26]. The latter was labeled "poor design" limit cycle and indicates the phenomenon of a moored vessel trying to converge to either its stable limit cycle or a stable AE while being pulled away by a line in high tension.

(vii) In the 1960's, 1970's and 1980's, several maneuvering models have been developed. Abkowitz's [1, 2] and Takashina's [65] models are among the physics-based models which are accurate but require extensive model tests to find the values of several hydrodynamic coefficients. Those are hereto forth referred to as the first school of maneuvering models. In the 1980's and in the 1990's a second school of modeling was developed with such models as the Obokata [54, 55] and the Short-Wing [46, 61]. Their contribution is the reduction of the required number of model tests by heuristically combining formulas for various sources of hull hydrodynamic forces. A number of maneuvering models widely used in practice are based on the Abkowitz model or are the product of a combination of the two schools [25, 49]. A recent comparison of the two schools of modeling based on the UM methodology reveals their advantages and drawbacks [49].

The problems involving towing and mooring have been studied widely theoretically, numerically and experimentally. Following the work by Strandhagen et al. [64] several studies in these fields have been published by Abkowitz [1], Benford [4], Bernitsas et al. [8, 10-12, 15, 16, 59], Brix [13], Eda [22], Chakrabarti [14], the authors of this paper [5-7, 9, 27-38, 43, 44] and others [23, 24, 46, 52, 61]. In recent years, mooring system design has attracted considerable attention particularly in deep waters. Presently, mooring systems are designed for specific purposes based mostly on experience and conservative calculations. Current practice [3] indicates that the existing rationale in the mooring system design process relies heavily on extensive nonlinear simulations and trial and error. This is due to the lack of fundamental understanding of the dynamics that mooring systems exhibit.

Several studies show that mooring system dynamics strongly depend on certain design parameters, such as the number of mooring lines; the fairlead position, material, orientation, pretension of lines, etc. [5-7, 11, 12, 15, 16, 24, 27-30, 33, 37, 38, 39, 43, 44, 46, 49, 53, 59, 61, 62]. Single Point Mooring (SPM) has been studied by Sharma et al. [62], Bernitsas and Papoulias [10, 11] , Faltinsen [23], Fernandes and Aratanha [24], Papoulias and Bernitsas [59], de Kat and Wichers [20], Nishimoto et al. [53]. The above references study the SPM problem in the case of a single floating mooring terminal. Turret Mooring Systems (TMS) have been studied by Garza-Rios and Bernitsas [30-33], Bernitsas and Garza-Rios [7], Nishimoto et al. [53], Leite et al. [46], Dercksen and Wichers [21], Laures and de Boom [45], Simos et al. [61], Mack et al. [47]. Occasionally, the Turret Mooring System (TMS) is referred to as SPM because the floating vessel is moored to the turret even though the latter is stationed via an array of spread mooring lines. It should be noticed that in [7, 30-33] the TMS was modeled properly taking into consideration the diameter of the turret and establishing the limitations of approximating the TMS by a SPM. Spread Mooring Systems (SMS) have been studied by Bernitsas and Garza-Rios [5, 6], Bernitsas and Kim [9], Chung and Bernitsas [15, 16], Chakrabarti [14], Davison et al. [19], Gottlieb and Kim [39], Garza-Rios and Bernitsas [27-29], Kim and Bernitsas [43, 44], van Oortmerssen et al. [68]. A variation of SMS, suitable for the Campos Basin offshore Brazil is the Differentiated Compliance Anchoring System (DICAS), a type of SMS in which different mooring line pretensions, and therefore stiffnesses, are used at the bow and at the stern of the ship allowing the vessel to partially weathervane under different environmental conditions. The lines moored forward of the center of gravity of the vessel have higher pretensions than the lines moored aft. This somewhat restricts the bow of the vessel from moving, while allowing the stern of the vessel to move relatively freely. Risers can then be installed near the bow of the vessel, where the horizontal motion is limited. DICAS have been studied by Garza-Rios et al. [37, 38].

5

In deep water, mooring chains become excessively heavy, and need to be supported by buoys. Their effect on spread mooring systems was studied by Garza-Rios and Bernitsas [34, 35]. The problem of coupled mooring and riser analysis was studied by Ormberg et al. [57] and Kim and Bernitsas [44]; and the memory effect was analyzed by Chung and Bernitsas [16], and Kim and Bernitsas [43].

3. PROBLEM DESCRIPTION

The station-keeping problem studied in this paper has four major elements which are described in this chapter: environment, station-keeping system, system dynamics, and design.

3.1 Environment

Water depth, current direction and velocity profile, wind velocity and direction, and wave directional spectrum are required for modeling the environment and calculating the environmental excitation on the floating production system including the moored vessel, the mooring lines and supporting buoys, and the riser(s). These factors along with availability of equipment largely determine the choice of the mooring system.

3.2 Station-Keeping System

For small and intermediate water depths, mooring is typically used for station-keeping of a floating vessel. For deeper waters, dynamic positioning has been used [19]. Presently, hybrid systems are considered for drilling at water depths approaching 3,000 meters. Depending on the water depth, the intensity of the environmental excitation, and the variation of direction of excitation, a different station-keeping system and configuration may be selected such as SPM, TPM, SMS, DICAS, or TMS. The number of mooring lines may vary from one to twelve or even higher. Lines may be of synthetic fiber, chains, steel cables, or a combination thereof. Anchoring at the sea bed is used and buoys may be attached to chains to support their weight. Other major components of the system are the marine risers whose flexibility of joints and strength determine the radius of offset of the moored vessel around the well head.

3.3 System Dynamics

In response to external excitation the various components of a mooring system respond dynamically in a wide range of frequencies. Four scales of frequencies can be identified in the system dynamics:

(i) Horizontal plane slow motions characterized by floating vessel maneuvering in response to time independent excitation from current, wind and mean wave drift. Surge, sway and yaw constitute the horizontal plane motions and have the common thread of zero hydrostatic restoring force.

7

(ii) Intermediate frequency motions due to slowly-varying wave drift forces and due to the wave frequency dependency of the radiation forces on horizontal plane dynamics. This is the memory effect which is non-autonomous [16, 43]. It is treated in the UM methodology using the method of extended dynamics [67] which renders the Cummins convolution integral [18] as a sequence of 12 autonomous first order differential equations (see equations (83) - (94)).

(iii) Wave frequency motions which cannot be controlled by a station-keeping system. Those are fast first order motions partially transmitted to the mooring lines and riser connected to the moored vessel. Fast frequency excitation is exerted on the lines and risers directly as well. The fast motions affect all six degrees of freedom of the vessel but may be more pronounced in heave, roll, and pitch due to the presence of hydrostatic restoring forces in these degrees of freedom.

(iv) Fluid-structure interaction frequencies due to flow induced vibrations of mooring lines and risers.

Mooring system dynamics is strongly nonlinear. Thus, solution of the complete problem can be achieved only by simulation. Extensive nonlinear simulations, however, provide only a very limited picture of the system dynamics. Fundamental understanding of the system physics is needed in order to provide the designer with tools that can reduce the need for trial and error and lengthy simulations. For that purpose, the approach used is to decouple the fast frequency scale and the fluid-structure interaction scale and study them separately from the coupled slow and intermediate frequency scales. The latter scales constitute the underlying dynamics which can be controlled by station-keeping. In addition, the two fast scales require input from the slow/intermediate dynamics.

3.4 Design

The design procedure that we have developed at the University of Michigan is based on the slow/intermediate motion, horizontal plane dynamics of mooring systems. These are the only controllable motions. The dynamics is still strongly nonlinear and the complete solution can be achieved only by simulation. Thus, the designer would be forced still to rely on his/her experience to reduce trial and error and lengthy simulations. An effective design methodology should be able to provide time independent features of the system dynamics which describe globally the mooring system performance and can be used for assessment. The global design information produced in our approach includes:

(i)   all system equilibria (attainable and non-attainable),

(ii) the system eigenvalues at each equilibrium,

(iii) the stable and unstable submanifolds at each equilibrium,

(iv) the bifurcation sequences of codimension one in any parametric design space,

(v) catastrophe sets (design graphs) in any parametric design space,

(vi) the associated morphogeneses for each bifurcation in any catastrophe set.

For autonomous systems, the above information suffices to assess a mooring system and to virtually eliminate trial and error and lengthy simulations. At the same time, it provides the complete picture of the slow and intermediate frequency dynamics because the design graphs define all regions of qualitatively different dynamics. The number of design graphs required to reveal the complete picture of the system dynamics is still very high due to the high number of design parameters, such as the number and orientation of the mooring lines, the material and pretension of each line, the coordinates of the two ends of each mooring line, and the location and tension of the riser(s).

In 1995-1996, we developed closed form analytical expressions of bifurcation sequences based on the system physics [6, 27-29]. Even though the expressions of both static and dynamic loss of stability are several pages long, it is straightforward to program them in a PC. Sensitivity information of the system dynamics on each design variable can be derived from those physics based expressions. Thus, these expressions make it possible to reduce to a minimum the design graphs (catastrophe sets) required for design.

Two environmental excitation components are in a nonautonomous form. The memory effect which is in the form of the Cummins convolution integral [18] and slowly-varying drift forces. The former can be made autonomous by the method of extended dynamics [16, 43, 67]. The slowly-varying drift forces are handled as an additional load on an otherwise autonomous system [9]. This makes it possible to reveal a more complete picture of the interaction between frequencies of the mooring system and wave-drift.

9

4. MATHEMATICAL FORMULATION

The nonlinear slow and intermediate frequency dynamics of the horizontal plane motions of a moored vessel is formulated mathematically. The model includes the vessel equations of motion with hydrodynamic memory and kinematics, maneuvering model, mooring line model, environmental excitation, and riser model. In this work, two mooring models are treated. The first models all Spread Mooring Systems (SMS), including the DICAS variation, SPM and TPM systems [5, 6, 9, 11, 15, 16, 37, 38, 43, 44]. The second models Turret Mooring System (TMS) which possesses an additional degree of freedom [7, 30, 31]. Additional degrees of freedom are needed to model buoy dynamics if buoys are used to support heavy chain lines. Each component of modeling is presented separately in the following sections of this chapter.

4.1 Equations of Motion and Kinematics of SPM, TPM, SMS, DICAS

Figure 1 depicts the general geometry of a SMS and two different coordinate systems: (i) A body fixed reference frame (X, Y, Z) with its origin located at the center of gravity (CG) of the moored vessel. In this frame, (X, Y) is the horizontal plane and (X, Z) is the center plane of symmetry. (ii) An inertial frame (x, y, z) fixed to the earth and with its origin located at Mooring Terminal 1. Further, n is the number of mooring lines, ($x_p^{(i)}$, $y_p^{(i)}$) are the body fixed coordinates of the i-th mooring line fairlead; and ($x_m^{(i)}$, $y_m^{(i)}$) are the mooring coordinates of the i-th mooring line with respect to (x, y). U is the current speed; u, v and r are the relative velocity components of the system in surge, sway and yaw, respectively; δ is the rudder angle; and ψ is the yaw (or drift) angle. The direction of external excitation ϕ with respect to (x, y, z) due to current, wind and waves is depicted in Figure 1.

The equations of motion of the system in the horizontal plane - surge, sway and yaw - are given by:

$$(m + m_{11})\dot{u} - mrv = X_H + \sum_{i=1}^{n}\left\{\left[T_H^{(i)} - F_P^{(i)}\right]\cos\beta^{(i)} + F_N^{(i)}\sin\beta^{(i)}\right\} + X_M + X_R + X_W + X_{WV} , \qquad (1)$$

$$(m + m_{22})\dot{v} + m_{26}\dot{r} + mru = Y_H + \sum_{i=1}^{n}\left\{\left[T_H^{(i)} - F_P^{(i)}\right]\sin\beta^{(i)} - F_N^{(i)}\cos\beta^{(i)}\right\} + Y_M + Y_R + Y_W + Y_{WV} , \quad (2)$$

$$m_{62}\dot{v} + (I_{zz} + I_{66})\dot{r} = N_H + \sum_{i=1}^{n}x_p^{(i)}\left\{\left[T_H^{(i)} - F_P^{(i)}\right]\sin\beta^{(i)} - F_N^{(i)}\cos\beta^{(i)}\right\}$$

$$- \sum_{i=1}^{n}y_p^{(i)}\left\{\left[T_H^{(i)} - F_P^{(i)}\right]\cos\beta^{(i)} + F_N^{(i)}\sin\beta^{(i)}\right\} + N_M + N_R + N_W + N_{WV} , \qquad (3)$$

where m is the mass of the vessel; I_{zz} is the moment of inertia of the system about the Z-axis; m_{11}, m_{22}, m_{26}, m_{62} and I_{66} are added mass and moment terms; $\dot{u}$ and $\dot{v}$ are the relative accelerations of the system in surge and sway with respect to water; $\dot{r}$ is the relative angular acceleration in yaw. X_H, Y_H and N_H are the hydrodynamic forces and moment acting on the vessel; X_M, Y_M and N_M are the velocity dependent hydrodynamic forces and moment due to the memory effect; X_R, Y_R and N_R are the forces and moment exerted by the riser on the vessel; X_W, Y_W and N_W are the forces and moment due to steady wind; X_{WV}, Y_{WV} and N_{WV} correspond to second order mean wave drift loads. In addition, for each mooring line, T_H is the horizontal tension component of the line; F_P and F_N are the mooring line drag components in the directions perpendicular and normal to the mooring line motion, respectively [36]; β is the horizontal angle between the X-axis and its corresponding mooring line.
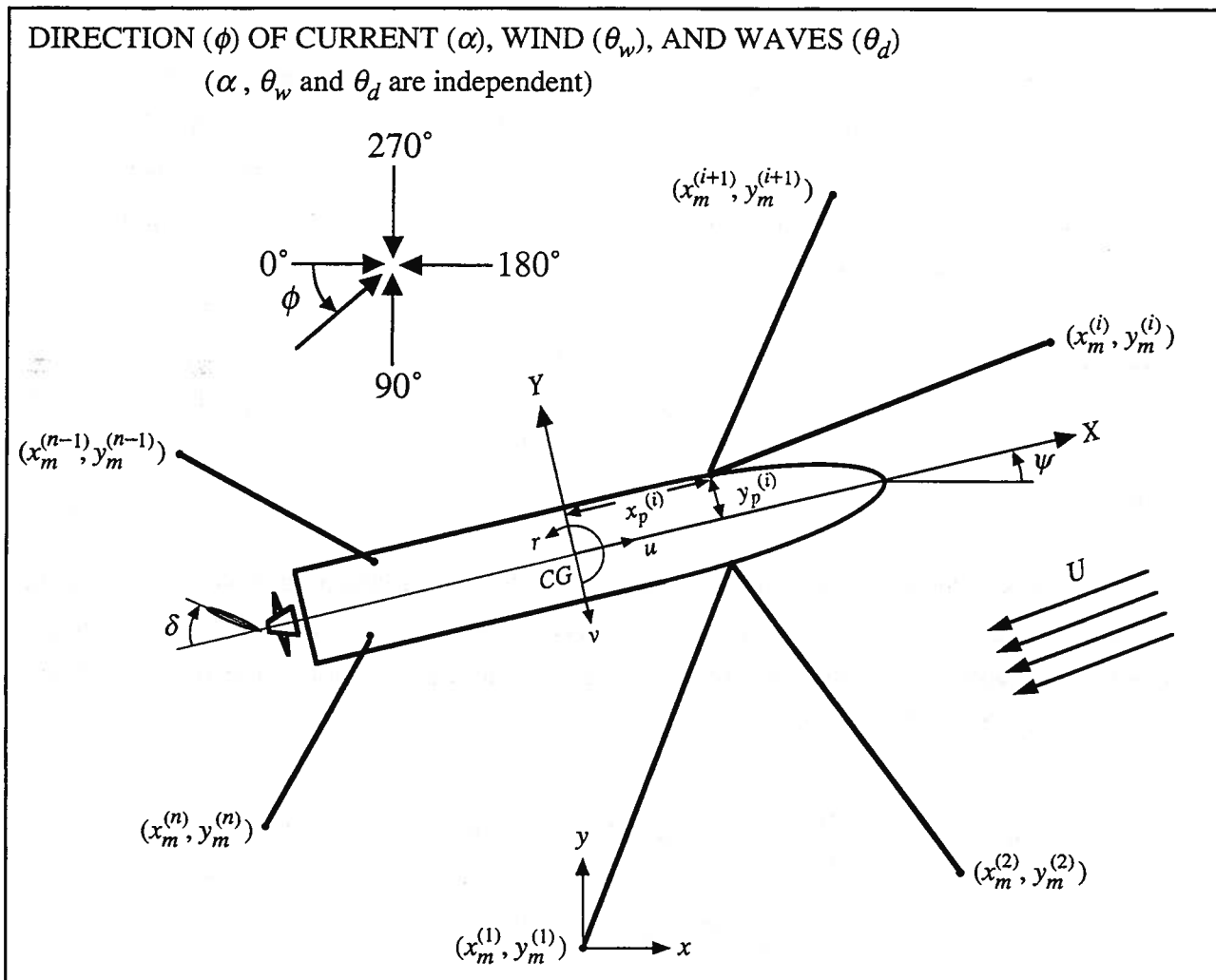
Fig. 1   Geometry of Spread Mooring System

The kinematics of the system are given by

$$\dot{x} = u\cos\psi - v\sin\psi + U\cos\alpha \ , \tag{4}$$

$$\dot{y} = u\sin\psi + v\cos\psi + U\sin\alpha \ , \tag{5}$$

$$\dot{\psi} = r \ , \tag{6}$$

where α is the current angle with direction of excitation as shown in Figure 1.

4.2 Equations of Motion and Kinematics of TMS

The geometry of a TMS is shown in Figure 2. As with SMS, the two principal reference frames are the inertial reference frame with its origin located on the sea bed at mooring terminal 1 (x,y,z); and the body fixed reference frame (X,Y,Z) with its origin located at the center of gravity of the system CG, i.e. of the vessel and turret combined. A third reference frame, (X',Y',Z') has its origin at the center of gravity of the turret (CG_T), with its Z'-axis parallel to the Z-axis on the body. The turret rotation is measured from this system and is denoted by ψ_T, the absolute yaw angle of the turret. D_{CG} is the distance between CG and CG_T; and γ_o is the angle at which the mooring line is attached to the turret with respect to the X'-axis (fixed to the turret). The rest of the symbols appearing in Figure 2 are defined as in Figure 1 for a general SMS.

The equations of motion of a TMS consist of three equations in the horizontal plane for the vessel and the corresponding equations for the turret. Since the surge and sway equations of the turret are related to the corresponding vessel equations [31], TMS possess four physical independent degrees of freedom.

The dynamics of the system can be recast in terms of four equations of motion, corresponding to the three equations of motion for the system (i.e. vessel and turret combined) in surge, sway and yaw, and one equation involving the rotation of the turret. The equations of motion of the system with respect to the (X,Y,Z) reference frame, are given by:

$$(m+m_{11})\dot{u} - mrv = X_H + \sum_{i=1}^{n}\left\{\left[T_H^{(i)} - F_P^{(i)}\right]\cos\beta^{(i)} + F_N^{(i)}\sin\beta^{(i)}\right\} + X_M + X_R + X_W + X_{WV} \ , \tag{7}$$

$$(m+m_{22})\dot{v} + m_{26}\dot{r} + mru = Y_H + \sum_{i=1}^{n}\left\{\left[T_H^{(i)} - F_P^{(i)}\right]\sin\beta^{(i)} - F_N^{(i)}\cos\beta^{(i)}\right\} + Y_M + Y_R + Y_W + Y_{WV} \ , \tag{8}$$

$$m_{62}\dot{v} + (I_{zz} + I_{66})\dot{r} = N_H + D_{CG}\sum_{i=1}^{n}\left\{\left[T_H^{(i)} - F_P^{(i)}\right]\sin\beta^{(i)} - F_N^{(i)}\cos\beta^{(i)}\right\} + N_T + N_M$$

$$+ N_R + N_W + N_{WV} \ . \tag{9}$$
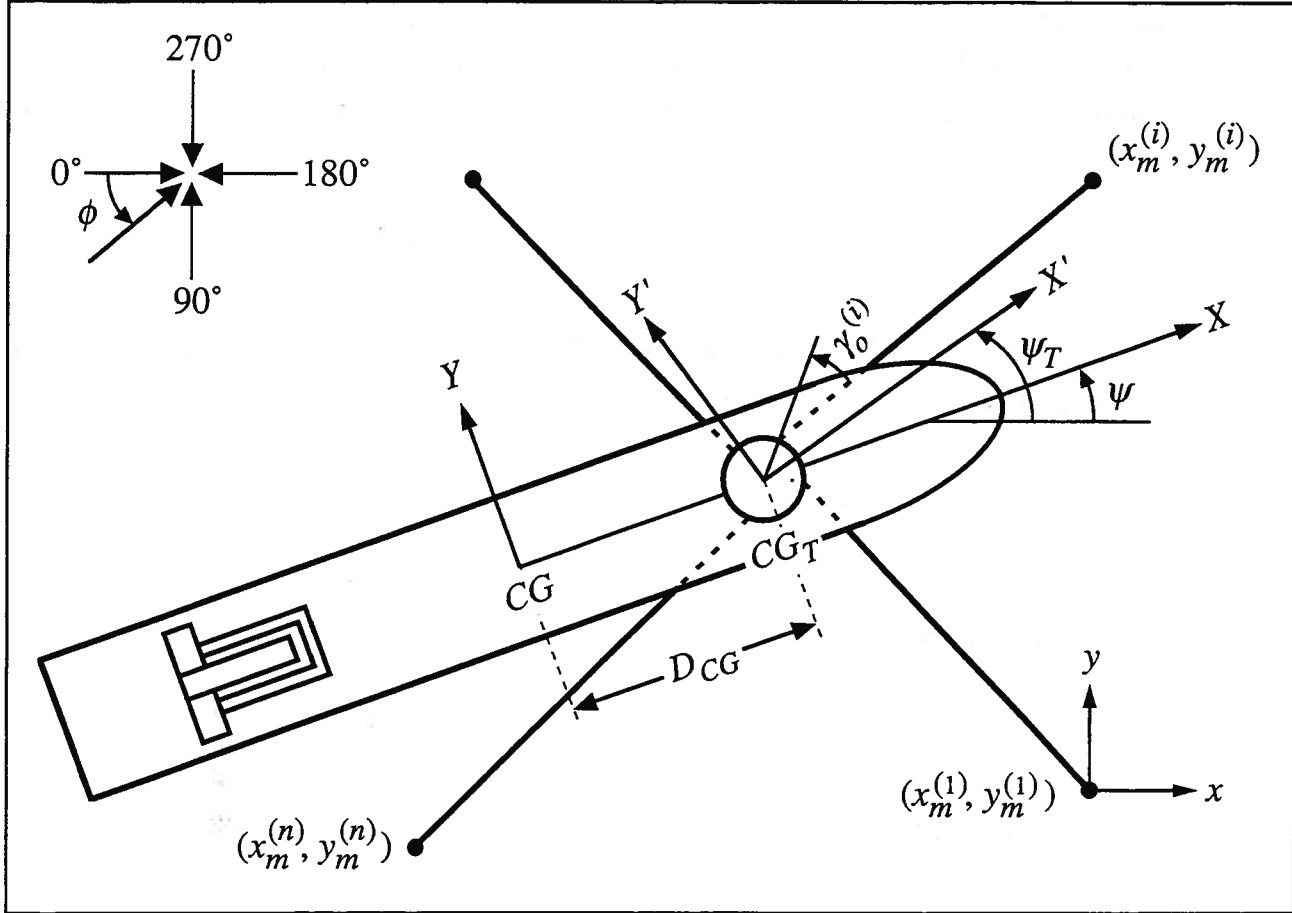
Fig. 2 Geometry of Turret Mooring System

Equations of motion in surge and sway remain as in SMS dynamics. In equation (9), N_T is the moment exerted on the vessel by the turret. The rotational equation of the turret about the Z'-axis is

$$I_T\dot{r}_T = \frac{D_T}{2}\sum_{i=1}^{n}f_a^{(i)}\left\{\left[T_H^{(i)} - F_P'^{(i)}\right]\sin\left(\beta'^{(i)} - \gamma_o^{(i)}\right)\right\} - \frac{D_T}{2}\sum_{i=1}^{n}f_a^{(i)}\left\{F_N'^{(i)}\cos\left(\beta'^{(i)} - \gamma_o^{(i)}\right)\right\} + N_V \ , \tag{10}$$

where I_T is the moment of inertia of the turret about the Z'-axis; $\dot{r}_T$ is the relative angular acceleration of the turret with respect to water; D_T is the turret diameter. The terms inside the summation in equation (10) for the i-th mooring line are defined as follows: f_a is the fraction of the turret diameter at which the mooring line is attached; F_P' and F_N' are the drag forces on the i-th mooring line in the directions parallel and perpendicular to the mooring line motion, respectively [36]; β' is the horizontal

13

angle between the X'-axis and the mooring line measured counterclockwise. In addition, N_V is the moment exerted on the turret by the vessel.

The exerted moments N_T and N_V are small compared to the other terms in equations (9) and (10), and are often neglected. Modeling these terms is difficult, as there are almost no existing experimental data. These are of equal magnitude, and represent the friction force exerted between the turret and the vessel. These moments are thus a function of their relative rotational velocities. A proposed model for these would be:

$$N_V = -N_T = \tau(r_T - r) \ , \tag{11}$$

where r_T is the turret rotational velocity and τ is a coefficient which depends on the friction between turret and vessel, the mooring line damping, geometry, and external system excitation.

The kinematics of TMS are given by

$$\dot{x} = u\cos\psi - v\sin\psi + U\cos\alpha \ , \tag{12}$$
$$\dot{y} = u\sin\psi + v\cos\psi + U\sin\alpha \ , \tag{13}$$
$$\dot{\psi} = r \ , \tag{14}$$
$$\dot{\psi}_T = r_T \ . \tag{15}$$

4.3 Maneuvering Models

Numerous hydrodynamic models have been developed to predict the velocity dependent hull hydrodynamic forces and moment X_H, Y_H and N_H in equations (1) - (3) and (7) - (9). Two main schools of modeling can be identified. The first one represented by the Abkowitz [1, 2] and Takashina [65] models are used in our work. The second is represented by the Obokata [54, 55] and the Short-Wing [46, 61] models. Next, these four models are described and compared briefly [49].

Each of the four hydrodynamic models compared in this paper has its own advantages and limitations. The first step in assessing a particular model is to understand how it approximates the physics of hydrodynamic force modeling. The reader is referred to original papers for a full rendition of each hydrodynamic model. Following, a brief description of each model is provided presenting some of its capabilities and limitations:

(i) The Abkowitz Model (A-M) assumes that the maneuvering characteristics of ships can be described properly by multi-variable Taylor expansions about the steady state condition of constant forward speed. The expressions for the hull hydrodynamic forces and moment are

$$X_H = X_o + X_u u + X_{vr} vr + X_{v\delta} v\delta + X_{r\delta} r\delta + X_{vru} vru + X_{v\delta u} v\delta u + X_{r\delta u} r\delta u$$
$$+ \frac{1}{2}\left(X_{uu} u^2 + X_{vv} v^2 + X_{rr} r^2 + X_{vvu} v^2 u\right) + \frac{1}{2}\left(X_{rru} r^2 u + X_{\delta\delta}\delta^2 + X_{\delta\delta u}\delta^2 u\right) + \frac{1}{6}X_{uuu} u^3 , \quad (16)$$

$$Y_H = Y_o + Y_{ou} u + Y_v v + Y_r r + Y_{vu} vu + Y_{ru} ru + Y_\delta \delta + Y_{\delta u}\delta u + Y_{vr\delta} vr\delta$$
$$+ \frac{1}{2}\left(Y_{ouu} u^2 + Y_{vrr} vr^2 + Y_{rvv} rv^2 + Y_{vuu} vu^2\right) + \frac{1}{2}\left(Y_{v\delta\delta} v\delta^2 + Y_{r\delta\delta} r\delta^2 + Y_{ruu} ru^2\right)$$
$$+ \frac{1}{2}\left(Y_{\delta vv}\delta v^2 + Y_{\delta rr}\delta r^2 + Y_{\delta uu}\delta u^2\right) + \frac{1}{6}\left(Y_{vvv} v^3 + Y_{rrr} r^3 + Y_{\delta\delta\delta}\delta^3\right) , \quad (17)$$

$$N_H = N_o + N_{ou} u + N_v v + N_r r + N_{vu} vu + N_{ru} ru + N_\delta \delta + N_{\delta u}\delta u + N_{vr\delta} vr\delta$$
$$+ \frac{1}{2}\left(N_{ouu} u^2 + N_{vrr} vr^2 + N_{rvv} rv^2 + N_{vuu} vu^2\right) + \frac{1}{2}\left(N_{v\delta\delta} v\delta^2 + N_{r\delta\delta} r\delta^2 + N_{ruu} ru^2\right)$$
$$+ \frac{1}{2}\left(N_{\delta vv}\delta v^2 + N_{\delta rr}\delta r^2 + N_{\delta uu}\delta u^2\right) + \frac{1}{6}\left(N_{vvv} v^3 + N_{rrr} r^3 + N_{\delta\delta\delta}\delta^3\right) , \quad (18)$$

where subscripts "o" and "δ" represent propeller and rudder angle effects.

Tests of deviation from the steady state condition provide the slow motion derivatives. In model tests, the hydrodynamic forces and moment are measured while in sea trials system identification techniques are used to calculate slow motion derivatives. Usually, terms to third-order are retained. In addition, A-M assumes that coupling between velocity and acceleration terms is negligible; thus, only first order accelerations are considered [1]. This model provides a very good estimation of the hydrodynamic forces and moment on a vessel in small deviations from a steady forward slow motion. In mooring applications, A-M is not so accurate for large incident angles of relative flow $\theta = \alpha - \psi$. These may be caused by large amplitude yaw or large θ. A-M for mooring systems can be improved by model tests and/or sea trials performed for larger drift angles.

(ii) The Takashina Model (T-M) approximates the hydrodynamic forces and moment using a Fourier series with respect to θ [65, 66]. Kinematic conditions are used to relate the vessel translational velocities to θ, thus expressing the hydrodynamic forces and moment in terms of the vessel velocity vector relative to current as follows:

$$X_H = X_u u + (X_{vr} + m_{22})vr , \quad (19)$$

$$Y_H = Y_v v + Y_{vvv} v^3 + Y_{vvvvv} v^5 + (Y_{ur} - m_{11})ur + Y_{ur|r|}ur|r| + Y_{v|r|}v|r| , \quad (20)$$

$$N_H = N_v v + N_{uv} uv + N_{vvv} v^3 + N_{uvvv} uv^3 + N_r r$$

15

$$+ N_{r|r|}r\,|\,r\,|+ N_{uv|r|}uv\,|\,r\,|+ N_{vvr}v^2r\,,\tag{21}$$

This approach makes the velocity components of the vessel dependent variables. Computation of the series coefficients relies on model tests. These consist of fixed θ (captive) and free running tests. The captive tests consist of static drift and yaw rotating tests, thus adding the capability of describing the forces and moments on the vessel for larger θ [65]. Due to the nature of the experiments, however, T-M does not take into account the coupled added mass components in sway and yaw, thus resulting in a small loss in the inertial forces and moment components. It should be pointed out that T-M uses only the linear term of the resistance $X_u u$ in equation (19). Throughout this work, this term has been replaced by a third-order resistance curve [38].

(iii) The Obokata Model (O-M) is based on the local cross flow principle [54] which is valid for large θ. O-M incorporates the inertia terms, static damping, and yaw damping of the hydrodynamic forces and moment. The static damping is modeled after the traditional velocity squared drag forces and moment acting on the vessel, with measured current force and moment coefficients for different θ. The yaw damping incorporates the viscous damping forces due to the yaw velocity of the vessel. Both damping components are calculated by a strip theory approach using the sectional speed and θ [55]. The approximation involved in the O-M approach is similar to that in the Morison equation. Specifically, the theoretically based inertia term and the semi empirical velocity squared drag term are added. The hydrodynamic coefficients which are measured experimentally in general do not account properly for all nonlinearities related to damping and viscosity.

(iv) The Short-Wing (SW-M) utilizes a similar approach as O-M, but instead of integrating the static and yaw damping components locally in each strip, SW-M separates them at the global ship level. The static component makes use of a heuristic formulation that blends the ship hydrodynamics in a cross flow and the ship hydrodynamics for small drift angles (short-wing theory), thus resulting in a relatively simple model that describes the generalized current forces acting on a vessel as a function of θ, vessel dimensions, and other vessel properties [46]. In addition, SW-M incorporates a linear correction for the presence of the rudder based on the work by Clarke et al. [17]. Model tests are performed with the ship fixed at a given θ to obtain the coefficients of forces and moment needed. Additional model tests consist of towing a model which is restricted to one degree of freedom (rotation), which serve to validate the static component of forces and moment. A heuristically determined transition function makes sure that the model fits the correct behavior in a continuous range of θ, and thus has the advantage of being able to preserve the

dependence of forces and moment on vessel dimensions. The yaw damping component consists of forces and moment due to the rotation of the ship, and is modeled starting from the cross flow principle [54, 61]. The two components are superposed. The original purpose of this model was to predict accurately static bifurcation phenomena [46] which it achieves satisfactorily. The physical limitations of SW-M are: First, the hydrodynamic forces and moment are measured for fixed θ, as is the case with O-M. Second, all damping components are computed using methods with different physics bases which are superposed expecting that experimentally measured coefficients account for coupling nonlinearities.

All four models depend on curve fitting of the measured forces. Both A-M and T-M rely on extensive tests to ensure that the curve fitting coefficients accurately represent the hull hydrodynamics. Both methods present experimental challenges, and are limited by model test precision. Specifically, higher order hydrodynamic derivatives may have a strong influence on the prediction of the system dynamics. Yet, different measurements may result even in sign discrepancies [42].

In SW-M and O-M, testing consists of a limited number of experiments that measure force coefficients with respect to θ. SW-M requires only a small number of measurements to construct the required expressions heuristically. O-M requires a larger range of measurements, and is limited in the sense that it employs only a number of force measurements for the whole range of incident angles, requiring interpolation to obtain a complete range of force coefficients. The fact that the force and moment coefficients are easily measured experimentally in O-M and SW-M, makes both models simple to validate [46, 54]. Both models, however, need corrections to account for the rotational forces and moment on the system since the coefficients are measured with the ship fixed.

Matsuura et al. [49] make further comparisons of the four models based on their ability to predict global system particulars such as equilibria and bifurcation sequences. In general, both schools predict well the static loss of stability. The first school predicts better the dynamic loss of stability.

Most of the maneuvering models used to predict X_H, Y_H, N_H follow one of the two schools of thought defined above. Several of those are summarized by Fossen [25].

4.4 Mooring Line Models

For the purpose of studying the slow motion dynamics of mooring systems, mooring lines are modeled quasi-statically. Mooring lines used in mooring operations are chains, cables, synthetic ropes or combinations thereof. The mathematical models are presented next.

4.4a Synthetic Fiber Ropes

Synthetic Fiber Ropes (SFR) are light and considerably extensible. Synthetic ropes function primarily out of the water, although sometimes are used in deep water mooring as components in hybrid lines. Their restoring force comes from their extensibility modeled as [50]

$$T = S_b p \left(\frac{\ell - \ell_w}{\ell_w} \right)^q , \tag{22}$$

where T is the tension in the rope, S_b is the average breaking strength of the line, ℓ_w is the length of the unstrained rope, ℓ is the length of the strained rope, and p and q are experimentally determined constants.

4.4b Steel Cables

Cables are heavier than synthetic fibers, are less extensible, and their deformation is three-dimensional [58]. Steel cables are modeled by a nonlinear cable model that takes into consideration partial submergence, three-dimensional deformation, effective tension, extensibility, and nonlinear drag [58]. The basic cable model is governed by the basic equations:

$$\frac{\partial}{\partial S} \left(\frac{T}{1 + E_S} \frac{\partial x}{\partial S} \right) + (1 + E_S) \left(f_{B_x} + f_{T_x} \right) = 0 , \tag{23}$$

$$\frac{\partial}{\partial S} \left(\frac{T}{1 + E_S} \frac{\partial y}{\partial S} \right) + (1 + E_S) \left(f_{B_y} + f_{T_y} \right) = 0 , \tag{24}$$

$$\frac{\partial}{\partial S} \left(\frac{T}{1 + E_S} \frac{\partial z}{\partial S} \right) + (1 + E_S) \left(f_{B_z} + f_{T_z} \right) = 0 , \tag{25}$$

$$x(0) = y(0) = z(0) = 0 , \tag{26}$$

$$\frac{T}{1 + E_S} \frac{\partial x}{\partial S} - F_{M_x} = \frac{T}{1 + E_S} \frac{\partial y}{\partial S} - F_{M_y} = \frac{T}{1 + E_S} \frac{\partial z}{\partial S} - F_{M_z} = 0 , \qquad \text{at} \quad S = \ell_w , \tag{27}$$

where (x, y, z) are the coordinates of a material point in the deformed configuration, S is the unstrained arc length, which is related to the real arc length s by the elongation rate relation

$$s = (1 + E_S) \, dS . \tag{28}$$

In addition, $(f_{T_x}, f_{T_y}, f_{T_z})$ is the body force vector; $(f_{B_x}, f_{B_y}, f_{B_z})$ is the traction force vector; $(F_{M_x}, F_{M_y}, F_{M_z})$ is the end force vector at $S = \ell_w$. In the case of a submerged cable, the tension T in equations (23) - (25) must be replaced by the effective tension T_e, where

$$T_e = T + \rho_w g A_s (H_w - z) , \tag{29}$$

ρ_w is the density of water, g is the gravitational acceleration, A_s is the strained cable cross sectional area, H_w is the free surface z-coordinate, and T is the actual tension in the cable

$$T = \frac{EA_o}{2} E_S (1 + E_S)(2 + E_S) . \tag{30}$$

E is the Young modulus of elasticity and A_o is the unstrained cable cross sectional area. Equation (30) is valid for Poisson ratio $v = 0$. In order to accurately integrate the hydrostatic pressure force on the surface of the submerged cable, the actual weight in the body force is replaced by the effective weight. For $v \neq 0$,

$$T = (1 + E_S) A_o \left[\frac{E}{2} E_x (2 + E_S) - 2 v \rho_w g (H_w - z) \right] . \tag{31}$$

4.4c   Chains

Chains are heavier than cables, have high hydrodynamic resistance, are usually fully submerged, only slightly extensible, and have two dimensional deformation in the vertical plane. Chains modeled by the catenary equations [36, 58]. In towing and mooring operations, two types of chains are commonly used, anchored and suspended catenaries.

The first type is Anchored Catenary (AC) used in intermediate depth mooring operations and includes nonlinear drag and touchdown. The horizontal and vertical components of the mooring line tension T_H and T_V at the attachment point on the vessel can be found by solving the following relations [36]:

$$\frac{T_H}{P} \sinh\left(\frac{P\ell}{T_H}\right) = \sqrt{h\left(h + 2\frac{T_H}{P}\right)} , \tag{32}$$

$$T_V = T_H \sinh\left(\frac{P\ell}{T_H}\right) , \tag{33}$$

19

where ℓ is the horizontal projection of the suspended part of the catenary, P is the weight of the catenary per unit length, and h is the water depth. The total tension in the chain, T is given by

$$T = \sqrt{T_H^2 + T_V^2} = T_H \cosh\left(\frac{P\ell}{T_H}\right) . \tag{34}$$

Thus, the tension in a given chain depends on the projection of the suspended part of the catenary and the water depth.

The second type of chain is called Suspended Catenary (SC) and is used in towing and occasionally in shallow mooring operations. The horizontal tension component T_H of a SC is obtained by solving the following implicit equation in T_H [58]

$$\sinh\left(\frac{P\ell}{2T_H}\right) = \frac{P\ell}{2T_H}\left[\frac{\sqrt{\ell_w^2 - h^2}}{\ell}\right] . \tag{35}$$

In equation (35), ℓ is also defined as the horizontal projection of the suspended part of the catenary. SC's are, by definition suspended, and thus ℓ is also the horizontal distance between end points of the catenary. The vertical tension component at each end of a SC is different if the endpoints are not at the same vertical level. This component may be calculated by decomposing the SC into two segments and using equation (33), provided that the horizontal projection of each segment is substituted instead of ℓ.

4.4d   Chains Supported by Buoys

In deep waters, the chain weight becomes a significant load on the moored vessel and the chain itself. In order to overcome this problem, buoys can be placed along a chain to support partially the weight of the chain. In this case, the chain model is made of a combination of one anchored and one or more suspended catenaries. Buoys make use of chains in deeper waters feasible by reducing the load on the vessel.

Figure 3 shows the geometry of a catenary mooring line, which consists of two line segments defined by a buoy [34]. Segment S1 is an anchored catenary moored to the sea bed with its upper end connected to the buoy. Segment S2 is a suspended catenary with its lower end connected to the buoy and its upper end connected to the moored vessel. Segment S2 is further divided into two parts:

Segment S2A, which extends from the point where SC is connected to the buoy to the lowest point of S2, and segment S2B which runs from the lowest point of S2 to the point of attachment of SC on the moored vessel. In Figure 3, (x,z) is the inertial reference frame of the catenary, located at the point where the mooring line is anchored to the sea bed; (x_m, z_m) are the coordinates of the anchoring point $(x_m = 0,\ z_m = 0)$; U is the current velocity in the $-x$ direction; ℓ_1' is the length of the horizontal projection of AC; ℓ_1 is the length of the horizontal projection of the suspended part of AC; d is the horizontal length of AC in the ground; ℓ_2 is the length of the horizontal projection of SC; ℓ_{2A} is the length of the horizontal projection of segment S2A; ℓ_{2B} is the length of the horizontal projection of segment S2B. These are related as follows:

$$\ell_1' = \ell_1 + d \ , \tag{36}$$
$$\ell_2 = \ell_{2A} + \ell_{2B} \ . \tag{37}$$
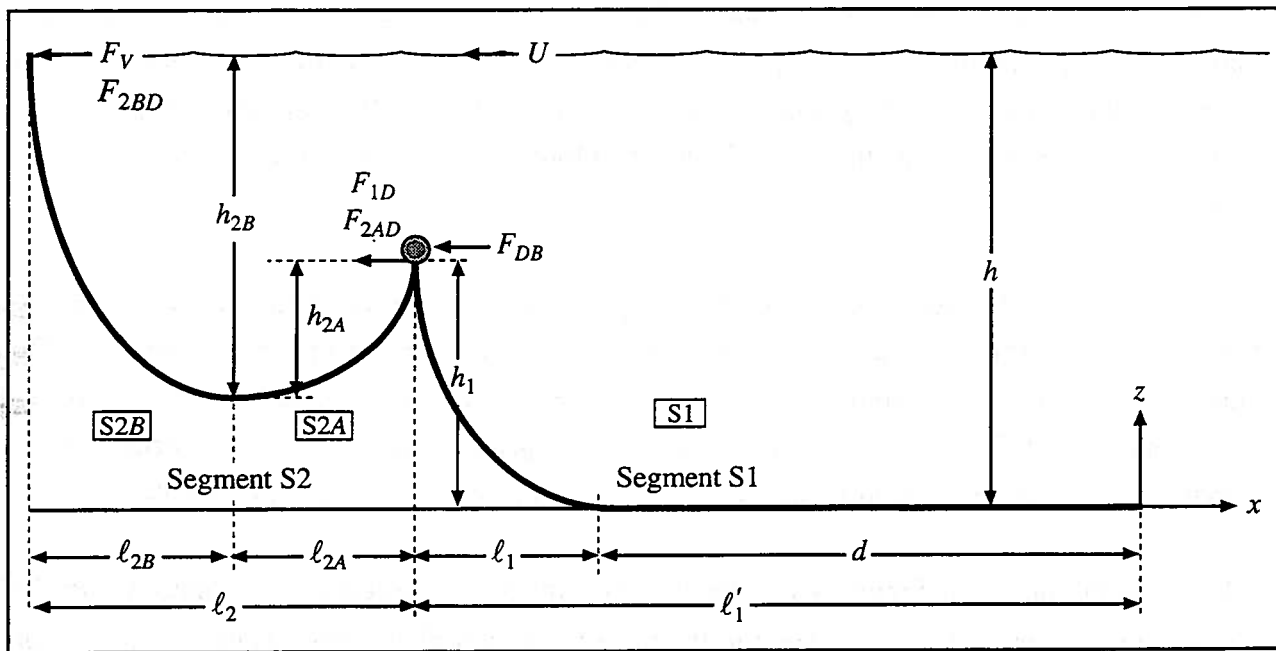
Fig. 3 Geometry of buoy-supported chain

In addition, h is the water depth; h_1 is the vertical distance from the lower point of the buoy to the sea bed; h_{2A} is the vertical distance from the lower point of SC to the lower point of the buoy; h_{2B} is the vertical distance from the lower point of SC to the point of attachment to the moored vessel. The total water depth is constant, and is related to the various vertical distances of Figure 2.1 as follows [34]:

$$h = h_1 - h_{2A} + h_{2B} \ , \tag{38}$$

21

where

$$h_1 = \frac{T_{H1}}{P}\left[\cosh\left(\frac{P\ell_1}{T_{H1}}\right) - 1\right],$$ (39)

$$h_{2A} = \frac{T_{H2}}{P}\left[\cosh\left(\frac{P\ell_{2A}}{T_{H2}}\right) - 1\right],$$ (40)

$$h_{2B} = \frac{T_{H2}}{P}\left[\cosh\left(\frac{P\ell_{2B}}{T_{H2}}\right) - 1\right].$$ (41)

In equations (39) - (41), T_{H1} and T_{H2} are the horizontal tension components of AC and SC, respectively.

The external forces acting on the catenary in Figure 3 are: F_{DB} is the current drag force acting on the buoy; the integrated drag force F_{1D} on catenary segment S1 concentrated at its upper end; the integrated drag components F_{2AD} and F_{2BD} on segments S2A and S2B, concentrated at the upper end of the respective segment; and the external horizontal force F_V imposed by the moored vessel at the top of the catenary.

Figure 4 shows the general horizontal plane geometry of a buoy-supported SMS. The system consists of n mooring lines and n_B buoys. In Figure 3.1, $n = n_B$, and $i = j$, where i is the line number and j is the buoy number. In addition to the inertial and vessel-fixed reference frames, there are n_B buoy-fixed right handed reference frames (X_B, Y_B, Z_B) with X_B pointing horizontally in the direction of its corresponding mooring terminal (x_m, y_m, z_m) and Z_B pointing upwards.

The system shown in Figure 4 can be modeled by $3 + 3n_B$ equations of motion and $3 + 3n_B$ kinematic relations. These correspond to the three horizontal plane vessel equations of motion and kinematics, and three equations of motion for each buoy in surge, sway, and heave as well as their corresponding kinematic relations. An additional equation of motion is required for the TMS as discussed previously. To facilitate discussion, one buoy is included per mooring line. A detailed derivation of the mathematical model for lines with multiple buoys is provided in [34].

In mooring systems where supporting buoys are present, the equations of motion remain as in (1) - (3) for SMS or (7) - (9) for TMS. For the system shown in Figure 4, these equations are:

$$(m+m_{11})\dot{u} - mrv = X_H + \sum_{i=1}^{n}\left\{T_{H2}^{(i)}\cos\beta^{(i)} - F_{2BDX}^{(i)}\right\} + X_M + X_R + X_W + X_{WV} \quad, \tag{42}$$

$$(m+m_{22})\dot{v} + m_{26}\dot{r} + mru = Y_H + \sum_{i=1}^{n}\left\{T_{H2}^{(i)}\sin\beta^{(i)} - F_{2BDY}^{(i)}\right\} + Y_M + Y_R + Y_W + Y_{WV} \quad, \tag{43}$$

$$m_{62}\dot{v} + (I_{zz}+I_{66})\dot{r} = N_H + \sum_{i=1}^{n}x_P^{(i)}\left\{T_{H2}^{(i)}\sin\beta^{(i)} - F_{2BDY}^{(i)}\right\} - \sum_{i=1}^{n}y_P^{(i)}\left\{T_{H2}^{(i)}\cos\beta^{(i)} - F_{2BDX}^{(i)}\right\}$$
$$+ N_M + N_R + N_W + N_{WV} \quad, \tag{44}$$
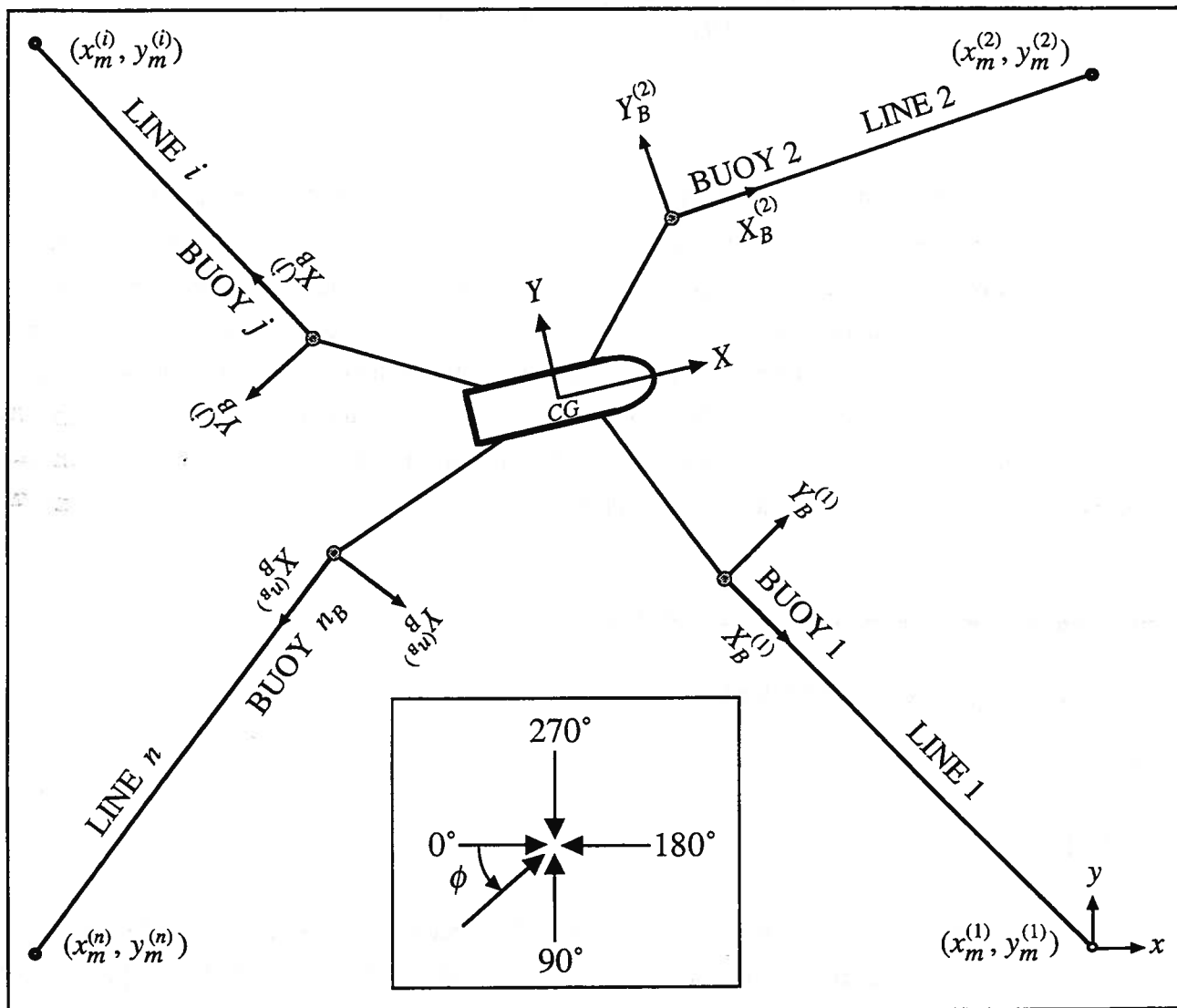
Fig. 4 Geometry of SMS with buoy-supported chains

23

where F_{2BDX} and F_{2BDY} are the drag forces on segment 2B of SC in the X and Y directions, respectively.

The equations of motion for each of the supporting buoys in surge, sway and heave for the system shown in Figure 4 are given by:

$$(m_B^{(i)} + A_{11}^{(i)})\dot{u}_B^{(i)} = T_{H1}^{(i)} + T_{H2}^{(i)} \cos\beta_B^{(i)} - F_{DBX}^{(i)} - F_{A1}^{(i)} - F_{2ADX}^{(i)} , \tag{45}$$

$$(m_B^{(i)} + A_{22}^{(i)})\dot{v}_B^{(i)} = T_{H2}^{(i)} \cos\beta_B^{(i)} - F_{DBY}^{(i)} - F_{L1}^{(i)} - F_{2ADY}^{(i)} , \tag{46}$$

$$(m_B^{(i)} + A_{33}^{(i)})\dot{w}_B^{(i)} = F_B^{(i)} - T_{H1}^{(i)} \sinh\left(\frac{P\ell_1^{(i)}}{T_{H1}^{(i)}}\right) - T_{H2}^{(i)} \sinh\left(\frac{P\ell_{2A}^{(i)}}{T_{H2}^{(i)}}\right) , \tag{47}$$

for $i = 1, \dots, n_B$.

For each buoy in the system, m_B is the buoy mass; A_{11}, A_{22} and A_{33} are the buoy added mass components in surge, sway and heave; $\dot{u}_B$, $\dot{v}_B$, and $\dot{w}_B$ are the buoy relative accelerations in surge, sway, and heave; F_B is the net buoyancy force of the buoy, i.e. the difference between its buoyancy and its weight; F_{DBX} and F_{DBY} are the drag forces on the buoy in surge and sway; F_{A1} and F_{L1} are the drag forces on AC in the directions parallel and perpendicular to the mooring line motion; F_{2ADX} and F_{2ADY} are the drag forces on segment S2A of SC in the X_B and Y_B directions, respectively; and β_B is the horizontal angle between the two segments of the catenary, measured counterclockwise from X_B. The $3\,n_B$ associated kinematic relations of the buoy system are:

$$\dot{x}_B^{(i)} = u_B^{(i)} \cos\gamma_B^{(i)} - v_B^{(i)} \sin\gamma_B^{(i)} + U\frac{z_B^{(i)}}{h}\cos\alpha , \tag{48}$$

$$\dot{y}_B^{(i)} = u_B^{(i)} \sin\gamma_B^{(i)} + v_B^{(i)} \cos\gamma_B^{(i)} + U\frac{z_B^{(i)}}{h}\sin\alpha , \tag{49}$$

$$\dot{z}_B^{(i)} = w_B^{(i)} , \tag{50}$$

for $i = 1, \dots, n_B$;

where u_B, v_B and w_B are the relative velocities of the buoy in surge, sway and heave; γ_B is the horizontal angle between the x-axis and S1, measured counterclockwise from the buoy; and z_B is the vertical ordinate of the center of gravity of the buoy. Kinematics (21) - (23) assume a linear current profile.

24

4.5 Riser Model

A three-dimensional, nonlinear, static, large deformation, riser finite element model STARI-3D (STAtic RIser - 3D) [12] is used to calculate quasistatically the riser dynamics in the analysis of mooring systems. The mathematical formulation and solution method for the riser are described briefly here. The assumptions involved in STARI-3D are the following:

(i) The riser material is homogeneous, isotropic, and linear elastic following Hooke's law.
(ii) Plane sections remain plane after deformation, i.e. warping deformation is neglected.
(iii) Plane sections normal to the centroid line remain normal after deformation, i.e. shear deformation is neglected.
(iv) The riser is initially undeformed and straight in the unloaded condition.

Considering the equilibrium of forces and moments for the static riser problem, we obtain the governing equation for bending

$$-(EI\vec{r}'')'' + [(P_e - EI\kappa^2)\vec{r}']' + [H(\vec{r}' \times \vec{r}'')]' + (\vec{r}' \times \vec{m})' + \vec{q} = \vec{0} \ , \tag{51}$$

and for torsion

$$H' + \hat{t} \cdot \vec{m} = 0 \ , \tag{52}$$

where EI is the bending rigidity of the riser; H is the torsional moment; $\vec{r}$ is the position vector from the origin located at the lower ball joint to a point on the centerline of the deformed riser; κ is the curvature in the osculating plane ($\kappa = |\vec{r}''|$); $\hat{t}$ is the unit local tangential vector; and $\vec{q}$ and $\vec{m}$ are the applied force and moment vectors per unit length, respectively. The effective tension P_e, which considers the effects of internal and external pressure, is given by

$$P_e = P_a + \rho_w g \frac{\pi D_o^2}{4}(H_w - z) - \rho_m g \frac{\pi D_i^2}{4}(H_m - z) \ , \tag{53}$$

where ρ_w is the density of the water; ρ_m is the density of the mud; g is the gravitational acceleration; H_w is the ordinate of the free surface of the water; H_m is the ordinate of the free surface of the mud; D_o is the external riser diameter; D_i is the internal riser diameter; and z is the vertical coordinate measured from the lower ball joint. Further, P_a is the actual tension inside the riser material given by

$$P_a = EA\,\varepsilon_t \; , \tag{54}$$

where EA is the stretching rigidity and ε_t is the strain of the riser centerline in the tangential direction. In equations (51) and (52), the external load per unit length $\bar{q}(s_1)$ consists of the fluid drag force for the static model. An incremental finite element method with an iterative scheme is employed to solve the governing equations for the riser. In this method, the weak form of equation (51) is derived by applying a Galerkin decomposition method. A predictor-corrector scheme is used to update the stiffness matrices, the boundary terms, the extensibility condition, and the deformation dependent loads. This scheme is repeated until convergence is achieved for each load increment. The iteration process is repeated until the entire load is applied. Upon obtaining the deformed riser configuration at equilibrium, the horizontal tension at the top of the riser is considered as an additional reaction force in the equations of motion of the mooring system.

4.6 External Excitation

External excitation is due to time independent current, wind, mean second-order wave drift forces; and slowly varying drift and memory effect. Each of these five loads is modeled in the sections below.

4.6a Current

Current load is implicitly included in the expressions of equations (1) - (3), (7) - (9) and (42) - (44) by using the relative velocity of the vessel with respect to water. Therefore, current loads are modeled accurately to third order in the Abkowitz model and to fifth-order in the Takashina model. This approach is more accurate than the usual method based on projected area and drag coefficients used in the Obokata and Short-Wing models (see Section 4.3).

4.6b Wind

Steady wind forces and moment exerted on the ship can be expressed as [48]:

$$X_W = \frac{1}{2}\rho_a U_w{}^2 C_{xw}(a_r)A_T \; , \tag{55}$$

$$Y_W = \frac{1}{2}\rho_a U_w{}^2 C_{yw}(a_r)A_L \; , \tag{56}$$

$$N_W = \frac{1}{2}\rho_a U_w{}^2 C_{zw}(a_r)LA_L \; , \tag{57}$$

where ρ_a is air density; U_w is wind velocity at a standard height of 10 m above water; a_r is the relative angle of attack between the wind direction and the ship heading; A_T and A_L are the transverse and longitudinal projected areas of the vessel, respectively; L is the length of the vessel; C_{xw}, C_{yw}, and C_{zw} are wind longitudinal and lateral force and moment coefficients, expressed in Fourier Series as follows:

$$C_{xw}(a_r) = \chi_o + \sum_{n=1}^{\infty} \chi_n \cos(na_r) , \tag{58}$$

$$C_{yw}(a_r) = \sum_{n=1}^{\infty} \vartheta_n \sin(na_r) , \tag{59}$$

$$C_{zw}(a_r) = \sum_{n=1}^{\infty} \zeta_n \sin(na_r) . \tag{60}$$

Coefficients χ_o, χ_n, ϑ_n, and ζ_n in Equations (58) - (60) depend on the type of vessel, superstructure location, loading conditions, and the relative angle of the wind direction a_r. These coefficients can be obtained from experimental and full-scale measurement data.

4.6c   Second Order Mean Drift and Slowly-Varying Drift

The common approach to formulation of nonlinear wave-body interaction problems in ship and offshore hydrodynamics is based on potential flow theory using the wave amplitude to length ratio as perturbation parameter. The solution to the second-order problem results in three types of wave excitation forces: mean, difference-frequency (slowly-varying), and sum-frequency (springing) forces. Mean and slowly-varying drift forces are of importance in mooring problems. Newman's approximation [51] for slowly-varying drift forces has been used extensively for many applications in ship hydrodynamics. The important practical consequence of this approach is that slowly-varying drift forces depend merely on evaluation of second-order mean drift forces, and this can reduce the computational time significantly. The formula for slowly-varying drift forces is

$$F_i^{SV} \equiv \left(X_{WV}, Y_{WV}, N_{WV} \right)^T = \sum_{j=1}^{N} \sum_{k=1}^{N} A_j A_k T_{jk}^i \cos\left[\left(\omega_k - \omega_j \right)t + \left(\varepsilon_k - \varepsilon_j \right) \right] , \tag{61}$$

where the coefficients $T_{jk}^i = 0.5(D_j^i + D_k^i)$ and $i = 1$, 2, 6 indicate surge, sway and yaw directions, respectively, and A, ω, and ε are the wave amplitude, circular frequency, and random phase angle of

component number j (or k) in the total number of wave components N. The random phase angles ε are uniformly distributed between 0 and 2π and remain constant in time. The wave amplitude A_j (or A_k) can be computed from the wave spectrum $S(\omega)$ as

$$A_j = \sqrt{2S(\omega_j)\Delta\omega} \; , \tag{62}$$

where $\Delta\omega = \omega_j - \omega_{j-1}$. The two-parameter Bretschneider wave energy spectrum formula is used to express $S(\omega)$. The two parameters are the significant wave height $H_{1/3}$ and the significant wave period $T_{1/3}$. The time mean value over the diagonal terms ($k = j$) in equation (61) gives the mean drift forces while the mean of the off-diagonal terms ($k \neq j$) vanishes.

Mean drift forces can be written as

$$\overline{F_i^{SV}} \equiv \left(X_{WV}, Y_{WV}, N_{WV}\right)^{\mathrm{T}} = \sum_{j=1}^{N} A_j^2 D_j^i \; . \tag{63}$$

The transfer functions D^i for mean wave drift force are approximated as

$$D^1 = \frac{X_{WV}}{\zeta_a^2} = \frac{1}{2}\rho_w g L C_{XD} \cos^3(\theta_o - \psi) \; , \tag{64}$$

$$D^2 = \frac{Y_{WV}}{\zeta_a^2} = \frac{1}{2}\rho_w g L C_{YD} \sin^3(\theta_o - \psi) \; , \tag{65}$$

$$D^6 = \frac{N_{WV}}{\zeta_a^2} = \frac{1}{2}\rho_w g L^2 C_{ZD} \sin 2(\theta_o - \psi) \; , \tag{66}$$

where ζ_a is the wave amplitude, ρ_w is the density of water, θ_o is the absolute angle of wave direction, and g is gravitational acceleration. Coefficients C_{XD}, C_{YD}, C_{ZD} can be obtained from the complete linear (first-order) solution of the seakeeping problem. Further details about the methods of predicting mean drift forces can be found, for example, in the study of Ogilvie [56]. In this paper, it is assumed that these can be given simply in terms of the ship particulars [41].

4.6d Hydrodynamic Memory Effect

In transient motions of a vessel, the time history of the surrounding fluid motion affects the hydrodynamic forces acting on the vessel. This is referred to as the hydrodynamic memory effect. In the time domain, the hydrodynamic radiation forces including the memory effect are given by the convolution integral involving the impulse response function [18]

28

$$F_i(t) = -\sum_j a_{ij}(\infty)\dot{V}_j(t) - \sum_j \int_{-\infty}^{t} K_{ij}(t-\tau)V_j(\tau)d\tau , \quad i, j = 1, 2, 6 , \qquad (67)$$

where $a_{ij}(\infty)$ is the added-mass coefficient at infinite frequency of vessel motion i due to acceleration in j, and V_j is the instantaneous vessel velocity at time t in the j-th mode. The impulse response function $K_{ij}(t)$ can be represented in terms of the frequency-dependent added-mass coefficient a_{ij} or damping coefficient b_{ij} as

$$K_{ij}(t) = \frac{2}{\pi}\int_0^{\infty} \omega[a_{ij}(\infty) - a_{ij}(\omega)]\sin\omega t\, d\omega = \frac{2}{\pi}\int_0^{\infty} b_{ij}\cos\omega t\, d\omega , \qquad (68)$$

where ω is the frequency of vessel motion. From the above equation, it can be noted that the convolution integrals should be evaluated at every time step during time simulation. These evaluations are computationally expensive and not efficient in simulations. An alternative approach to avoid this problem is the use of the method of extended dynamics [67] which replaces the convolution integrals by a set of first-order linear ordinary differential equations. Furthermore, this approach converts the non autonomous expression for $F_i(t)$ given by equation (67) to autonomous.

Following the method of extended dynamics, the convolution integral is approximated by time-varying state variables S_i^0 and is defined by a finite set of recursive first-order linear ordinary differential equations as follows:

$$\dot{S}_i^{m-k}(t) = S_i^{m+1-k}(t) - \sum_j A_{ij}^k S_j^0(t) - \sum_j B_{ij}^k V_j(t) , \quad k = 0, 1, \dots , m , \qquad (69)$$

where

$$S_i^{m+1}(t) = 0 , \qquad (70)$$

and

$$S_i^0 \cong -\sum_j \int_{-\infty}^{t} K_{ij}(t-\tau)V_j(\tau)d\tau . \qquad (71)$$

A_{ij}^k and B_{ij}^k are coefficients of state-space parameter matrices that should be estimated optimally to model the frequency-dependent added mass and damping coefficients by polynomial filter of degree m. The polynomial filter selected has the following rational form

$$\frac{\sum_{k=0}^{m}(i\omega)^k\left[B_{ij}^k\right]}{(i\omega)^{m+1}\left[I_{ij}\right]+\sum_{k=0}^{m}(i\omega)^k\left[A_{ij}^k\right]} = i\omega[a_{ij}(\omega)] - i\omega[a_{ij}(\infty)] + [b_{ij}(\omega)] - [b_{ij}(\infty)] \ , \tag{72}$$

where $i=\sqrt{-1}$ and $\left[I_{ij}\right]$ is the identity matrix. Equation (72) leads to a linear system of equations for the unknowns A_{ij}^k and B_{ij}^k. The cubic polynomial filter ($m=3$) is used to determine A_{ij}^k and B_{ij}^k because this provides a sufficient accuracy of fit. Since we consider only three motion degrees of freedom (surge, sway, yaw) in the horizontal plane and we use a cubic polynomial filter with four coefficients ($k=0, 1, 2, 3$), equation (69) results in twelve extended equations. The final expression of hydrodynamic forces and moment due to the memory effect to be substituted in the equations of motion becomes

$$(X_M, Y_M, N_M)^\mathrm{T} = F_i^M = \sum_j [a_{ij}(0) - a_{ij}(\infty)]\dot{V}_j(t) + S_i^0 \ , \quad i, j = 1, 2, 6 \ , \tag{73}$$

because the added-mass terms at zero frequency are already considered in the expressions of X_H, Y_H, and N_H in equations (16) - (18) and (19) - (21).

4.7 Dimension of the System Dynamics

The physical dimension of the system (N_s) is determined by its number of degrees of freedom. A general spread mooring system, for example, has three physical degrees of freedom - surge, sway and yaw - and thus, for a general SMS $N_s=3$. A TMS has four degrees of freedom - surge, sway, yaw and turret rotation - and thus, $N_s=4$. A SMS with n_B number of buoys has three degrees of freedom for the vessel and three degrees of freedom for each of the buoys in surge, sway and heave. In this case, $N_s=3+3n_B$. Similarly, a buoy supported TMS would have $N_s=4+3n_B$ physical degrees of freedom. Obviously, the number of physical degrees of freedom is related to the number of mathematical degrees of freedom in the state space defined in Section 6.1.

5. RICHNESS OF MOORING DYNAMICS

The dynamical behavior of specific mooring systems can be illustrated by nonlinear time simulations. In this chapter, a few simulations are performed to demonstrate numerically the richness of nonlinear dynamic behavior that mooring systems (TPM, SMS, TMS) may exhibit. In the numerical applications in this paper, the current velocity U is set equal to 2 knots, unless specified otherwise. Two vessels of widely different stability characteristics are used:

(i) A barge with stabilizing skegs, which is marginally unstable in forward motion.
(ii) A tanker without propeller, which is unstable in forward motion.

The mooring systems considered in the numerical applications in this paper have symmetric configurations with up to four mooring lines.

5.1 Notation for SMS and TMS

To facilitate the notation regarding mooring system configuration, let $FmAs$ represent a $(m+s)$-line mooring system with m lines attached forward of the CG and s lines aft. For example, F1A2 denotes a three line mooring system with one line attached forward of the CG and two lines attached aft. This notation is especially useful for symmetric mooring system configurations, and is widely used in this work. Exceptions are SPM and TPM systems, where $s=0$ and $m=1,2$ respectively. In TMS, all lines are moored around the turret, and thus it is impractical to use the notation above. The rest of the notation appearing in the Figures is explained in the Nomenclature at the end of the paper.

5.2 Solution by Simulation

SMS and TMS may exhibit the following qualitatively different dynamical behavior:

(i) Stable node behavior as shown in Figure 5 around an Alternate Equilibrium (AE).
(ii) Unstable node behavior.
(iii) Stable focus behavior as shown in Figure 5 around the Principal Equilibrium (PE).
(iv) Unstable focus behavior as shown in Figure 5 around PE.
(v) Stable limit cycle as shown in Figure 6 around PE and in Figure 7 around AE.
(vi) "Poor design" limit cycle as shown in Figure 8. We define this cycle as one caused by improper distribution of mooring lines where the moored vessel diverges from PE trying to converge to

31

either a stable limit cycle or to AE. In this case, the mooring lines alternatingly become both taut and slack, working against each other, thus preventing the vessel from achieving its natural stable limit cycle.

(vii)   Chaotic caused by a strange attractor such as the one at PE in Figure 9.

(viii) Resonance in surge due to slowly-varying drift forces as shown in Figure 10 around PE.

In Figures 5-10, all relevant information and parameter values are presented to ensure that the reader can reproduce these results. Data include the type of mooring line; mooring line length, orientation, fairlead coordinates and pretension (or initial strain) in the mooring lines; mean and slowly-varying drift forces; the mooring line configuration, mooring line model and material (AC - anchored catenary; SFR - synthetic fiber rope; BSC - buoy supported catenary), maneuvering model, external excitation, etc. In the simulations, the yaw angle (ψ) is plotted, except for Figure 8, where the mooring line tensions nondimensionalized by vessel resistance are plotted; and Figure 10, which shows displacement in surge.

In Figure 5, a F1A2 tanker SMS converges to AE in a head current without waves, while PE is unstable. When mean drift forces are added to the excitation, PE becomes stable in Figure 5. In this case, mean wave drift forces have a favorable effect on the stability of PE. The system becomes unstable again and the yaw angle fluctuates about AE when slowly-varying drift forces are added to the excitation from head seas [9]. Figure 6 shows limit cycle behavior about PE for a F1A1 barge SMS. In this Figure, slowly-varying drift forces stabilize oscillatory motions instigated by mean drift forces [9].
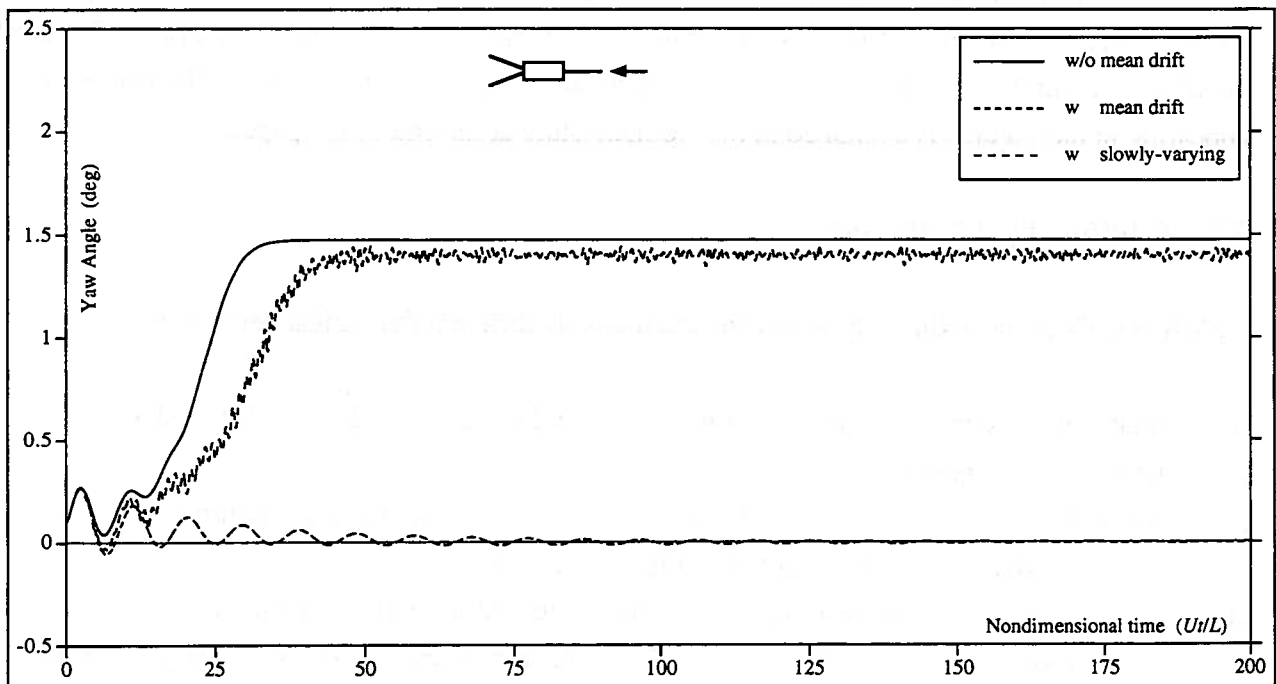
Fig. 5 Effect of slow-drift loads on F1A2 Tanker SMS: ℓ_w/L =0.15, x_p/L =0.52, y_p/B =0.5, Ω =5°, E_I =0.04, SFR, A-M

32

Fig. 6 Effect of slow-drift loads on F1A1 Barge SMS: $\ell_w/L = 0.4$, $x_p/L = 0.3$, $y_p/B = 0.0$, $E_l = 0.013$; SFR, A-M

Figure 7 shows a time simulation of a four line TMS in which the trajectories diverge from PE and converge to a stable limit cycle around AE [30]. The F2A1 tanker SMS of Figure 8 shows a "poor design" limit cycle, as indicated by alternating slack forward mooring lines [26].
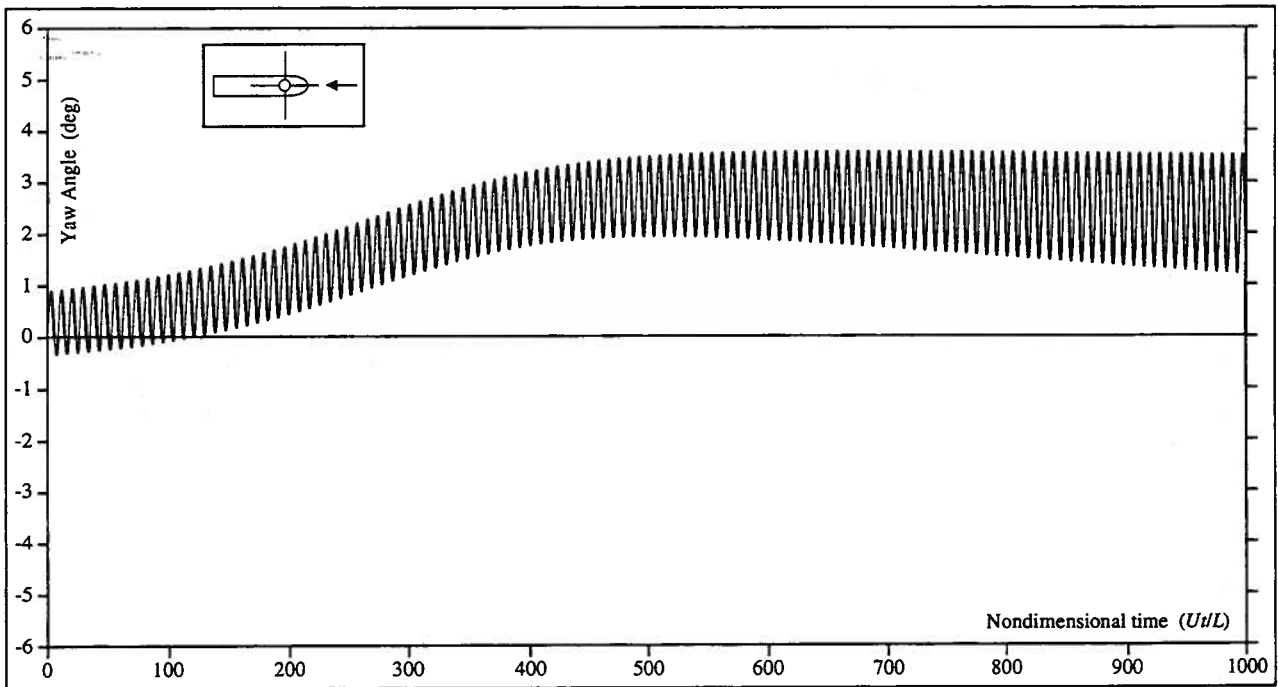
Fig. 7 Stable limit cycle about AE, 4 line TMS: $\ell_w/h = 3.5$, $D_{CG}/L = 0.355$, $h = 2000$ m, $T_P = 3071.59$ kN; AC, T-M

33
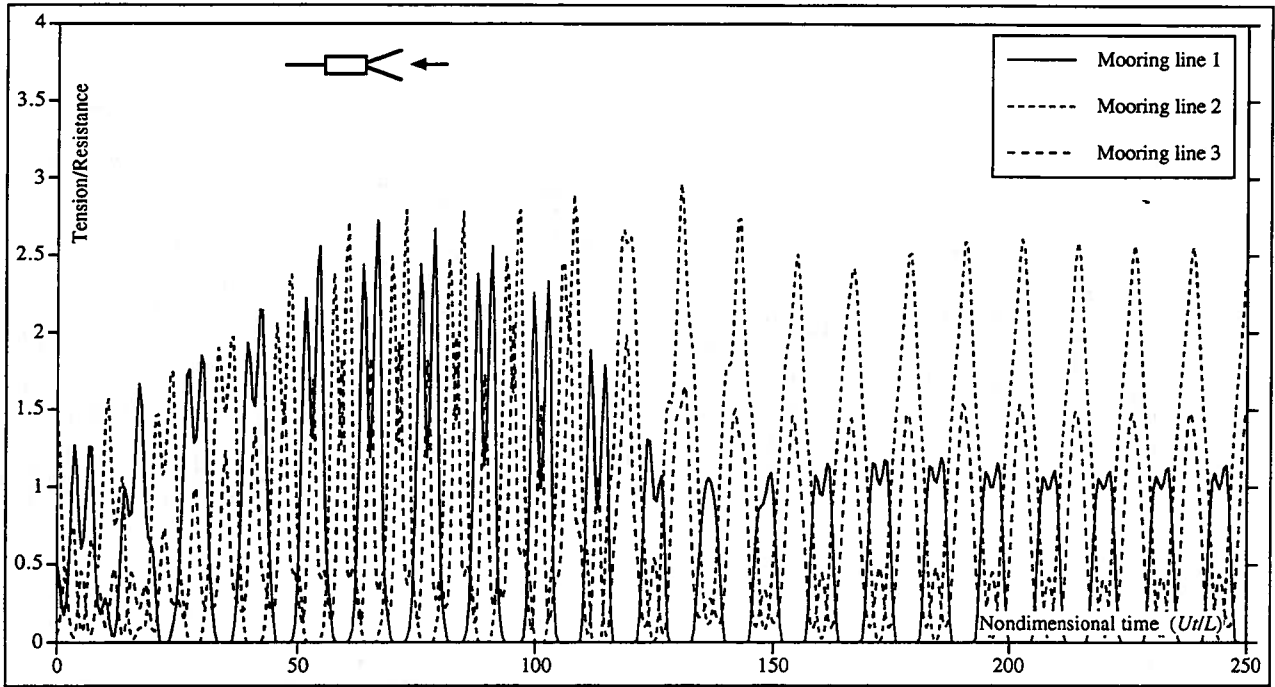
Fig. 8 Line tension, F2A1 Tanker SMS: $\ell_w/L = 1.0$, $x_p/L = 0.5$, $y_p/B = 0.0$, $\Omega = 15°$, $E_I = 0.04$, SFR, A-M

Cases of chaotic dynamics, caused by a strange attractor near an equilibrium, may result in large (but bounded) oscillations, and eventually line breakage. Figure 9 shows this type of behavior for a tanker TPM [26].
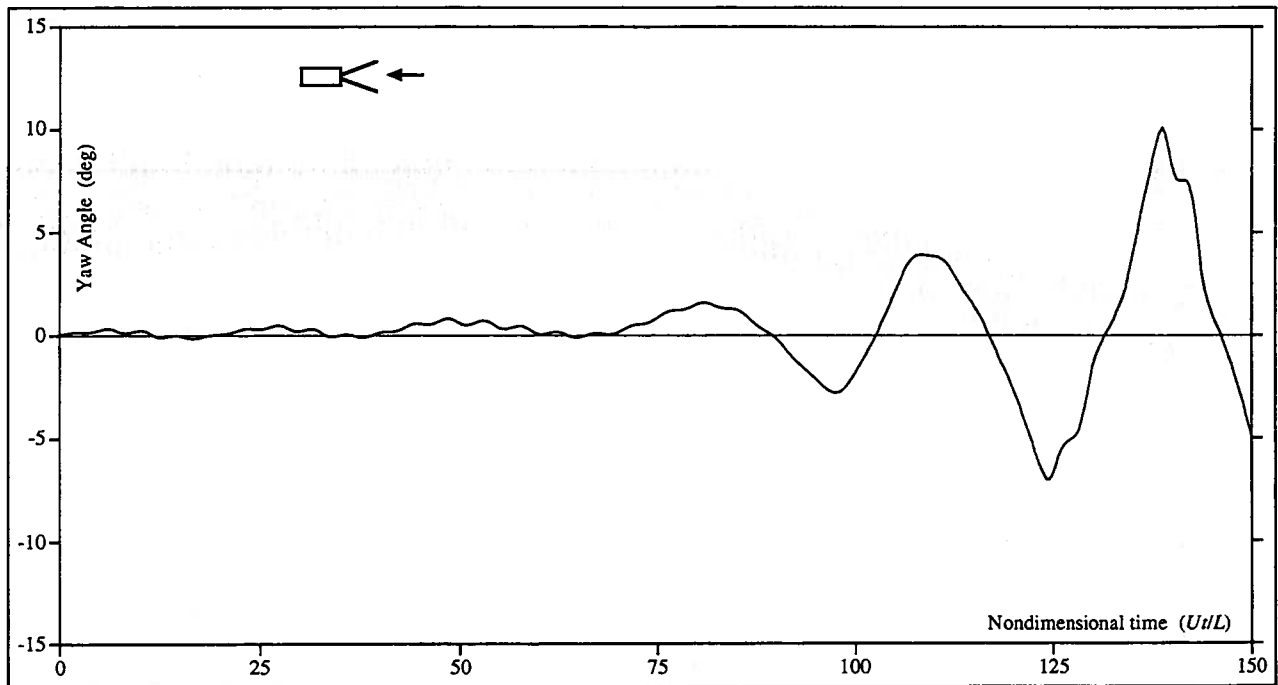
Fig. 9 Drift Angle, Tanker TPM: $\ell_w/L = 1.0$, $x_p/L = 0.45$, $y_p/B = 0.1$, $\Omega = 10°$; SFR, A-M

34

Finally, Figure 10 shows resonance motion on top of the periodic motion of Figure 6 due to loss of stability about PE of the F1A1 barge SMS in surge. Slowly-varying drift forces produce the resonant beating behavior observed in Figure 10. Such behavior is indicative of narrow band excitation near a natural frequency [9].
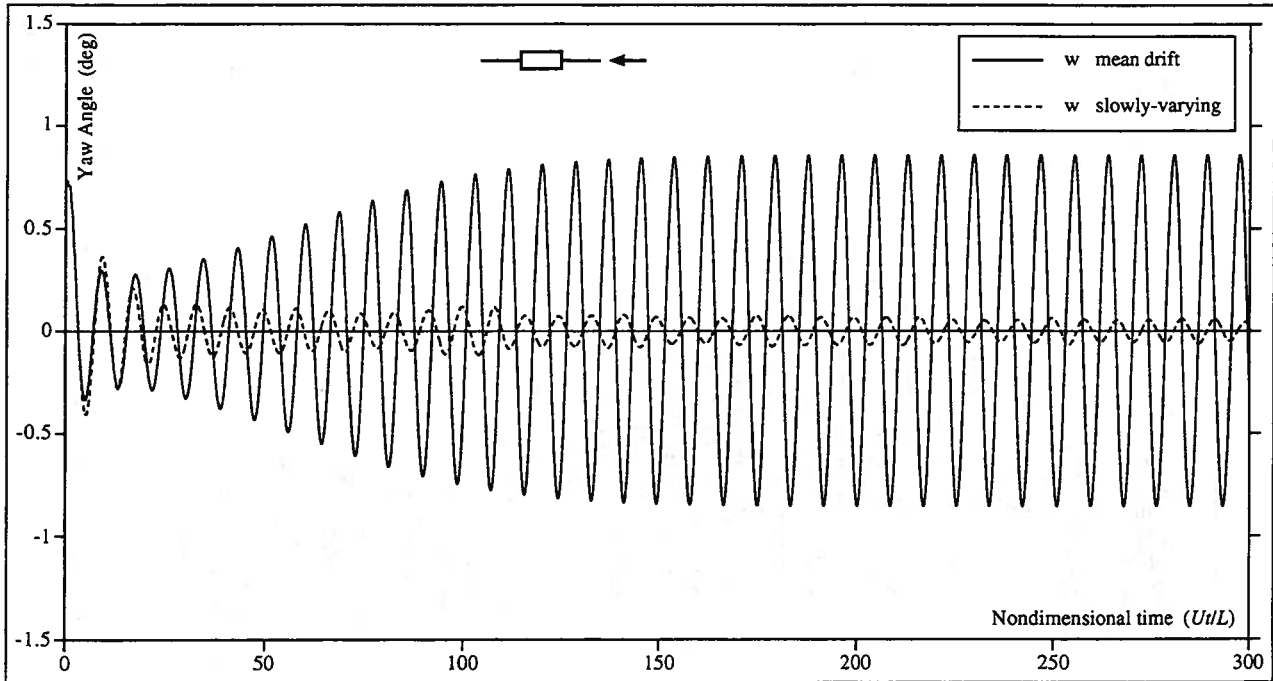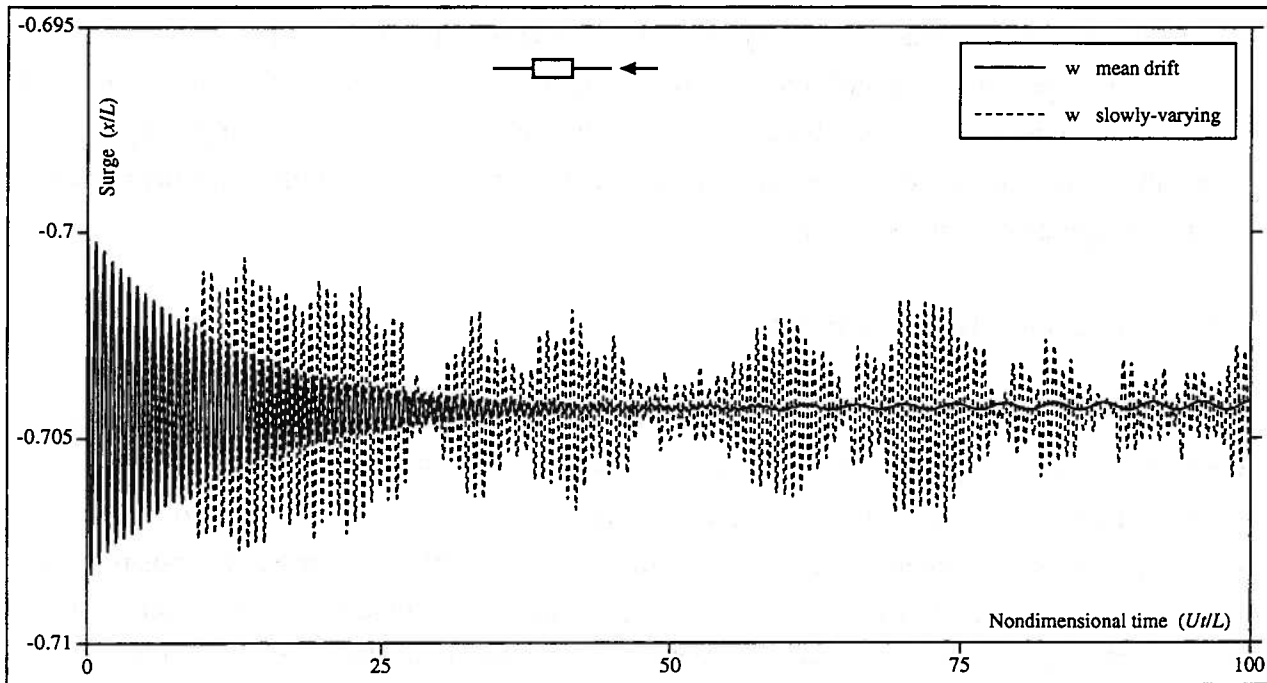

Fig. 10 Effect of slow-drift loads on F1A1 Barge SMS: ℓ_w/L =0.4, x_p/L =0.3, y_p/B =0.0, E_I =0.013; SFR, A-M

The nonlinear time simulations in Figures 5 - 10 demonstrate some of the richness of the nonlinear dynamics of mooring systems. They also show that the dynamical behavior of mooring systems varies widely with mooring line arrangement, vessel properties, external excitation, etc. Such differences in behavior are inherent stability properties exhibited by the mooring system, and are explained Chapter 6.

35

6. STABILITY AND BIFURCATIONS OF EQUILIBRIA OF NONLINEAR SYSTEMS

Equilibria of nonlinear dynamical systems and the behavior of such systems near equilibrium provide local information on dynamical flows (trajectories) [40, 60, 69]. Such information is useful in surmising the global behavior of a system in the time domain or in a phase space. Consequently, knowing all equilibria and their nature provides global information which renders time simulations unnecessary in general. Further, bifurcations of equilibria and their corresponding morphogeneses make it possible to identify areas of qualitatively acceptable dynamics. That eliminates the need for trial and error in design of mooring systems.

6.1 State Space Representation

The mathematical models presented in Chapter 4 can be recast into a set of N_{ss} first-order nonlinear coupled differential equations, where N_{ss} is the dimension of the state space. This can be achieved in several equivalent ways [5]. For general mooring, where the number of mooring lines may be unspecified, it is convenient to represent the state space variables in terms of the position and velocity vectors of the moored vessel. The SMS and TMS model presented in the previous chapters can be modeled by N_{ss} nonlinear coupled first order ordinary differential equations in the form:

$$\dot{x} = f(x), \qquad f \in C^1, \qquad f : \Re^{N_{ss}} \to \Re^{N_{ss}}, \tag{74}$$

where $\Re^{N_{ss}}$ is the N_{ss}-dimensional Euclidean space and C^1 is the class of continuously differentiable functions. In addition,

$$N_{ss} = N_{EOM} + N_{KR} + N_{ME}, \tag{75}$$

where N_{EOM} is the number of equations of motion (3 for SMS; 4 for TMS; additional $3n_B$ for supporting buoys); N_{KR} is the number of associated kinematic relations (3 for SMS; 4 for TMS; 3 per buoy); and N_{ME} is the number of extended dynamics equations due to the memory effect.

Due to the potentially high number of equations of motion and kinematics in the system, the following example is provided which corresponds to the state space representation of a SMS with memory effect and without supporting buoys. In such case, $N_{ss} = 3 + 3 + 12 = 18$, and the following state variables are selected:

$$x = [x_1 = u, \ x_2 = v, \ x_3 = r, \ x_4 = x, \ x_5 = y, \ x_6 = \psi, \ x_7 = S_1^0, \ x_8 = S_1^1, \ x_9 = S_1^2, \ x_{10} = S_1^3,$$
$$x_{11} = S_2^0, \ x_{12} = S_2^1, \ x_{13} = S_2^2, \ x_{14} = S_2^3, \ x_{15} = S_6^0, \ x_{16} = S_6^1, \ x_{17} = S_6^2, \ x_{18} = S_6^3]^T . \tag{76}$$

The subscripts and super subscripts in the extended state variables x_7 - x_{18} represent modes of horizontal motions (surge, sway and yaw) and the order of extended variables, respectively. In Cauchy standard form, the nonlinear system in the state space defined by (76) is written as:

$$\dot{x}_1 = \frac{X_H + mx_2x_3 + X_R + F_{surge} + x_7}{m + m_{11} - a_{11}^*} + \frac{\sum_{i=1}^{n}\left\{\left[T_H^{(i)} - F_P^{(i)}\right]\cos\beta^{(i)} + F_N^{(i)}\sin\beta^{(i)}\right\}}{m + m_{11} - a_{11}^*} , \tag{77}$$

$$\dot{x}_2 = \frac{(I_{zz} + I_{66} - a_{66}^*)}{M}\left\{Y_H - mx_1x_3 + Y_R + F_{sway} + x_{11}\right\} + \frac{(I_{zz} + I_{66} - a_{66}^*)}{M}\left\{\sum_{i=1}^{n}\left[T_H^{(i)} - F_P^{(i)}\right]\sin\beta^{(i)}\right\}$$

$$- \frac{(I_{zz} + I_{66} - a_{66}^*)}{M}\left\{\sum_{i=1}^{n}F_N^{(i)}\cos\beta^{(i)}\right\} - \frac{(m_{26} - a_{26}^*)}{M}\left\{N_H + N_R + N_{yaw} + x_{15}\right\}$$

$$- \frac{(m_{26} - a_{26}^*)}{M}\left\{\sum_{i=1}^{n}x_P^{(i)}\left[T_H^{(i)} - F_P^{(i)}\right]\sin\beta^{(i)}\right\} + \frac{(m_{26} - a_{26}^*)}{M}\left\{\sum_{i=1}^{n}x_P^{(i)}F_N^{(i)}\cos\beta^{(i)}\right\}$$

$$+ \frac{(m_{26} - a_{26}^*)}{M}\left\{\sum_{i=1}^{n}y_P^{(i)}\left[T_H^{(i)} - F_P^{(i)}\right]\cos\beta^{(i)}\right\} + \frac{(m_{26} - a_{26}^*)}{M}\left\{\sum_{i=1}^{n}y_P^{(i)}F_N^{(i)}\sin\beta^{(i)}\right\} , \tag{78}$$

$$\dot{x}_3 = -\frac{(m_{62} - a_{62}^*)}{M}\left\{Y_H - mx_1x_3 + Y_R + F_{sway} + x_{11}\right\} - \frac{(m_{62} - a_{62}^*)}{M}\left\{\sum_{i=1}^{n}\left[T_H^{(i)} - F_P^{(i)}\right]\sin\beta^{(i)}\right\}$$

$$+ \frac{(m_{62} - a_{62}^*)}{M}\left\{\sum_{i=1}^{n}F_N^{(i)}\cos\beta^{(i)}\right\} + \frac{(m + m_{22} - a_{22}^*)}{M}\left\{N_H + N_R + N_{yaw} + x_{15}\right\}$$

$$+ \frac{(m + m_{22} - a_{22}^*)}{M}\left\{\sum_{i=1}^{n}x_P^{(i)}\left[T_H^{(i)} - F_P^{(i)}\right]\sin\beta^{(i)}\right\} - \frac{(m + m_{22} - a_{22}^*)}{M}\left\{\sum_{i=1}^{n}x_P^{(i)}F_N^{(i)}\cos\beta^{(i)}\right\}$$

$$- \frac{(m + m_{22} - a_{22}^*)}{M}\left\{\sum_{i=1}^{n}y_P^{(i)}\left[T_H^{(i)} - F_P^{(i)}\right]\cos\beta^{(i)}\right\} - \frac{(m + m_{22} - a_{22}^*)}{M}\left\{\sum_{i=1}^{n}y_P^{(i)}F_N^{(i)}\sin\beta^{(i)}\right\} , \tag{79}$$

$$\dot{x}_4 = x_1\cos x_6 - x_2\sin x_6 + U\cos\alpha , \tag{80}$$

$$\dot{x}_5 = x_1\sin x_6 + x_2\cos x_6 + U\sin\alpha , \tag{81}$$

$$\dot{x}_6 = x_3 , \tag{82}$$

$$\dot{x}_7 = x_8 - A_{11}^3 x_7 - B_{11}^3 x_1 , \tag{83}$$

$$\dot{x}_8 = x_9 - A_{11}^2 x_7 - B_{11}^2 x_1 , \tag{84}$$

$$\dot{x}_9 = x_{10} - A_{11}^1 x_7 - B_{11}^1 x_1 , \tag{85}$$

$$\dot{x}_{10} = -A_{11}^0 x_7 - B_{11}^0 x_1 \ , \tag{86}$$

$$\dot{x}_{11} = x_{12} - A_{22}^3 x_{11} - A_{26}^3 x_{15} - B_{22}^3 x_2 - B_{26}^3 x_3 \ , \tag{87}$$

$$\dot{x}_{12} = x_{13} - A_{22}^2 x_{11} - A_{26}^2 x_{15} - B_{22}^2 x_2 - B_{26}^2 x_3 \ , \tag{88}$$

$$\dot{x}_{13} = x_{14} - A_{22}^1 x_{11} - A_{26}^1 x_{15} - B_{22}^1 x_2 - B_{26}^1 x_3 \ , \tag{89}$$

$$\dot{x}_{14} = -A_{22}^0 x_{11} - A_{26}^0 x_{15} - B_{22}^0 x_2 - B_{26}^0 x_3 \ , \tag{90}$$

$$\dot{x}_{15} = x_{16} - A_{62}^3 x_{11} - A_{66}^3 x_{15} - B_{62}^3 x_2 - B_{66}^3 x_3 \ , \tag{91}$$

$$\dot{x}_{16} = x_{17} - A_{62}^2 x_{11} - A_{66}^2 x_{15} - B_{62}^2 x_2 - B_{66}^2 x_3 \ , \tag{92}$$

$$\dot{x}_{17} = x_{18} - A_{62}^1 x_{11} - A_{66}^1 x_{15} - B_{62}^1 x_2 - B_{66}^1 x_3 \ , \tag{93}$$

$$\dot{x}_{18} = -A_{62}^0 x_{11} - A_{66}^0 x_{15} - B_{62}^0 x_2 - B_{66}^0 x_3 \ , \tag{94}$$

where

$M = (I_{zz} + I_{66} - a_{66}^*)(m + m_{22} - a_{22}^*) - (m_{62} - a_{62}^*)(m_{22} - a_{26}^*)$, and $a_{ij}^* = a_{ij}(0) - a_{ij}(\infty)$. It should be noted that the number of extended equations depends on the degree of the polynomial filter to approximate the frequency dependent added mass and damping coefficients; e.g. twelve for cubic filter, nine for quadratic filter, six for linear filter. In deriving the cross-coupling coefficients A_{12}^k, A_{21}^k, A_{16}^k, A_{61}^k, B_{12}^k, B_{21}^k, B_{16}^k, and B_{61}^k ($k = 0, 1, 2, 3$) are assumed to be zero due to port/starboard symmetry of the vessel. In equations (77) - (79), T_H, X_R, Y_R, N_R and β depend explicitly on the position vector x_4 - x_6; F_P and F_N, are functions of x_1 - x_6; and the external excitation terms (wind and second order mean drift) X_W, Y_W, N_W, X_{WV}, Y_{WV}, and N_{WV} are explicit functions of x_6.

Since the vector field f in evolution equation (74) does not depend explicitly on time, the system is *autonomous*. Inclusion of slowly-varying wave drift forces would render the system *nonautonomous*.

6.2 Equilibria of Mooring Systems

Equilibria of the nonlinear SMS and TMS models are stationary flows of the vector field (74), and can be computed as intersections of null clines [60]. Accordingly, all equilibria (singular flows or stationary solutions) can be found by setting the time derivative of the state variable vector equal to zero, i.e.

$$\bar{x} \in \Re^{N_{ss}} \quad \text{is an equilibrium of} \quad \dot{x} = f(x) \quad \Leftrightarrow \quad f(\bar{x}) \equiv 0 \ , \tag{95}$$

where the overbar on the state variable vector x represents the equilibrium state. The solution to the nonlinear component equations in (95) produces the system equilibria. TMS may possess one or three equilibria, depending on the location of the mooring lines. The number of equilibria that exist in SMS

strongly depends on the number and tension of the mooring lines, the system configuration, and the environmental conditions. For mooring systems with buoy supported chains, the number of possible equilibria may be even higher due to the high number of degrees of freedom in the system. This is an important design issue since a small variation in line arrangement may allow a mooring system to reach a different equilibrium. SMS with relatively small pretension in the mooring lines, for example, may inherently have several equilibria, since the vessel is not overly restrained from moving. In such cases, one or several mooring lines may become slack, and thus an initial mooring line configuration may be transformed into a different one after equilibrium is achieved. Highly pretensioned systems, on the other hand, are configured to restrain the vessel from moving, thus limiting the number of equilibria that can be attained. As mentioned previously, the Principal Equilibrium of the system is denoted by PE. Other equilibria that may exist are denoted as Alternate Equilibria (AE).

6.3 Asymptotic Stability of Equilibria

To determine the stability of a nonlinear system near an equilibrium point, we linearize the vector field with respect to that point. The local behavior of the nonlinear system in the vicinity of the equilibrium point can be predicted by studying the following linear state equation [40, 69]

$$\dot{\xi} = [A]\xi , \qquad \xi \in \mathfrak{R}^{n_{ss}} , \qquad [A] \in \mathfrak{R}^{N_{ss} \times N_{ss}} , \tag{96}$$

where $\xi(t) = x(t) - \bar{x}$ is the deviation from equilibrium, and $[A]$ is the Jacobian matrix of f evaluated at that equilibrium condition. If all eigenvalues of $[A]$, λ_i, have nonzero real parts (usually called hyperbolic or nondegenerate), the trajectories of the nonlinear system in a small neighborhood of an equilibrium point are close to the trajectories of its linearization at that point. Equilibrium position $\bar{x}$ is asymptotically stable if $\text{Re}[\lambda_i] < 0$ for all λ_i. Then, all sufficiently small perturbations vanish as time increases, and nearby trajectories approach $\bar{x}$. If there exists at least one eigenvalue such that $\text{Re}[\lambda_i] > 0$, then $\bar{x}$ is unstable, and all trajectories initiated near such an equilibrium will deviate exponentially from it in forward time [69]. Depending on the nature of the positive real parts of the eigenvalues, an equilibrium position may be an unstable node, an unstable focus, a stable limit cycle, or chaotic in nature, as described later. Eigenvalue analysis at each equilibrium position yields the characteristic global behavior of the system.

Local stability analysis must be performed near each and every equilibrium position of a particular system configuration to determine its global behavior.

6.4 Bifurcations of Equilibria and Associated Morphogeneses

As pointed out in the previous section, the stability properties of the system equilibria persist under small perturbations of the vector field. Large variations in parameters, however, may result in a significant change of the system behavior, which is called a bifurcation. A bifurcation is a qualitative change in a limit set of the system as a parameter is infinitesimally perturbed. Appearance/disappearance of a limit set or change in the stability type of a limit set is a bifurcation. A bifurcation also occurs when an unstable limit set remains unstable but undergoes a change in the unstable manifold dimension. Saddle-node, pitchfork, and Hopf bifurcations are the typical types of bifurcation found in the nonlinear dynamics of mooring systems [59].

The dynamic behavior of a mooring system changes significantly with variation of system parameters, such as the number, length, material and orientation of the mooring lines; fairlead position; location of turret; location of risers; etc. Systematic variation of all system parameters is prohibitively time consuming and graphical representation of bifurcations and catastrophe sets in a multidimensional design space is too complex. Thus, in this paper, we limit numerical applications to symmetric mooring systems. Systematic variation of design variables allows us to determine pitchfork, saddle node (turning point), simple stationary, and Hopf bifurcations; as well as fold and cusp singularities of bifurcations. These results reveal the morphogeneses of dynamical phenomena and show the richness of SMS dynamics. It may be possible, however, to identify other bifurcations like hysteresis points or isola centers; and other singularities in the stability charts like swallowtail and butterfly [60] due to codimension higher than one. In this section, bifurcation sequences are studied to find qualitative changes in the dynamic behavior of mooring systems by varying design parameters for specific mooring configurations. The study of the bifurcation phenomena is absolutely necessary for the complete understanding of the system dynamics and ultimately for determining the appropriate ranges of design parameters for safe operations. In order to perform bifurcation analysis, evolution equations (74) are written as

$$\dot{x} = f(x,\mu) , \qquad x \in \Re^{N_{ss}} , \qquad \mu \in \Re^{N_P} , \tag{97}$$

where μ is the design parameter vector and N_P is the number of parameters in the system. In bifurcation analysis, parameters vary slowly (quasi-statically); that is $(d\mu/dt)$ is small. When a bifurcation occurs due to a parameter change, the Jacobian at equilibrium becomes singular and the system degenerates. In bifurcation analysis, not only is this degeneracy identified, but the system metamorphosis and the associated morphogeneses are described as well. The behavior of the solutions

to the dynamical system described by equation (97) in the N_P-dimensional space is illustrated graphically by stability or design charts.

Mooring systems exhibit both static as well as dynamic loss of stability. The former occurs when there is a change in the structure of the set of zeroes of equation (97) as parameters change. Pitchfork, saddle node, and simple stationary bifurcations are of static nature [40]. In mooring system dynamics, this is due to the action of external excitation which maintains a constant magnitude and heading. Dynamic loss of stability occurs when there is a change in the structure of the limit sets of solutions of the vector field as parameters are varied. A Hopf bifurcation is of dynamic nature. In mooring systems, oscillations may occur due to Hopf bifurcations. Dynamic loss of stability in mooring systems is analogous to beam buckling under a compressive follower force which gives rise to the phenomenon of fluttering. The mooring line restoring forces and moment, and the hydrodynamic pressure applied to the hull as the vessel is moving, are follower forces. The set of all bifurcation boundaries is called a *catastrophe set*. When those sets are produced, theoretical conclusions can be drawn regarding the system dynamics, permitting direct selection of values of parameters. Those lines constitute the boundaries between regions of qualitatively different dynamics. Elementary catastrophes, which correspond to the bifurcations presented above, play an important role in the analysis of nonlinear dynamics. Depending on the mooring line configuration, a mooring system may exhibit a fold singularity (projection of the boundary of a simply connected domain onto a plane), or a cusp singularity (occurring at the intersection of stationary and Hopf bifurcation stability boundaries or two Hopf bifurcations). A detailed mathematical presentation of these concepts is provided in [59]. A catastrophe set is thus the set of all loci of bifurcations in a parametric design space. These loci are the boundaries between regions of qualitatively different dynamics and reveal the morphogeneses occurring as boundaries are crossed. Therefore, the catastrophe set can provide qualitative conclusions regarding the system dynamics in the initial design stage of mooring systems, thus enabling the designer to select appropriate parameters for design.

The catastrophe sets presented in Chapters 8 - 10 pertain to PE, unless otherwise specified (bifurcation sequences around other equilibria are out of the scope of this paper), and possess five regions of qualitatively different dynamics. These regions, numbered I to V and denoted as R-I to R-V, are defined below. For mnemonic purposes, the number of a region minus one is equal to the dimension of the unstable manifold.

Region I (R-I): PE is stable. All trajectories starting near PE equilibrium converge toward it in forward time. Since there are no other equilibria that may attract or repel the trajectories, the system eventually

converges to PE irrespectively of the initial conditions of the system, resulting in a stable principal equilibrium.

Region II (R-II): PE is unstable with a one-dimensional unstable manifold. Static loss of stability of PE occurs when crossing from R-I to R-II, with the development of a pitchfork bifurcation and the appearance of two statically stable equilibria. Trajectories diverge from PE and are attracted to one of such alternate equilibria (AE), if present or attainable, depending on the initial conditions. Such equilibria, while statically stable, may be dynamically stable or unstable, resulting in trajectories converging to either equilibrium or to a limit cycle around it, respectively.

Region III (R-III): PE is unstable with a two-dimensional unstable manifold. Dynamic loss of stability, also called Hopf bifurcation - occurs when crossing from R-I to R-III, with the development of a limit cycle around PE. In this region, the system oscillates around PE, unless other equilibria that may attract the trajectories exist. The frequency and amplitude of oscillations vary with system parameters and can be found by numerical simulations or approximated using the Center Manifold Theorem [40].

Region IV (R-IV): PE is unstable with a three-dimensional unstable manifold. In this region, PE is statically and dynamically unstable; i.e. the system has undergone both static and dynamic loss of stability by crossing both bifurcation boundaries. This region is characterized by the merging of unstable R-II and R-III, and the unstable manifold has the minimum dimension for the onset of chaos [60]. Simulations show, however, that occasionally the system initiates in chaos but trajectories are quickly attracted by AE. That AE is a result of either the static bifurcation occurring when crossing from R-III to R-IV or from other equilibria present in the system.

Region V (R-V): PE is unstable with a four-dimensional unstable manifold. Ann application with region R-V corresponds to dynamic loss of stability of the two forward buoys which support chains in deep water SMS dynamics (see Figure 30). In this case, the system is chaotic about PE. Another case was shown in [59] where the tanker motions in a SPM system becomes chaotic.

6.5 Physics-Based Expressions for Bifurcation Boundaries, and Morphogeneses

A breakthrough in the development of the UM methodology was achieved in 1995-1996 when physics-based analytical expressions were derived for the bifurcation boundaries of equilibria [6, 27-29]. Up to that time, presentations of design graphs (catastrophe sets) were limited to three dimensions - two dimensions and a parameter. Following the derivation of those physics-based expressions, it has

become possible to eliminate trial and error with respect to any design variable in addition to virtually eliminating the need for simulations.

The design methodology of mooring systems developed at the University of Michigan is based on the stability coefficients presented in this section. This methodology consists on deriving analytical expressions for the bifurcation boundaries and the associated morphogeneses of mooring systems, and applying them to design based on their slow motion dynamics. These expressions have been derived in [27] for symmetric SMS, in [28, 29] for general SMS, and in [33] for TMS.

6.5.a Analytical Expressions of Stability Criteria and Bifurcation Sequences

Due to the complexity of such expressions, only a brief example of a SMS moored via synthetic ropes, without riser, memory effect, supporting buoys, mooring line drag, and excitation due to wind and waves is shown to illustrate the derivation of analytical expressions for the stability criteria of the system and its bifurcation sequences. In brief, the equations of motion, kinematics of the system and all expressions relating mooring lines, external excitation, etc. are perturbed about an equilibrium position and only linear terms retained. After perturbation of the system, the equations of motion (surge, sway, yaw) in this example can be recast as:

$$(m + m_{11})\cos\overline{\psi}\Delta\ddot{x} + \left(\frac{\overline{\partial X_H}}{\partial v}\sin\overline{\psi} - \frac{\overline{\partial X_H}}{\partial u}\cos\overline{\psi}\right)\Delta\dot{x} + E_{1x}\Delta x + (m + m_{11})\sin\overline{\psi}\Delta\ddot{y}$$

$$- \left(\frac{\overline{\partial X_H}}{\partial u}\sin\overline{\psi} + \frac{\overline{\partial X_H}}{\partial v}\cos\overline{\psi}\right)\Delta\dot{y} + E_{1y}\Delta y + \left(m_{11}\overline{v} - \frac{\overline{\partial X_H}}{\partial r}\right)\Delta\dot{\psi} + E_{1\psi}\Delta\psi = 0 \ , \tag{98}$$

$$- (m + m_{22})\sin\overline{\psi}\Delta\ddot{x} + \left(\frac{\overline{\partial Y_H}}{\partial v}\sin\overline{\psi} - \frac{\overline{\partial Y_H}}{\partial u}\cos\overline{\psi}\right)\Delta\dot{x} + E_{2x}\Delta x + (m + m_{22})\cos\overline{\psi}\Delta\ddot{y}$$

$$- \left(\frac{\overline{\partial Y_H}}{\partial u}\sin\overline{\psi} + \frac{\overline{\partial Y_H}}{\partial v}\cos\overline{\psi}\right)\Delta\dot{y} + E_{2y}\Delta y + m_{26}\Delta\ddot{\psi} + \left(m_{22}\overline{u} + \frac{\overline{\partial Y_H}}{\partial r}\right)\Delta\dot{\psi} + E_{2\psi}\Delta\psi = 0 \ , \tag{99}$$

$$- m_{62}\sin\overline{\psi}\Delta\ddot{x} + \left(\frac{\overline{\partial N_H}}{\partial v}\sin\overline{\psi} - \frac{\overline{\partial N_H}}{\partial u}\cos\overline{\psi}\right)\Delta\dot{x} + E_{3x}\Delta x + m_{62}\cos\overline{\psi}\Delta\ddot{y}$$

$$- \left(\frac{\overline{\partial N_H}}{\partial u}\sin\overline{\psi} + \frac{\overline{\partial N_H}}{\partial v}\cos\overline{\psi}\right)\Delta\dot{y} + E_{3y}\Delta y + (I_z + m_{66})\Delta\ddot{\psi} - \left(m_{62}\overline{u} + \frac{\overline{\partial N_H}}{\partial r}\right)\Delta\dot{\psi} + E_{3\psi}\Delta\psi = 0 \ . \tag{100}$$

Expressions for the "E" terms in equations (98) - (100) involve coupling terms between stiffness (mooring line tension) and damping (velocity dependent first order derivatives of the hydrodynamic forces and moment) terms. These are derived in [29]. In general, equations (98) - (100) are coupled. The surge equation of motion (98) decouples from sway and yaw equations (99) and (100) for

43

symmetric systems, i.e., SMS which preserve geometric symmetry under symmetric excitation after an equilibrium position has been achieved [27, 28]. By introducing the differential operator $D = d/dt$, these equations can be written in the form:

$$(a_{11}D^2 + a_{12}D + a_{13})\Delta x + (a_{21}D^2 + a_{22}D + a_{23})\Delta y + (a_{31}D^2 + a_{32}D + a_{33})\Delta \psi = 0 , \tag{101}$$

$$(b_{11}D^2 + b_{12}D + b_{13})\Delta x + (b_{21}D^2 + b_{22}D + b_{23})\Delta y + (b_{31}D^2 + b_{32}D + b_{33})\Delta \psi = 0 , \tag{102}$$

$$(c_{11}D^2 + c_{12}D + c_{13})\Delta x + (c_{21}D^2 + c_{22}D + c_{23})\Delta y + (c_{31}D^2 + c_{32}D + c_{33})\Delta \psi = 0 . \tag{103}$$

For mooring lines with no drag, term a_{31} would be zero. The characteristic equation for Δx, Δy, or $\Delta \psi$ derived from equations (101) - (103) is:

$$A\sigma^6 + B\sigma^5 + C\sigma^4 + D\sigma^3 + E\sigma^2 + F\sigma^1 + G = 0 , \tag{104}$$

where coefficients A - G are the Routh-Hurwitz coefficients and were derived in [29]. These are related to the system eigenvalues ($\sigma_i = \lambda_i$, $i = 1, 2, ..., 6$) as follows:

$$B/A = -(\sigma_1 + \sigma_2 + \sigma_3 + \sigma_4 + \sigma_5 + \sigma_6) , \tag{105}$$

$$\begin{aligned} C/A = (&\sigma_1\sigma_2 + \sigma_1\sigma_3 + \sigma_1\sigma_4 + \sigma_1\sigma_5 + \sigma_1\sigma_6 + \sigma_2\sigma_3 + \sigma_2\sigma_4 + \sigma_2\sigma_5 + \sigma_2\sigma_6 + \sigma_3\sigma_4 + \sigma_3\sigma_5 \\ &+ \sigma_3\sigma_6 + \sigma_4\sigma_5 + \sigma_4\sigma_6 + \sigma_5\sigma_6) , \end{aligned} \tag{106}$$

$$\begin{aligned} D/A = -(&\sigma_1\sigma_2\sigma_3 + \sigma_1\sigma_2\sigma_4 + \sigma_1\sigma_2\sigma_5 + \sigma_1\sigma_2\sigma_6 + \sigma_1\sigma_3\sigma_4 + \sigma_1\sigma_3\sigma_5 + \sigma_1\sigma_3\sigma_6 + \sigma_1\sigma_4\sigma_5 \\ &+ \sigma_1\sigma_4\sigma_6 + \sigma_1\sigma_5\sigma_6 + \sigma_2\sigma_3\sigma_4 + \sigma_2\sigma_3\sigma_5 + \sigma_2\sigma_3\sigma_6 + \sigma_2\sigma_4\sigma_5 + \sigma_2\sigma_4\sigma_6 + \sigma_2\sigma_5\sigma_6 \\ &+ \sigma_3\sigma_4\sigma_5 + \sigma_3\sigma_4\sigma_6 + \sigma_3\sigma_5\sigma_6 + \sigma_4\sigma_5\sigma_6) , \end{aligned} \tag{107}$$

$$\begin{aligned} E/A = (&\sigma_1\sigma_2\sigma_3\sigma_4 + \sigma_1\sigma_2\sigma_3\sigma_5 + \sigma_1\sigma_2\sigma_3\sigma_6 + \sigma_1\sigma_2\sigma_4\sigma_5 + \sigma_1\sigma_2\sigma_4\sigma_6 + \sigma_1\sigma_2\sigma_5\sigma_6 \\ &+ \sigma_1\sigma_3\sigma_4\sigma_5 + \sigma_1\sigma_3\sigma_4\sigma_6 + \sigma_1\sigma_3\sigma_5\sigma_6 + \sigma_1\sigma_4\sigma_5\sigma_6 + \sigma_2\sigma_3\sigma_4\sigma_5 + \sigma_2\sigma_3\sigma_4\sigma_6 \\ &+ \sigma_2\sigma_3\sigma_5\sigma_6 + \sigma_2\sigma_4\sigma_5\sigma_6 + \sigma_3\sigma_4\sigma_5\sigma_6) , \end{aligned} \tag{108}$$

$$\begin{aligned} F/A = -(&\sigma_1\sigma_2\sigma_3\sigma_4\sigma_5 + \sigma_1\sigma_2\sigma_3\sigma_4\sigma_6 + \sigma_1\sigma_2\sigma_3\sigma_5\sigma_6 + \sigma_1\sigma_2\sigma_4\sigma_5\sigma_6 \\ &+ \sigma_1\sigma_3\sigma_4\sigma_5\sigma_6 + \sigma_2\sigma_3\sigma_4\sigma_5\sigma_6) , \end{aligned} \tag{109}$$

$$G/A = \sigma_1\sigma_2\sigma_3\sigma_4\sigma_5\sigma_6 . \tag{110}$$

As noted in the previous section, the stability of an equilibrium position in the system depends on the values of the real part of the eigenvalues. If all the eigenvalues have negative real parts, the system is stable around that equilibrium position. For the SMS example, the necessary and sufficient conditions for stability are the following six [29]:

$$C_{R1} = \frac{B}{A} > 0 , \tag{111}$$

$$C_{R2} = \frac{BC - AD}{AB} > 0 \ , \tag{112}$$

$$C_{R3} = \frac{D}{A} + \frac{B}{A}\frac{(AF - BE)}{(BC - AD)} > 0 \ , \tag{113}$$

$$C_{R4} = \frac{E}{A} + \frac{(BG - CF)(BC - AD) - AF(AF - BE)}{A[D(BC - AD) + B(AF - BE)]} > 0 \ , \tag{114}$$

$$C_{R5} = \frac{F}{A} + \frac{G}{A}\left[\frac{(BC - AD)(D^2 - BF)}{(BC - AD)(CF - DE - BG) + (AF - BE)^2}\right]$$

$$+ \frac{G}{A}\left[\frac{BD(AF - BE) + B^3 G}{(BC - AD)(CF - DE - BG) + (AF - BE)^2}\right] > 0 \ , \tag{115}$$

$$C_{R6} = \frac{G}{A} > 0 \ . \tag{116}$$

The number of positive real parts in the eigenvalues corresponds to the number of sign changes in the above stability criteria [28]. The first stability criterion (111) is always satisfied [29], indicating that the maximum number eigenvalues with positive real parts for the sample mooring system can be at most five. Thus, the maximum dimension of the unstable manifold cannot be higher than five in this case.

6.5.b Analytical Expressions of Bifurcation Boundaries

Numerically, the types of bifurcation present in a system are determined by studying its eigenvalues and their change as parameters are varied. In this section, it is shown that for general mooring systems the boundaries that correspond to loss of stability in the system may be obtained in closed form analytical expressions without the need of numerically obtaining the eigenvalues and performing bifurcation search. The analytical expressions (111) - (116) shown in the previous subsection can serve to identify boundaries where loss of stability occur. Such bifurcation boundaries denote regions where the system exhibit singular dynamics in the parametric space.

(i) Static loss of stability: Static loss of stability arises when a real eigenvalue crosses from the negative to the positive real axis as a single parameter is varied [40]. We have shown in [28] that the Boundary for Static Loss (BSL) is

$$BSL = C_{R6} = C_{RS} = \frac{G}{A} = 0 \ . \tag{117}$$

The term G/A is the product of the six eigenvalues of the system, as shown in equation (110). As one real eigenvalue crosses the real axis from negative to positive or vice versa as a parameter is varied,

45

equation (117) becomes active, thus establishing the boundary where static loss of stability occurs. The bifurcation boundary generated by making BSL active (i.e. setting C_{R6} equal to zero), provides the necessary and sufficient conditions for static loss of stability.

(ii) <u>Dynamic loss of stability</u>: Dynamic loss of stability corresponds to Hopf bifurcation, where a pair of complex eigenvalues crosses from the negative to the positive real axis with nonzero speed [40]. We have shown in [28] that the Boundary of Dynamic Loss (BDL) of stability in the system can be determined by multiplying the remaining stability criteria, and setting this new expression equal to zero [28].

$$C_{RC} = C_{R1}C_{R2}C_{R3}C_{R4}C_{R5} \ . \tag{118}$$

This resulting expression can be recast as:

$$\text{BDL} = C_{RC} = 0 \ , \tag{119}$$

where C_{RC} is given in terms of the system eigenvalues in our example as:

$$
\begin{aligned}
C_{RC} = -[&(\sigma_1 + \sigma_2)(\sigma_1 + \sigma_3)(\sigma_1 + \sigma_4)(\sigma_1 + \sigma_5)\,(\sigma_1 + \sigma_6)(\sigma_2 + \sigma_3)(\sigma_2 + \sigma_4)(\sigma_2 + \sigma_5) \\
&(\sigma_2 + \sigma_6)(\sigma_3 + \sigma_4)(\sigma_3 + \sigma_5)(\sigma_3 + \sigma_6)\,(\sigma_4 + \sigma_5)(\sigma_4 + \sigma_6)(\sigma_5 + \sigma_6)] \ .
\end{aligned}
\tag{120}
$$

The equivalent analytical expression of (46) in terms of the Routh-Hurwitz coefficients is given by [29]

$$C_{RC} = \frac{(BC - AD)(DEF + 2BFG - D^2G - CF^2)}{A^5} - \frac{F(BE - AF)^2 + BG(ADF + B^2G - BDE)}{A^5} \ . \tag{121}$$

Expression (120) consists of the product of fifteen terms, each containing the sum of two roots, or eigenvalues, of the sixth order system. When the system loses its stability dynamically, the real part of a complex conjugate pair of eigenvalues becomes zero. Expression (120) vanishes when one or more complex pairs of eigenvalues cross the real axis from negative to positive, thus establishing a boundary when dynamic loss of stability occurs. Such a boundary is therefore obtained by setting C_{RC} to zero.

The boundary determined by equation (119) is necessary for determining the dynamic loss of stability of the system with respect to any equilibrium position. Setting C_{RC} to zero, however, does not necessarily imply that the system has undergone dynamic loss of stability. A pair of real eigenvalues with the same magnitude and opposite signs, or two or more real zero eigenvalues, for example, will

also satisfy (119). Thus, the bifurcation boundary generated by setting C_{RC} equal to zero yields a necessary and sufficient condition for dynamic loss of stability of the TMS, provided that the exceptions noted above do not occur. If, however, these are to occur, the stability criteria (111) - (116) and relations (105) - (110) can be used to establish whether or not the system has lost its stability dynamically.

Cases where two or more real eigenvalues go to zero would yield both BSL and BDL active. Such cases in which two or more static losses of stability occur have not been observed in mooring dynamics. In such a case, we can include expressions (105)-(110) to determine the number of eigenvalues with zero real part. If two real eigenvalues are zero, for example, F/A will be zero; if three real eigenvalues are zero, then F/A and E/A will be zero as well; if four real eigenvalues are zero, then F/A, E/A and D/A will be zero, and so on. In addition, with no formal proof, we state the following cases in which C_{RC} may be zero without the occurrence of dynamic loss of stability: (i) Two real eigenvalues have the same magnitude and opposite sign. In this case, C_{R5} will be zero as well. (ii) If four real eigenvalues satisfy this condition, then C_{R3} and C_{R5} will be zero. (iii) If all six real eigenvalues satisfy this condition, then C_{R1}, C_{R3} and C_{R5} will be zero (auxiliary relations B/A, D/A and F/A are zero as well). The boundaries that define regions of different dynamics experienced by the mooring system as parameters are varied can be obtained analytically by setting expressions (117) and (121) to zero (i.e. making C_{RS} and C_{RC} active).

The stability criteria and the analytical expressions for the bifurcation boundaries and associated morphogeneses occurring in mooring systems are very powerful tools that can be used in the design of mooring systems without the need of trial and error and endless nonlinear simulations. These expressions serve to evaluate the stability of the system, construct bifurcation boundaries, study the change in dynamical behavior of the system as parameters are varied, and understand their effects in the process of design. The complexity of the analytical expressions for the morphogeneses and bifurcation boundaries, show that it is unlikely that rules of thumb for design of mooring systems can be derived. Instead, these expressions should be used in design without extensive computational time. Furthermore, proper use of these tools helps the designer to improve understanding of the slow motion dynamics of SMS and TMS and their dependence on design parameters. The order of the characteristic polynomial (104) equals the dimension of the state space N_{ss}. The example shown in this section corresponds to a SMS with $N_{ss} = 6$, and thus the analytical expressions correspond to a sixth order polynomial expansion. In TMS, where $N_{ss} = 8$, the level of complexity of such expressions increases considerably [33]. Memory effect and buoy supported catenaries in the system further increase the dimension of the state space, thus resulting in more complicated expressions.

7. OUTLINE OF THE MOORING DESIGN METHODOLOGY

The mathematical formulation presented in Chapter 4, the process of producing catastrophe sets for design developed in Chapter 6, along with the simulations in Chapter 5 provide a complete picture of the UM methodology to mooring system design. It is used in Chapters 8 - 10 to assess the effects of a wide range of modeling issues, as well as environmental and design parameters on mooring system design. Before proceeding to that assessment, the steps of the methodology are listed below.

(i)   Specify the environmental conditions including water depth, wind, wave, and current particulars.

(ii) Select the mooring system particulars that will remain unchanged during this design cycle. For example, select the moored vessel, an API recommended [2] or other mooring line pattern, and the mooring line material.

(iii) Select parameters that the designer is willing to change to achieve a satisfactory design. Such design parameters may be the mooring line orientation, length, and pretension; number, size and distribution of supporting buoys; coordinates of anchoring and vessel attachment point for each line; vessel orientation; size and particulars of stabilizing fins; location of turret and riser top tension; vessel offset with respect to well head.

(iv) Set up the mathematical model as presented in Chapter 4. It is recommended that a maneuvering model from the first school of thought is adopted, such as the Abkowitz or Takashina models.

(v)   Select a state space representation, preferably the one used in Section 6.1. This will make it possible to identify the eigenmode components corresponding to each eigenvalue.

(vi) Calculate numerically the system equilibria and their eigenvalues. This information fully characterizes the asymptotic system behavior in the vicinity of each equilibrium with the exception of strange attractors. In the latter case, further analysis is required such as calculating the Lyapunov characteristic exponents and the associated fractal dimension [15, 59]; or at least perform time simulations. Next, global tendencies of trajectories in the time domain or in any phase space can be surmised.

(vii) Produce design graphs (catastrophe sets) by calculating bifurcation sequences and their singularities. These would be accompanied by identification of morphogeneses such as pitchfork (static) and Hopf (dynamic) bifurcations, and fold and cusp singularities.

(viii) Select a satisfactory design by direct reading of the design graph.

(ix) If a satisfactory design is not available, more design graphs need to be produced. For mooring systems with high number of design parameters, the physics-based analytical expressions of bifurcation sequences presented in Section 6.5 should be used to perform sensitivity analysis with respect to design variables. Since in most cases mooring systems have many design parameters, these expressions provide the needed breakthrough for design.

(x) Search for a better design if so desired. This step cannot be defined properly since criteria for assessment and optimization of mooring systems have not been developed. The issue of course is that current practice aims at avoiding first excursion failure of mooring lines which is a time domain constraint, not a design criterion. What can be done at this point is to compare by simulation designs that fall within the regions of acceptable dynamic behavior identified in the developed design graphs.

Upon completion of this design procedure based on slow and intermediate frequency dynamics, the underlying motions become available in the time domain. These results make it possible to proceed with the next step in design. That is, computation of fast motions for the moored vessel and risers as well as their effect on extreme and fatigue loads on the mooring lines.

In the next two chapters, the developed methodology is used to assess the effects of environmental and design factors on the slow and intermediate frequency scale dynamics and the design of mooring systems.

8. ASSESSMENT OF MODELING

In Chapters 8 - 10, catastrophe sets are developed for specific mooring systems to investigate the effects of modeling issues, environmental factors, and operational parameters on the design of mooring systems. To facilitate graphical representation, only the bifurcation sequences around PE are discussed to show the dependence of SMS dynamics on such parameters. The current angle α is set equal to $180°$ (head seas) and the current speed U is set to 2 knots unless specified otherwise. Nonlinear simulations are important in determining the quantitative nature of the system dynamics, and they provide important information regarding amplitudes of motion, tension in the mooring lines, deformation of riser, etc. Due to space limitations, however, only qualitative comparisons are made without simulations. The only simulations are shown in Chapter 5, and in Sections 8.1 and 8.2, which were deemed necessary.

The values of the various parameters for each numerical application are included in the caption of each Figure. In Section 9.5, slowly-varying drift force effects are studied by selected simulations since they are nonautonomous forces.

8.1 Comparison of Hydrodynamic Maneuvering Models

Figure 11 shows a series of catastrophe sets for a 4-line TMS as a function of turret position D_{CG}/L and current direction α (no other external excitation) for the various hydrodynamic maneuvering models discussed in Chapter 4 (A-M, T-M, O-M and SW-M) [49]. As can be inferred from Figure 11, the predicted dynamics vary between models of the same school, and vary considerably between models of the two schools.

In the catastrophe sets of Figure 11, the models of the first school (A-M and T-M) exhibit only regions R-I, R-II and R-III in the parametric design space. The second school, O-M and SW-M, exhibits only unstable regions R-II, R-III and R-IV about PE. Based on the catastrophe sets in Figure 2, the following observations can be made:

(i) Even though the selected vessel characteristics are as similar as possible for each model, it was not possible to obtain all hydrodynamic coefficients for all models for exactly the same vessel. Thus, the results in Figure 11 were expected to be different, even for the models of the same modeling school. The bifurcation boundary resulting from static loss of stability (straight line in all cases) should be approximately the same for all models. This is indeed the case for T-M, O-M and SW-M. The difference for A-M is due to incomplete data of the slow motion nonlinear derivatives [2].
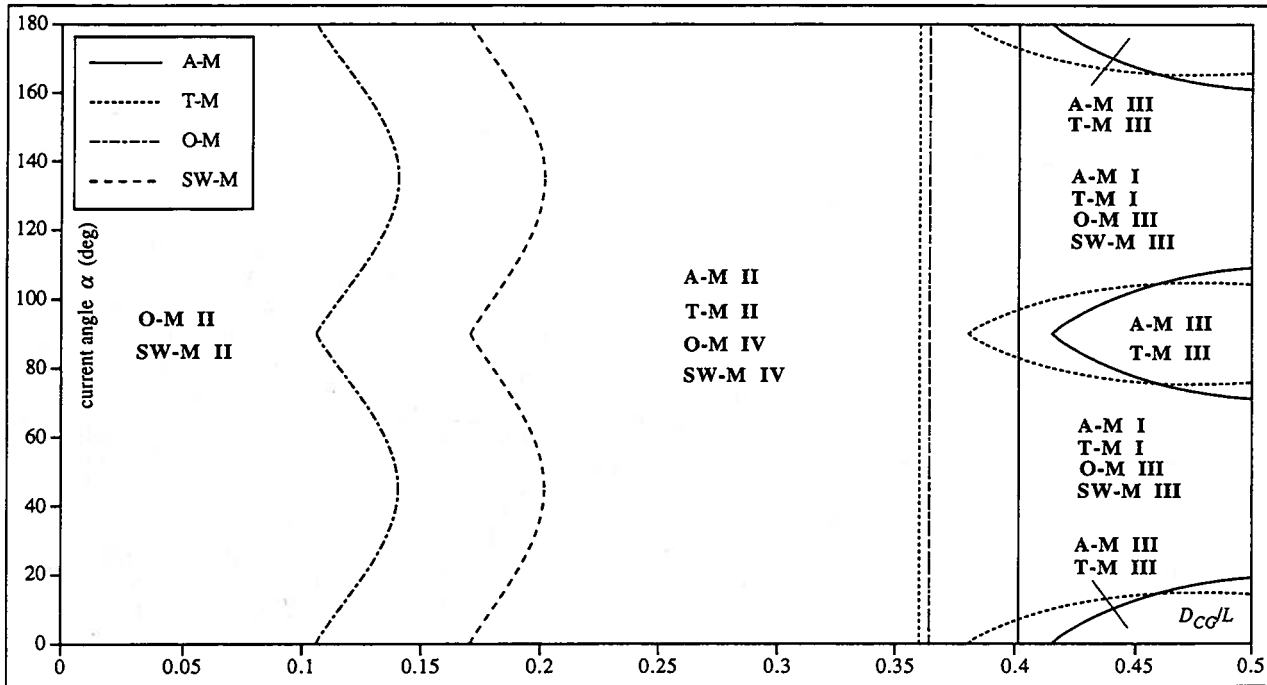
50

Fig. 11 Effect of turret location and current direction, 4-line TMS: All hydrodynamic models; $\ell_w/L = 6.0$, $h = 700$ m, $U = 3.5$ kts, $T_P = 1327.8$ kN, AC

(ii) The catastrophe sets of TMS around PE in Figure 11, show that the two groups of modeling predict dynamic loss of stability differently. This is expected since the physics behind each of the schools is different. According to Figure 11, neither O-M nor SW-M renders a stable PE in the design space, and therefore the system either results in a limit cycle around PE (R-III), or its trajectories are attracted by an alternate equilibrium AE (R-II, R-IV).

The difference in nature of the catastrophe sets with variations of the current angle α is a consequence of changes in the incident angle of the water with respect to the catenaries.

These variations change the drag in the mooring lines. As the drag in the mooring lines increases, A-M and T-M models become dynamically stable. Nonlinear time simulations show this to be the case, and show that even if the dynamic behavior of all systems is oscillatory in nature, major differences exist between the two groups in amplitudes of oscillations [49].

Figures 12 and 13 show simulations of the four maneuvering models separated by schools for the same mooring line arrangement which lies in R-III [49]. As expected from Figure 11, all models show convergence to a limit cycle around PE. The first group shows relatively large amplitude oscillations (Figure 12) with respect to the second group (Figure 13).

The large amplitude oscillations for A-M and T-M in Figure 12 show that the TMS goes asymptotically to a stable limit cycle, but the system is unsafe for operations. Additional dynamic analyses are required to verify the viability of the system; selecting different parameters to stabilize the TMS is possible by just looking at the design graphs in Figure 11. In Figure 13, the

51

qualitative behavior of O-M and SW-M is oscillatory about PE, and thus PE is unstable even though the motions of the vessel are relatively small.
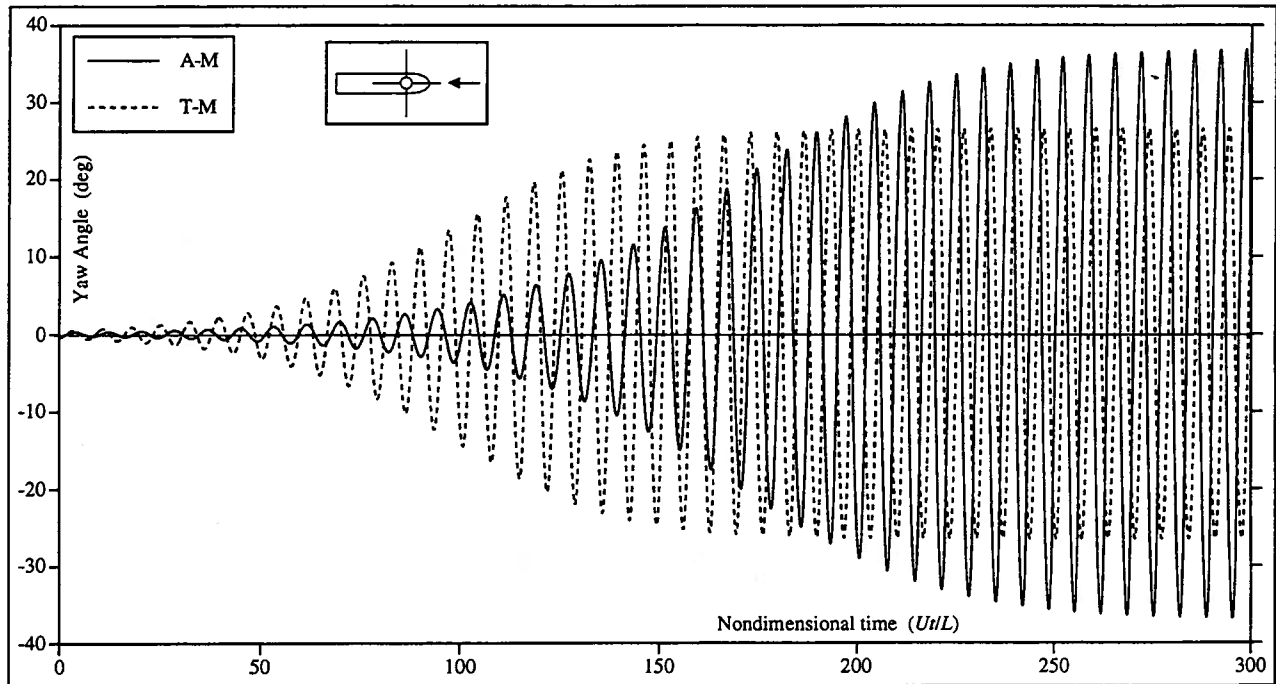

Fig. 12 Stable limit cycle, 4-line TMS, A-M and T-M: $\ell_w/L = 6.0$, $D_{CG}/L = 0.45$, $h = 700$ m, $U = 3.5$ kts, $T_p = 1327.8$ kN, $\alpha = 180°$, AC
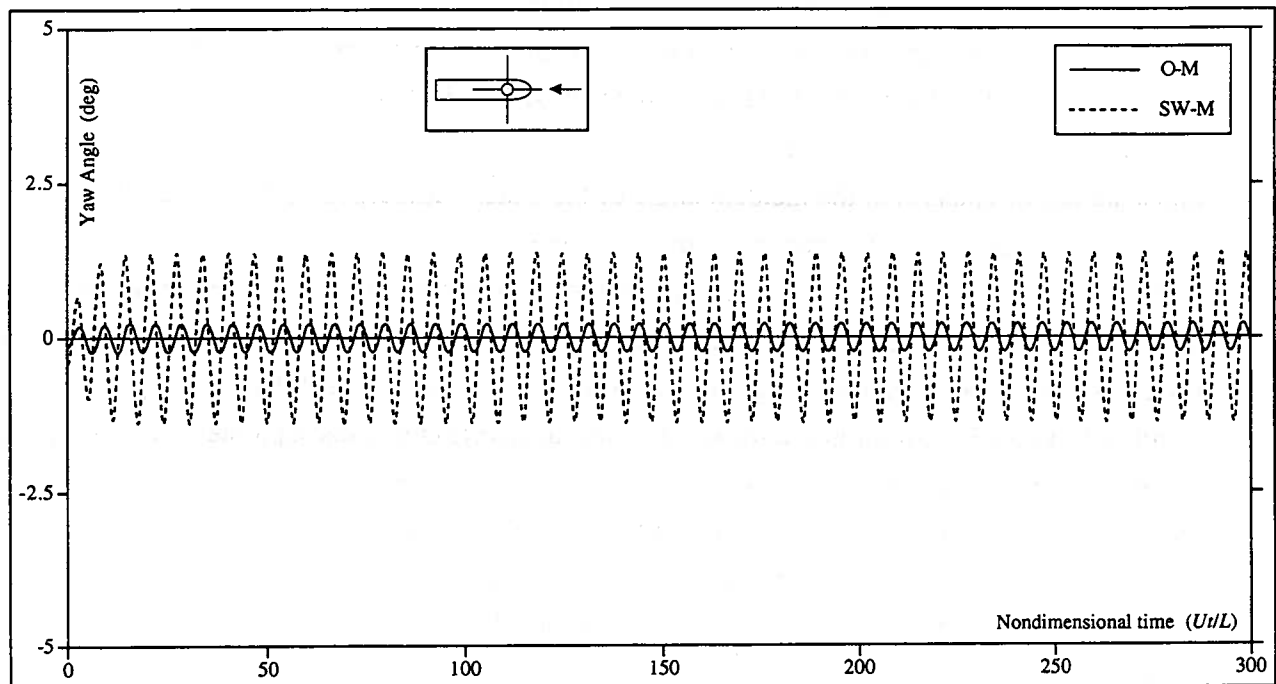

Fig. 13 Stable limit cycle, 4-line TMS, O-M and SW-M: $\ell_w/L = 6.0$, $D_{CG}/L = 0.45$, $h = 700$ m, $U = 3.5$ kts, $T_p = 1327.8$ kN, $\alpha = 180°$, AC

52

8.2 Modeling TMS as SPM

Presently, several TMS have been designed and deployed in relatively deep waters under harsh environmental conditions. Due to the complexity of these types of systems, TMS are often modeled mathematically as Single Point Mooring (SPM) systems with a number of lines or as a single line [21, 24, 46, 53]. Limited experimental and field data for TMS in shallow and intermediate water depths [46], show that SPM models have proven useful, especially in determining the turret locations for which the system is statically stable. The TMS model, however, differs from the classical Single Point Mooring (SPM) model in three ways: (i) The friction moment exerted between the turret and the vessel. (ii) The mooring line damping moment resulting from the turret rotation. (iii) The point of attachment of the mooring lines on the turret [32]. Some of the qualitative differences in the dynamical behavior between TMS and SPM are identified in the catastrophe sets of Figure 14 [32].

Figure 14 shows a series of catastrophe sets about PE in the (D_{CG}/L, ϕ) plane for both SPM and TMS (D_{CG} in TMS is equivalent to x_p in SPM). External excitation consists of current, wind and second order mean drift, which are collinear acting in direction ϕ. For TMS the non-dimensionalized moment friction factor τ is set equal to 0.001 (very high) and 0.000001 (low). To establish an appropriate basis of comparison between SPM and TMS, both systems have the same vessel hydrodynamics, mooring line model, center of gravity, added and structural mass, added and structural second moment of inertia. Qualitatively, the dynamics of the TMS and SPM systems are similar in the (D_{CG}/L, ϕ) plane as shown in Figure 14. The static stability of both systems depends mostly on the value of D_{CG}, and to a lesser extent on the environmental excitation. The location of the turret (mooring lines in the SPM case) largely determines whether or not PE will bifurcate to create two additional equilibria irrespective of the direction of the external excitation. Both SPM and TMS tend to achieve their principal weathervaning equilibrium as the turret (or location of the mooring lines) is moved forward, i.e. with increasing D_{CG} values, as shown by stable region R-I.

The static bifurcations that occur in both SPM and TMS in Figure 14 are very similar. This characteristic of TMS is captured well by SPM model. The position of the turret has important design ramifications, since higher hydrodynamic forces act on the vessel when achieving a non-weathervaning configuration. The dynamic stability for both systems in Figure 14 is affected by the direction of external excitation. Both SPM and TMS dynamics may fall in R-III achieving a stable limit cycle around PE for large values of D_{CG}. This occurs for excitation angles at which the total projected area of the catenaries to the inflow is smaller, resulting in less damping due to the mooring lines.
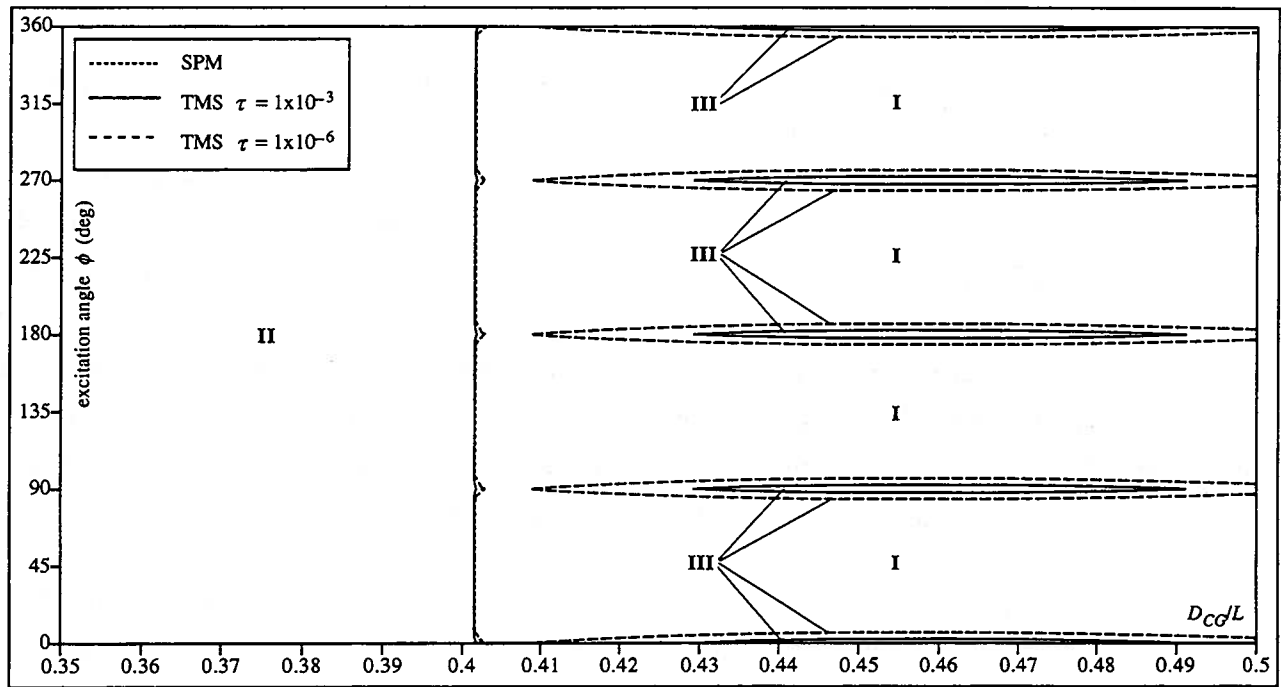
53

Fig. 14 Effect of turret location and external excitation, comparison of SPM and TMS dynamics: ℓ_w/L =10.12, h =750 m, T_P =1444 kN, U =3.3 kts, U_w =15 kts, $H_{1/3}$ =3.66 m, $T_{1/3}$ =8.5 s, AC, T-M
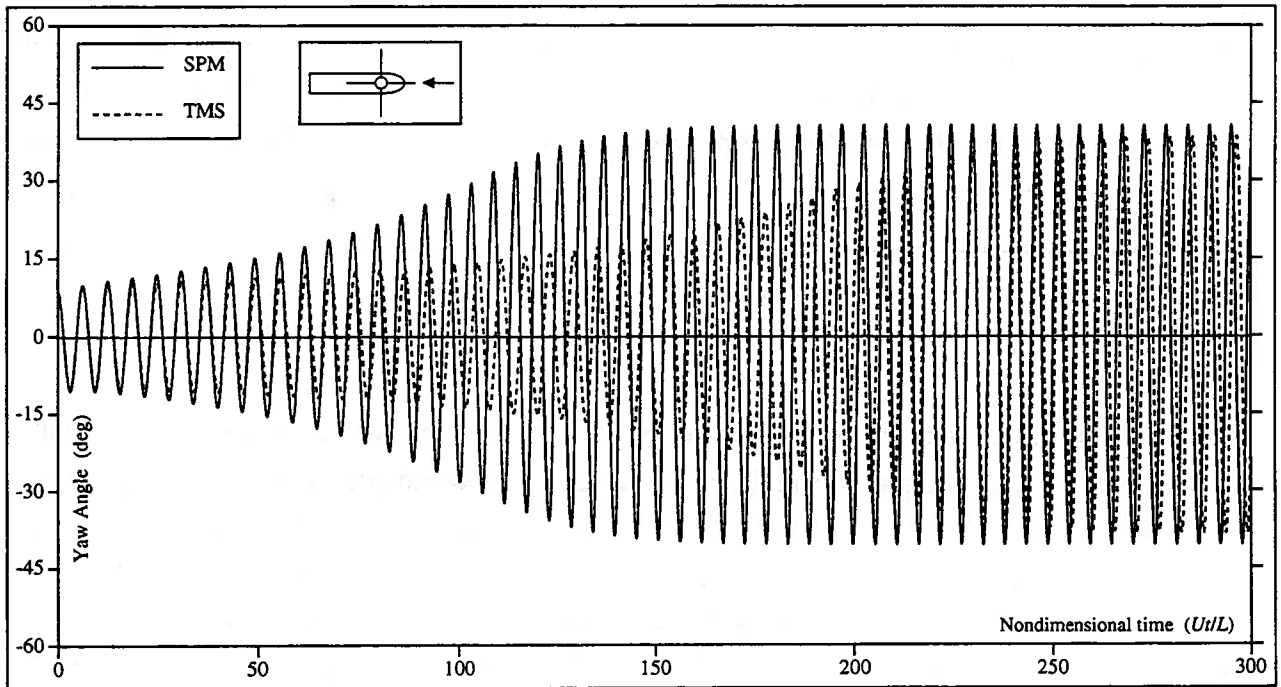

Fig. 15 Stable limit cycle, TMS and SPM; ℓ_w/L =10.12, D_{CG}/L =0.45, h =750 m, ϕ =180°; U =3.3 knots, U_w =15 knots, $H_{1/3}$ =3.66 m, $T_{1/3}$ =8.5 s, T_P =1444 kN, AC, T-M

The third parameter, which corresponds to the magnitude of the moment exerted between the turret and the vessel, is shown to alter significantly the region where dynamic loss of stability occurs. For nonzero friction coefficient τ, TMS dynamic stability increases with increasing values of τ. As the friction coefficient decreases, the region of limit cycles (R-III) exhibited by TMS approaches that of SPM system. It is significant to point out that the static bifurcation boundaries (i.e. the boundary between R-I and R-II) for TMS and SPM systems do not coincide as shown in Figure 14. As the turret diameter decreases (and therefore its mass decreases), the TMS catastrophe set approaches that of the SPM system, and their bifurcation boundaries between regions R-I and R-II, and R-I and R-III, converge in the limit of zero turret mass.

Other discrepancies between SPM and TMS models can be discerned with nonlinear time simulations. The major quantitative differences between TMS and SPM result from the mooring line damping moment which is a consequence of the turret rotation. This is shown by simulations in Figure 15 where the frequency of oscillation of the TMS is lower than that of SPM [32].

9 ASSESSMENT OF ENVIRONMENTAL FACTORS

The environment determines the type of mooring that is appropriate for operations. All environmental factors have their characteristics and affect the mooring system differently. In this chapter, qualitative changes in the dynamics of mooring systems due to environmental changes are assessed using design graphs.

9.1 Memory Effect

The effect of memory is shown in the catastrophe sets in Figure 16 for a F2A1 tanker SMS in the $(x_p/L, \Omega)$ plane [43]. This Figure shows that the memory effect causes the bifurcation boundaries to move to the left. As a result, the memory effect may stabilize the system both statically and dynamically, and all trajectories that result in a limit cycle around PE may converge to a stable PE. Figure 16 also shows the effect of pretension in the system. Unstable R-III, where periodic solutions exist, disappears as the pretension in the mooring lines is increased. Statically unstable R-II also shrinks with increasing pretension.
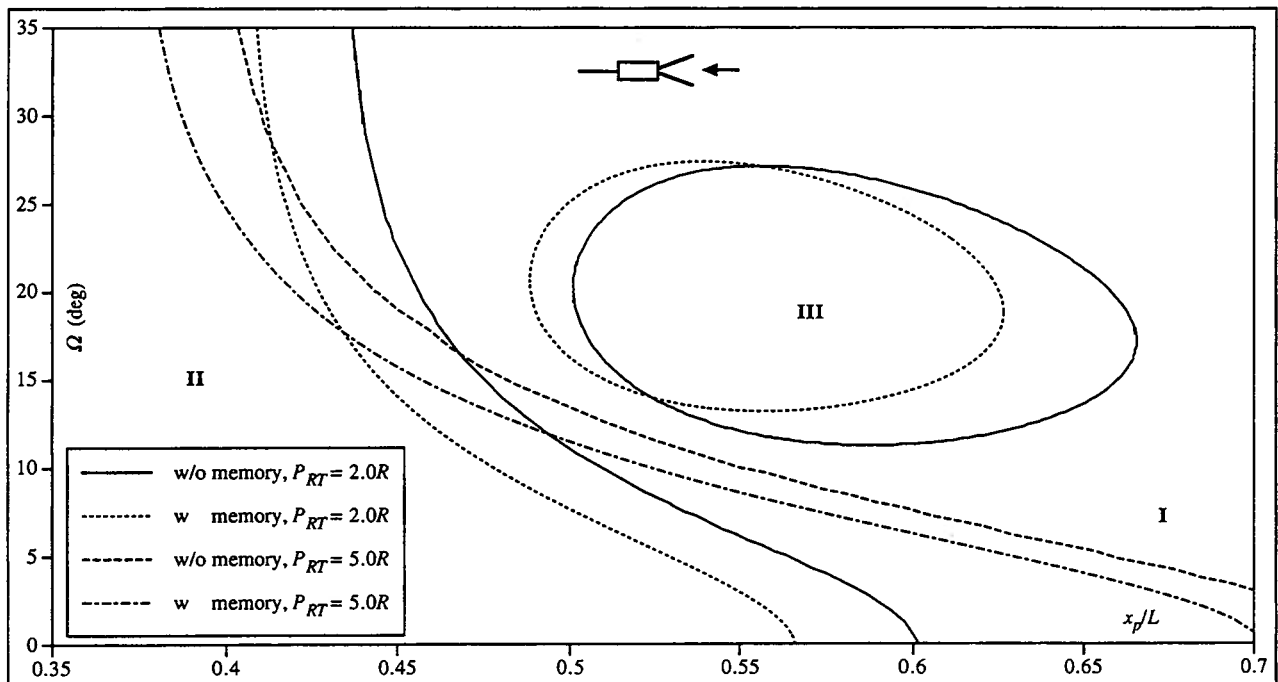

Fig. 16 Effect of memory, F2A1 Tanker SMS: ℓ_w/L =6.0, y_p/B =0.0, h =450 m, $H_{1/3}$ =3.0 m, $T_{1/3}$ =8.0 s, AC, A-M

9.2 Current

The effect of current speed on a F1A2 tanker SMS is shown in Figure 17 for various current speeds in the parametric space (x_p/L, ℓ_w/L). The four regions are marked with respect to the case where $U = 2$ knots. As shown in the Figure, current speed significantly affects the behavior near PE. For $U = 1$ knot, PE is statically unstable in most of the practical range except for very small values of ℓ_w. As the current speed increases, the cusp singularity moves to the left and to lower values of ℓ_w, and unstable R-IV enters the range of practical values of x_p and ℓ_w. The case for which $U = 3$ knots corresponds to the catastrophe set of the tanker SPM. As the current speed increases, the vessel is pushed back and the two aft lines become slack and the system turns into a SPM system.

The effect of current direction on TMS is shown in Figure 11. The bifurcation boundary corresponding to static loss of stability (BSL) is not affected by a change in current direction. The dynamic loss of stability of the system (BDL), however, is affected due to the change in the inflow angle of the mooring lines to the direction of current, as previously explained. The direction of the current alone does not affect single point - single line mooring dynamics, as the system weathervanes.
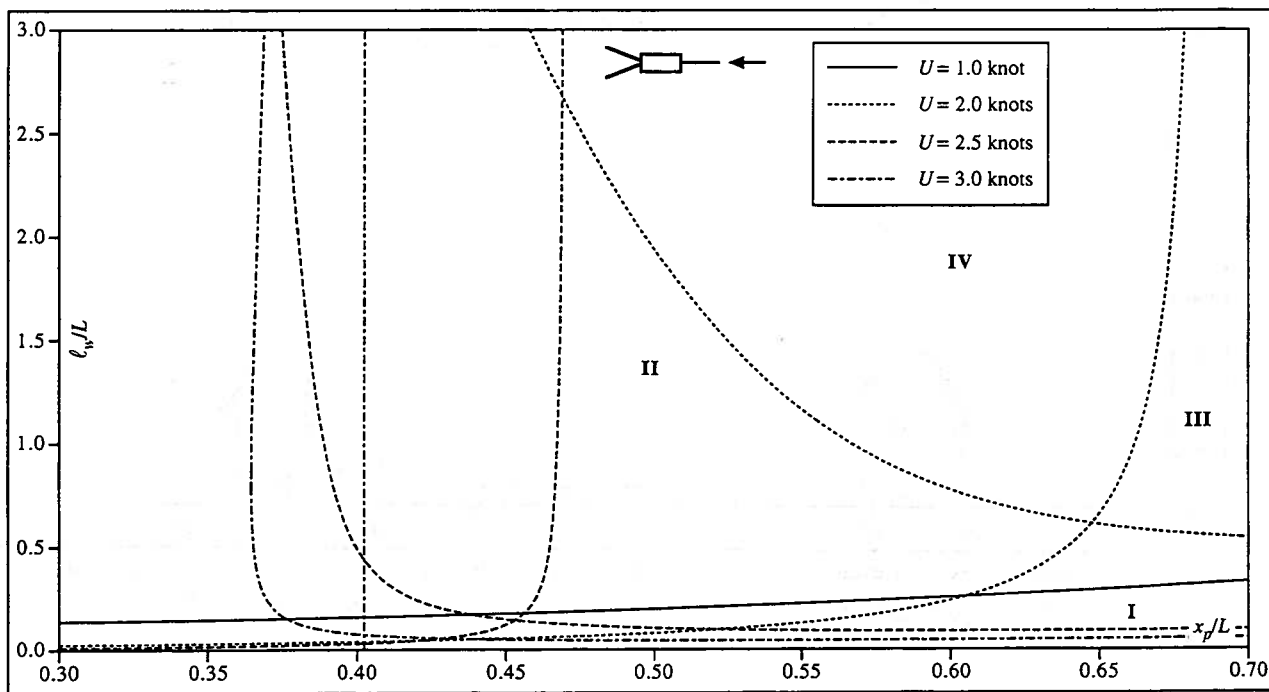

Fig. 17 Effect of current speed on F1A2 Tanker SMS: $y_p/B = 0.5$, $\Omega = 5°$, $E_l = 0.04$, SFR, A-M

The effect of current direction on SMS, however, may have a considerable effect on SMS dynamics, as shown in Figures 18, 20 and 26 [37, 38], which correspond to a F6A3 DICAS in water depth of 300

m. In those figures, the current direction tends to destabilize a DICAS at or near beam seas, as noted by R-III. In this region, the system oscillates around PE with no other equilibria that may attract the trajectories.

9.3 Wind

The effect of wind in mooring systems also depends on the system configuration. To illustrate some of the effects of wind, Figure 18 shows a catastrophe set of a F6A3 DICAS for various directions of wind excitation [37]. As shown in Figure 18, DICAS is stable under a large range of excitation. Wind destabilizes DICAS in the range of following to beam seas, and stabilizes the system in or near head seas. This is partly due to the fact that this orientation of the wind forces provides additional forces to the already pretensioned forward mooring lines, thus limiting the motions of the system.
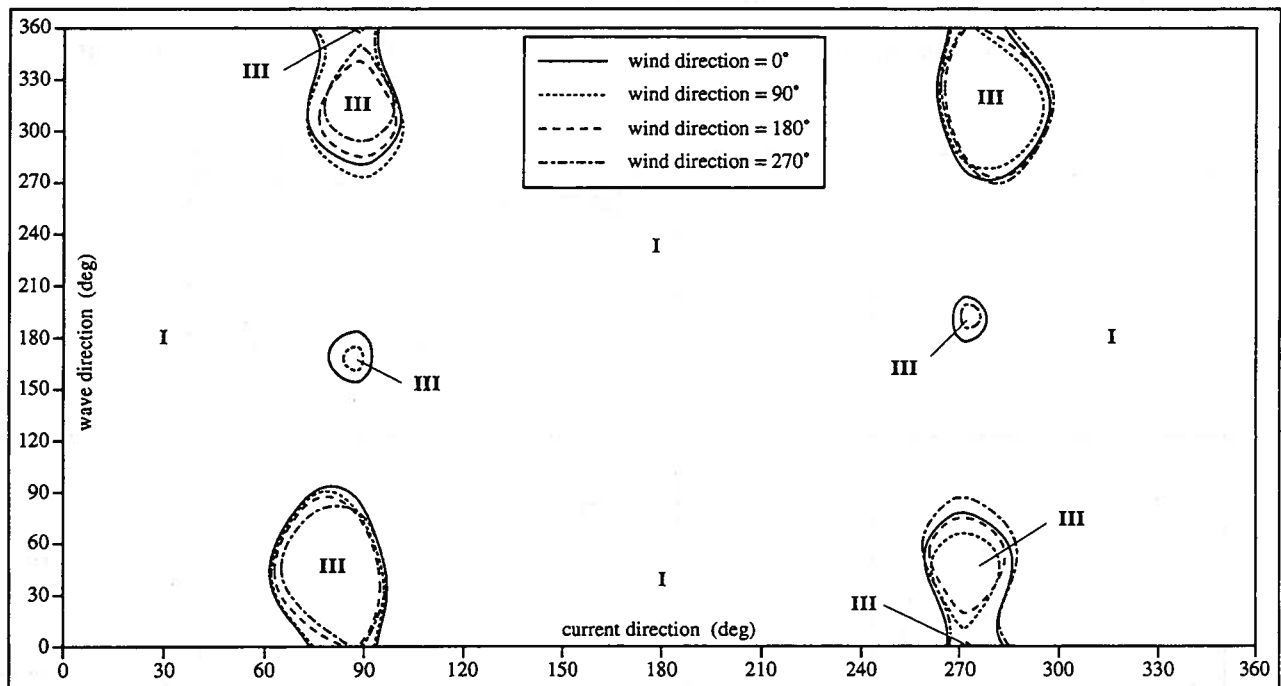

Fig. 18 Effect of external excitation, F6A3 DICAS: ℓ_w/L =7.36, $(x_p/L)_{fwd}$ =0.25, $(x_p/L)_{aft}$ = −0.5, $(y_p/B)_{fwd}$ =0.354, $(y_p/B)_{aft}$ =0.0, h =300 m, U =3.08 kts, U_w =48.7 kts, $H_{1/3}$ =4.7 m, $T_{1/3}$ =9.2 s, AC, T-M

The direction and speed of wind also affect the stability of TMS as shown in the catastrophe sets of Figure 14, where the external excitation consists of collinear current, wind and mean drift. Compared to Figures 11 and 21 [30], for which only current is included as external excitation, static loss of stability of TMS occurs for larger values of D_{CG} when wind excitation is added. Note that Figure 14

also includes the effect of mean drift on the system. The point of static bifurcation at equilibrium, D_{CG}^{SB}, of the symmetric system $\psi = \phi - 180°$ is given by:

$$D_{CG}^{SB} = \frac{\overline{N}_H + \overline{N}_M + \overline{N}_W + \overline{N}_{WV}}{\overline{Y}_H + \overline{Y}_M + \overline{Y}_W + \overline{Y}_{WV}} \ . \tag{122}$$

This ratio corresponds to the center of pressure of the system. The other terms that affect BSL are thus the memory effect, wind, and second order mean drift.

9.4 Mean Wave Drift

Some mean wave drift effects can be illustrated in the catastrophe sets in Figures 18 and 19. In Figure 18, the effect of wave direction is shown. The F6A3 DICAS falls into oscillatory region R-III, undergoing a limit cycle behavior, for waves in the range of following to beam seas; PE is stable for wave direction at or near head seas. This effect is similar to that of wind.

Figure 19 shows a series of catastrophe sets for a F1A2 tanker SMS configuration without wave drift and for various values of the significant wave height, $H_{1/3}$ [9]. As $H_{1/3}$ increases, the set of bifurcation boundaries move to the left. As a result, stable R-I and unstable R-IV move to the left in Figure 19, shrinking unstable R-II. A point in R-II under no mean drift forces, for example, may become a stable PE (R-I) or an oscillatory PE (R-III) depending on the value of $H_{1/3}$. In Figure 5, a statically unstable PE under no mean drift forces becomes stable. Mean wave drift has a similar effect as the current speed in Figure 17.

As mentioned in Section 9.3, mean wave drift also affects the static stability of TMS. This is shown by comparing the catastrophe sets in Figures 11 and 25 [7]. As noted in Figure 25, mean drift forces shift BSL to the right with respect to its position in Figure 11.

9.5 Slowly-Varying Drift

When the spectrum of slowly-varying drift forces is added as an external excitation, the system becomes nonautonomous. There is no general stability theory to analyze a nonautonomous system subjected to spectral excitation. Only nonlinear time simulations can provide useful information on the dynamics that mooring systems exhibit due to slowly-varying drift. The following observations can be made regarding the possible effects of slowly-varying drift on mooring systems dynamics [9]:

(i) Slowly-varying drift forces may stabilize oscillatory motions instigated by mean drift forces, as shown in the simulation of a F1A1 barge SMS in Figure 6, where a significant reduction in the oscillations is observed. Actually, slowly varying drift forces of higher $H_{1/3}$ totally eliminate the oscillations of the system in Figure 6.

(ii) Slowly-varying drift may also produce resonant beating behavior as in Figure 10 for the surge motion, resonating with a natural frequency of the system.

(iii) Finally, slowly-varying drift may render a stable PE unstable and take the system to non-resonant oscillations around AE, as shown for the F1A2 tanker SMS in Figure 5.
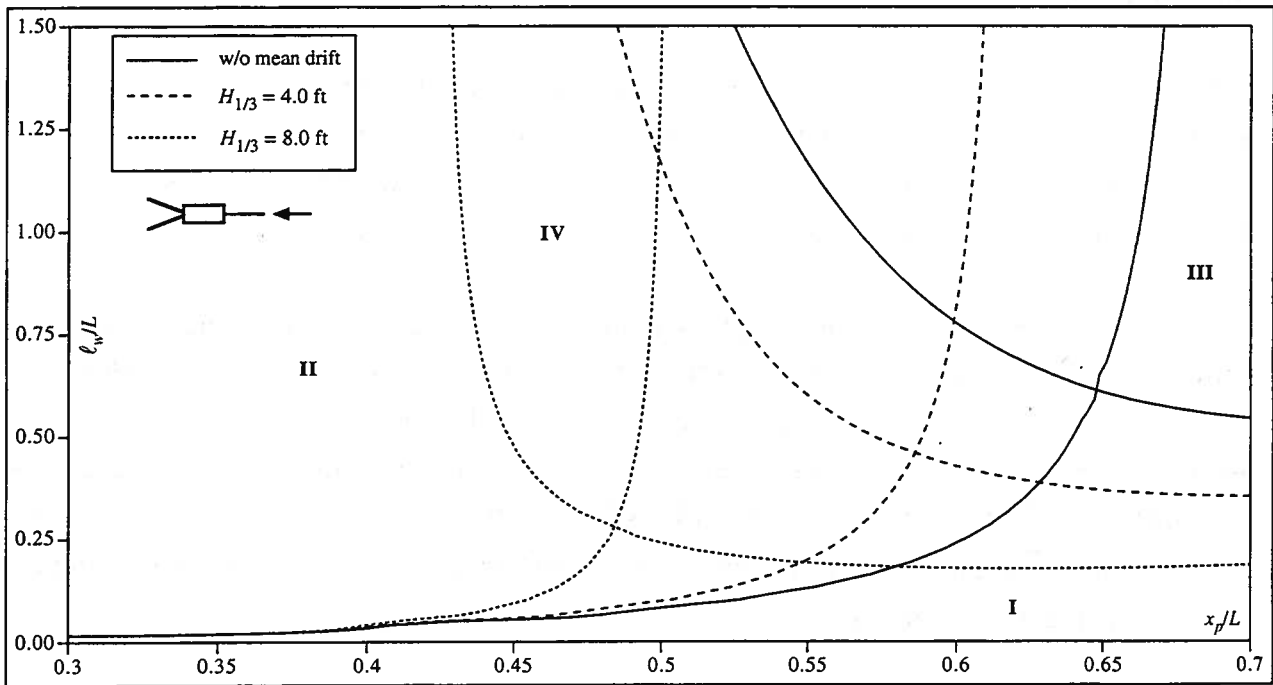

Fig. 19 Effect of mean drift on F1A2 Tanker SMS: $y_p/B = 0.5$, $\Omega = 5°$, $E_l = 0.04$, SFR, A-M

9.6 Water Depth

The loads exerted on the mooring lines and the risers as well as the lack of understanding of the dynamics of mooring systems in deep water make water depth an important design factor. Depending on the system configuration, the depth of water may have stabilizing or destabilizing effects, as shown by the catastrophe sets in Figures 20, 21 and 30.

The catastrophe sets in Figure 20 pertain to the F6A3 DICAS discussed previously. Stable region R-I tends to increase with increasing water depth, while unstable R-III disappears. This is due to higher

resistance (drag) on the system as a result of an increase in the suspended portion of length of each of the chains. The opposite effect is shown in Figure 21 [30], which corresponds to catastrophe sets of a 4-line TMS. Oscillatory R-III increases with increasing water depth, and thus a specific TMS configuration may be stable for water depth h <800 m but unstable for h >850 m. Due to the nature of the turret, the drag in the mooring lines does not provide the necessary restoring moment for stability to occur.
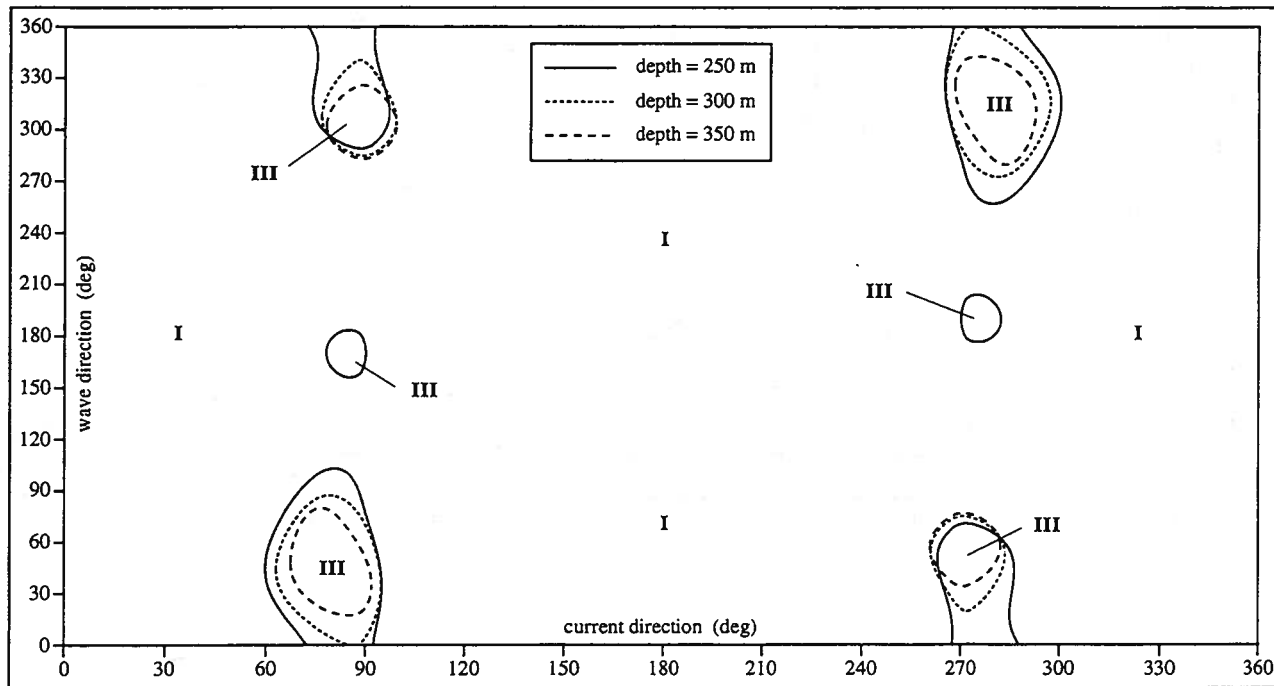

Fig. 20 Effect of external excitation on F6A3 DICAS: ℓ_w/L =7.36, $(x_p/L)_{fwd}$ =0.25, $(x_p/L)_{aft}$ = −0.5, $(y_p/B)_{fwd}$ =0.354, $(y_p/B)_{aft}$ =0.0, h =300 m, U =3.08 kts, U_w =48.7 kts, $H_{1/3}$ =4.7 m, $T_{1/3}$ =9.2 s, AC, T-M

The catastrophe sets in Figure 30 for a buoy-supported F2A2 DICAS [35] show different effects of water depth depending on the system configuration. Two different geometries of the DICAS, denoted as G1 and G2, are used to illustrate this concept. The only difference between G1 and G2 lies in the orientation of the forward mooring lines. In G1, the angle of aperture between the two forward mooring lines is 20°, while in geometry G2 is 90°.

For a symmetric mooring system, we define Ω as the horizontal angle between the X-axis and the mooring line, and thus Ω = 10° for G1, and Ω =45° for G2 (the angle of aperture between lines equals 2Ω). Figure 30 shows that, in the case of G1, stable R-I increases with water depth. On the other

hand, R-I decreases with water depth for G2. The bifurcations involved in each of these geometries are different in nature, and will be discussed further in Section 10.8.
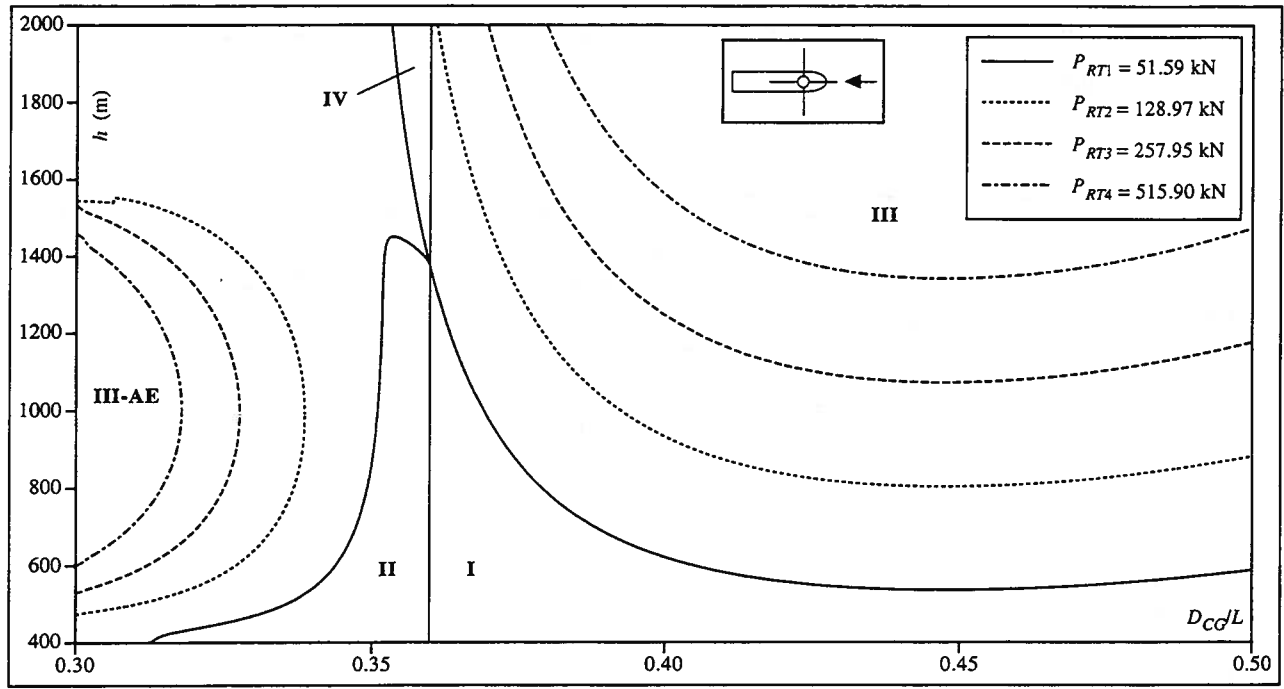

Fig. 21 Effect of turret location, water depth and horizontal pretension, 4-Line TMS: ℓ_w/h =3.5, AC, T-M

10. ASSESSMENT OF OPERATION PARAMETERS

In the design procedure of mooring systems, several operation parameters (design variables) are selected by the designer. These are, among others, the number, material, length, orientation and pretension of the mooring lines; fairlead position; location of turret; location of riser; etc.

To illustrate the complex behavior of mooring systems, some of the effects of those parameters are graphically shown in the catastrophe sets in Figures 11-31. These sets can be compared to establish a rationale for determining trends in behavior for different mooring systems with different mooring line configurations.

10.1 Mooring Line Material

The material of the mooring lines significantly affects the dynamical behavior of the system. To illustrate this, consider the catastrophe set in Figure 22 for a barge SPM in the $(x_p/L, \ell_w/L)$ parametric design space [11]. In Figure 22, the dynamics of the SPM is compared for three types of mooring lines: synthetic fiber rope, suspended catenary without drag, and 3-D cable FEM model with drag. The SPM system may fall in either stable R-I or oscillatory R-III, depending on the particular values of x_p and ℓ_w. It is shown that the material of the mooring line significantly affects the SPM stability boundaries.

Based on the results of Figure 22, we can draw the following conclusions:

(i)   For small values of ℓ_w/L, the mooring line restoring force is provided by its extension. For this reason, the three line models considered give near identical results.

(ii) For intermediate values of ℓ_w/L, the line restoring force is mainly governed by its weight. Hydrodynamic drag forces are still not important to induce any visible difference between the SC and the 3-D cable.

(iii) For large values of ℓ_w/L, hydrodynamic drag forces on the cable become very significant, thus resulting in considerable differences between the SC and the 3-D cable stability boundaries.

The results of Figure 22 indicate that for the SPM system considered, the heavier the mooring line results in a larger unstable region, as denoted by a larger region R-III. Spread mooring systems that provide restoring moments on the mooring lines may show the opposite behavior.
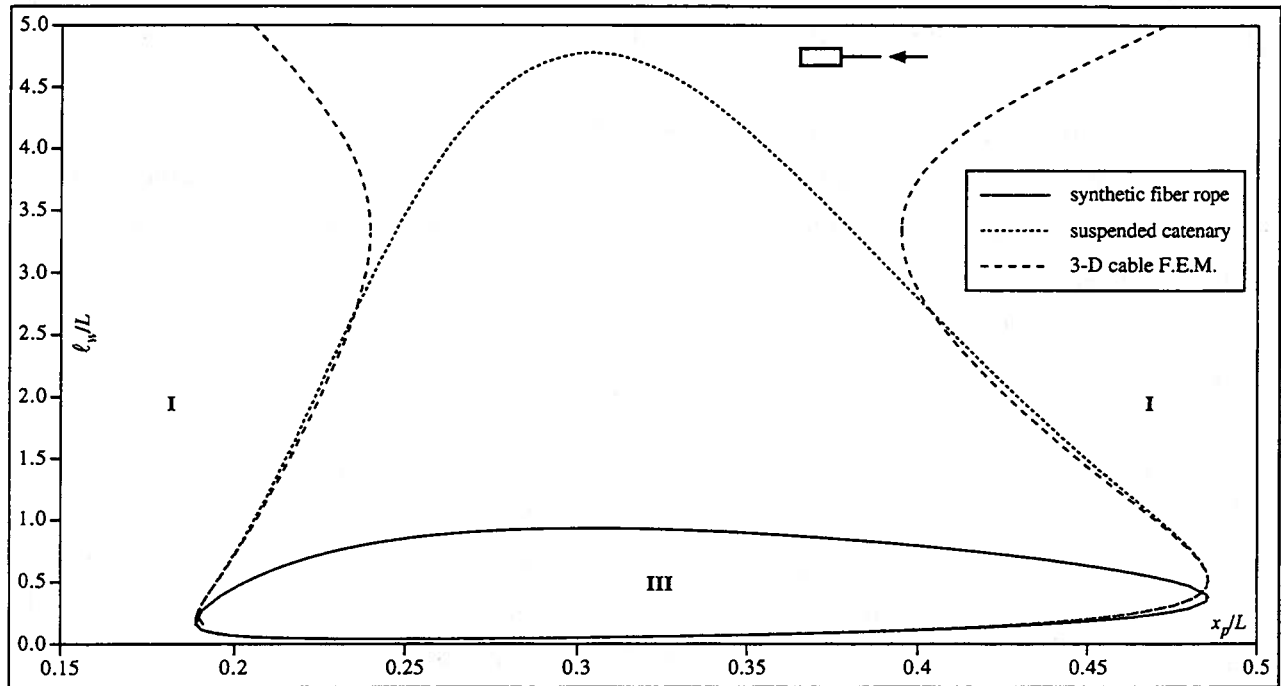

Fig. 22 Effect of mooring line material on barge SPM; A-M

10.2 Mooring Line Pattern

Due to the wide selection of arrangements that mooring systems may have, one of the most important parameters to consider in the design process is that of mooring line pattern. As seen in Section 9.6 and depicted in Figure 30, a mooring system (F2A2 DICAS) may exhibit entirely different qualitative dynamics by changing the angle of aperture in the forward mooring lines.

The effect of mooring line pattern can also be illustrated with the catastrophe sets in Figures 23 and 24 [5]. In each figure, two different configurations of 3-line tankers SMS in the (x_p/L, ℓ_w/L) parametric design space are shown. Figure 23 corresponds to a F1A2 tanker SMS and it shows that - with increasing Ω in the aft lines, - the bifurcation boundaries move to the right, expanding unstable R-IV. The exact opposite effect is observed in Figure 24 where instead of F1A2, a F2A1 arrangement is considered. In both cases, the cusp singularity moves toward higher values of ℓ_w with increasing Ω.
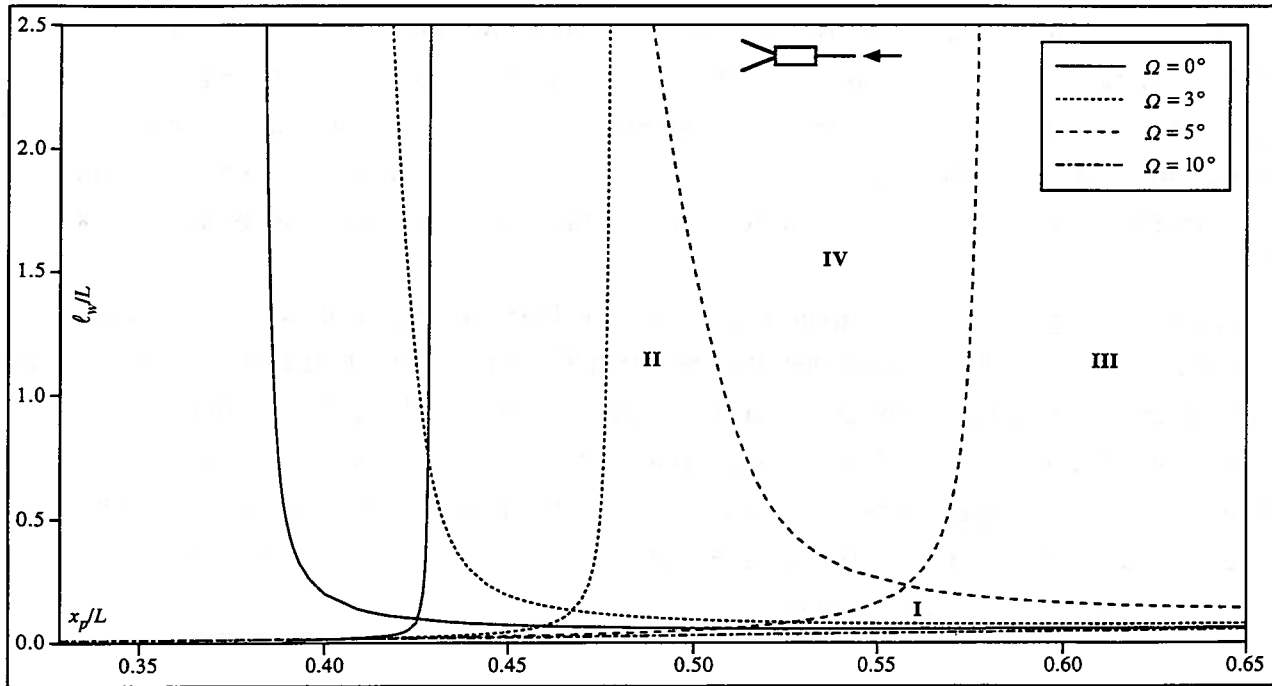
Fig. 23 Effect of Ω on F1A2 Tanker SMS: $y_p/B = 0.0$, $E_I = 0.03$, SFR, A-M
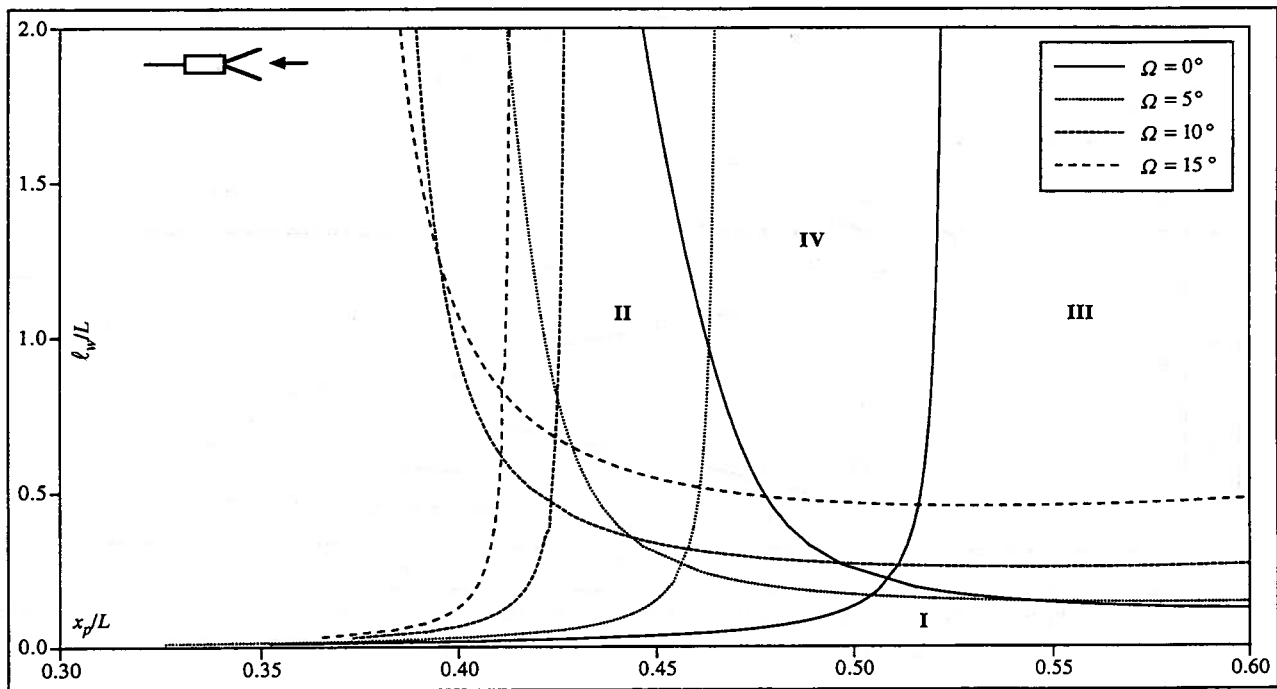

Fig. 24 Effect of Ω on F2A1 Tanker SMS: $y_p/B = 0.0$, $E_I = 0.03$, SFR, A-M

65

10.3 Mooring Line Pretension

Mooring line pretension is one of the most important parameters in the design of mooring systems, because it has significant effects on catastrophe sets and it is easy to control during operations. It is generally considered that an increase in pretension will render an unstable system stable. This assertion is based on the fact that highly pretensioned systems further restrict the motions of the system. From the dynamics point of view, however, this is not always the case as shown next.

Figures 14 and 25 show the effect of pretension in TMS. In Figure 14, since the catastrophe sets include the water depth as a parameter, the pretension P_{RT} corresponds to the horizontal component of the pretension in each mooring line. The total pretension of each line, T_P, is a function of the water depth. In Figure 25, the total pretension is used instead. Both Figures show that pretensioning the TMS does not have an effect on BSL but can considerably reduce BDL, and thus shrink unstable R-III and R-IV to the point of disappearance. For the parameters shown in Figures 14 and 25, increasing pretension improves the TMS dynamics.
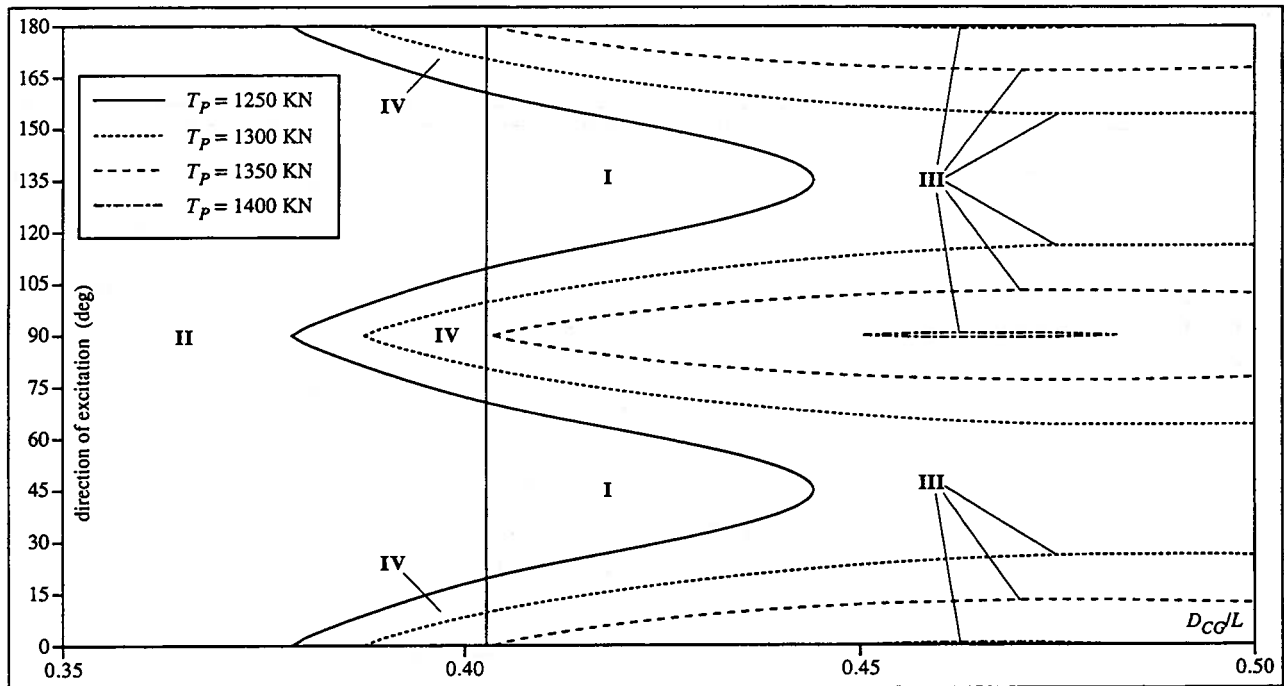

Fig. 25 Effect of turret location, external excitation and pretension, 4-Line TMS: $\ell_w/L = 10.12$, $h = 750$ m, $U = 3.2$ kts, $U_w = 0.0$ kts, $H_{1/3} = 3.66$ m, $T_{1/3} = 8.5$ s, AC, T-M AC, T-M

66

The catastrophe sets if Figure 26 correspond to a F6A3 DICAS, and show the effect of pretension in the system. In this Figure, three cases of total pretension, denoted as T_{P1}, T_{P2} and T_{P3} are used. For this particular system, each mooring line has a different pretension [38], and thus it is not necessary to specify all values of pretension involved. Suffice to say that T_{P1} corresponds to the case of lower pretension and T_{P3} to the case of higher pretension. In addition, the values for $(y_p/B)_{fwd}$ are not included in the caption, since they depend on x_p, which is a parameter in the Figure. The effects of increasing pretension in Figure 26 are two-fold: to increase stable R-I, and to shift BDL toward the center of the Figure for high values of x_p. This second effect may throw a stable system into periodic oscillations.

In addition to the effects of pretension observed in Figures 14, 25 and 26, consider the catastrophe sets for tanker SPM and F1A1 SMS in the $(x_p/L, \ell_w/L)$ plane in Figure 27 [5]. The pretension in this figure is defined in terms of the initial strain, E_I, of the forward synthetic rope. Thus higher values of E_I imply higher pretension. As shown in the figure, increasing pretension tends to expand R-I and to move BSL and BDL toward the right of the Figure until disappearing. For reasonable pretension values, however, R-I does not fall within the range of practical values of x_p and ℓ_w. Figure 27 also shows that a system for which PE originally lies in R-III, may fall in region R-IV with increasing the pretension.
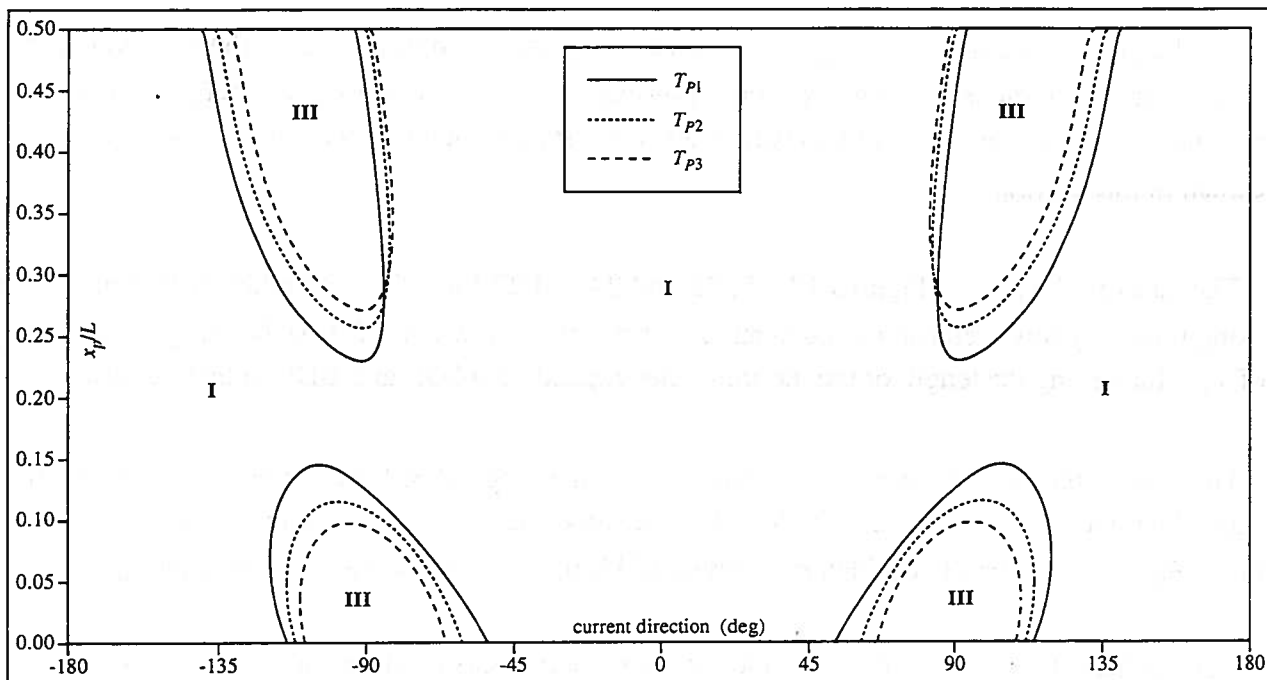

Fig. 26   Effect of pretension and current direction, F6A3 DICAS: ℓ_w/L =7.36, $(x_p/L)_{aft}$ = −0.5, $(y_p/B)_{aft}$ =0.0, h =300 m; AC, T-M
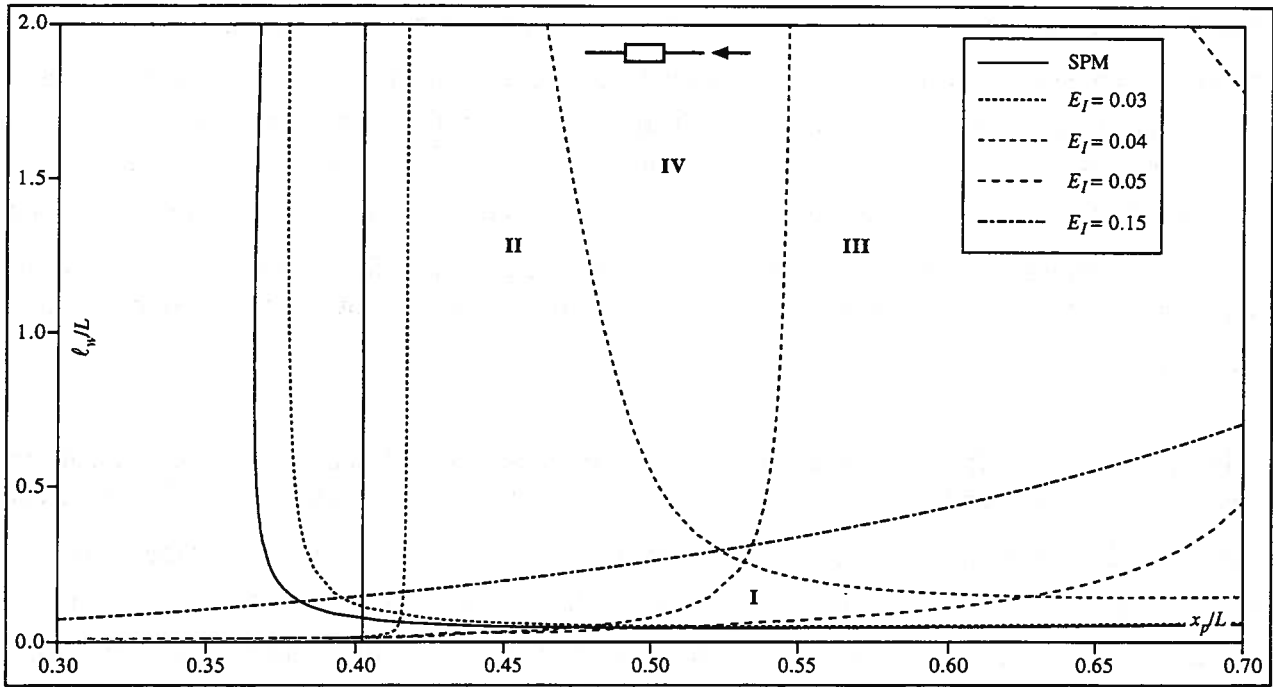
Fig. 27 Effect of pretension on F1A1 Tanker SMS: $y_p/B = 0.0$, SFR, A-M

10.4 Mooring Line Length

The length of a mooring line is generally dictated by the depth of the water, the desired touchdown length, and the pretension. The designer, however, may choose amongst a range of mooring line lengths ℓ_w. Small variations in this parameter may have profound effects on the system dynamics as shown in this section.

The catastrophe sets in Figures 17, 19, 23 and 24 and 27 for different tanker SMS configurations using relatively low pretensions and synthetic fiber ropes, show that PE is stable only for small values of ℓ_w. Increasing the length of the mooring lines expand both BSL and BDL in these cases.

The catastrophe sets in Figure 22 corresponding to the barge SPM for different mooring line models, show the effect of ℓ_w on BDL. The length of the mooring line does not affect BSL [11]. As shown in the Figure, an originally oscillatory behavior of PE may become stable by increasing ℓ_w.

Yet another effect of ℓ_w in the dynamics of the system is shown in the catastrophe sets of Figure 29 for a F2A1 tanker SMS moored with catenaries. Region R-II falls under small values of ℓ_w, and R-III under large values. Operation under intermediate values of ℓ_w renders a stable PE.

68

10.5 Fairlead Position

Some of the possible effects of mooring line fairlead position are shown in the catastrophe sets in Figures 16, 17, 19, 22, 23, 24, 26, 27 and 28. It is not possible to generalize the effect of fairlead position on specific mooring systems. In general, however, an increase in x_p tends to either stabilize PE or cause the system to fall into a limit cycle.

Garza-Rios and Bernitsas [27] provide the following guidelines to stabilize a statically unstable system:

(i)   For lines moored forward of CG, increase the values of x_p. If possible, decrease the value of y_p (i.e. move the mooring lines as close as possible to the centerline).

(ii) For lines moored aft the CG, decrease the values of x_p. If possible, increase the value of y_p.

Such guidelines are useful when the system is statically unstable, i.e. PE has bifurcated to yield additional AE.
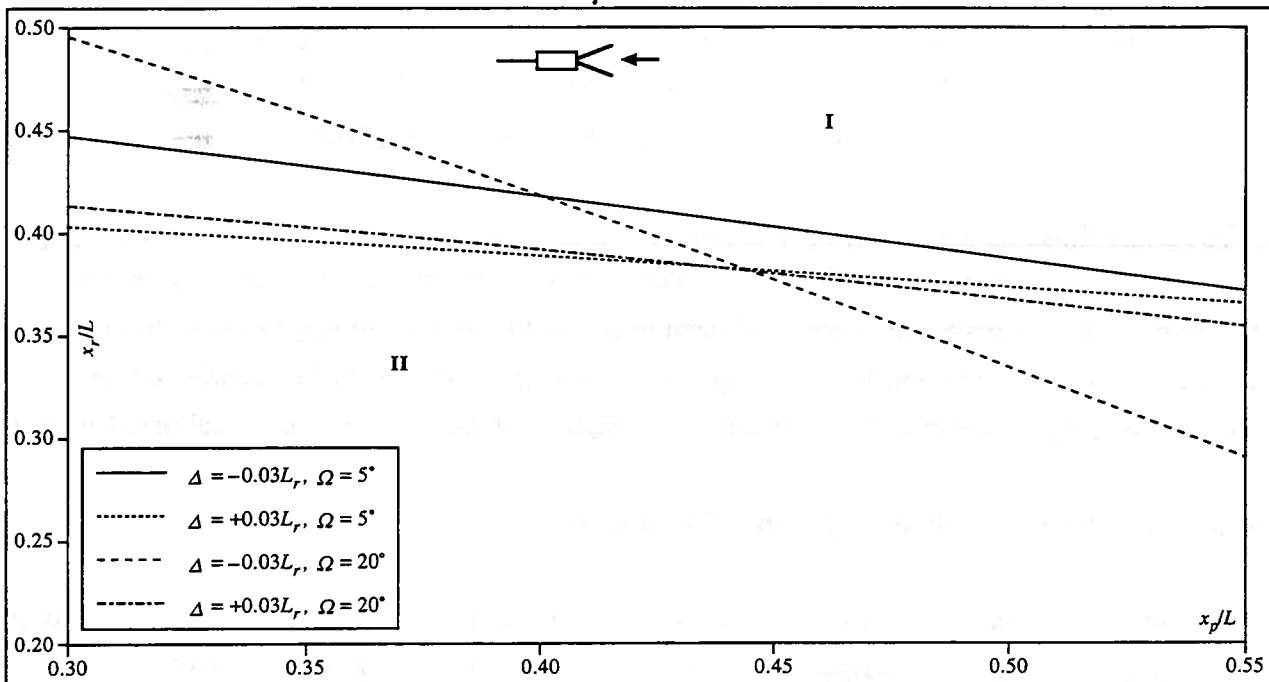

Fig. 28   Effect of Δ and Ω on F2A1 Tanker SMS: $\ell_w/h = 3.5$, $y_p/B = 0.0$, $h = 450$ m, $H_{1/3} = 3.0$ m, $T_{1/3} = 8.0$ s, $P_{RT} = 2\,R$, AC, A-M

69

10.6 Location of Turret

The effect of turret location is shown in the catastrophe sets in Figures 11, 14, 21, and 25. The position of the turret determines whether the system possesses one or three equilibria, which is determined by the location of BSL in those figures. The location of the turret has a strong influence on the position of BSL. For small values of D_{CG}, the TMS converges to AE and such equilibrium is either stable or oscillatory, depending on the system configuration and the external excitation. For large values of D_{CG}, the system possesses only one equilibrium, which may be stable or fall in a limit cycle.

10.7 Location of Riser

To study the effect of riser location on system dynamics, the catastrophe sets for a F2A1 tanker SMS in the (x_p/L, x_r/L) plane, for two different half aperture angles Ω in the forward mooring lines (5° and 20°), and two different riser offsets $\Delta = -0.03\,L_r$ (bottom of riser downstream) and $\Delta = +0.03\,L_r$ (bottom of riser upstream), are shown in Figure 28 [44]. Only regions R-I and R-II exist in this parametric design range, and show that, in general, the riser must be placed as forward as necessary to achieve stable PE. This value of x_r can be decreased with increasing x_p. For $\Omega = 5°$, placing the bottom end of the riser in the upstream (positive Δ) is favorable to the stability of the system. However, for the larger half aperture angle $\Omega = 20°$, it is observed that the downstream placement of the riser (negative Δ) has the opposite effect for $x_p/L \geq 0.445$. The system is unstable about PE irrespective of the placement of the riser when the location of the riser at the top is near CG.

To further illustrate the effects of riser position on the dynamics of PE, consider the catastrophe sets in Figure 29 [44] in the (T_P, ℓ_w/L) design space, where T_P is the pretension in the mooring lines. In this Figure, x_r is superposed as the third parameter. As the riser location gets closer to the bow of the vessel, the oscillatory region R-III disappears, and the set of stationary boundaries denoted by R-II, move to the left, and eventually disappear. As a result, the F2A1 tanker SMS is stabilized around PE.

10.8 Location and Size of Supporting Buoys

As discussed in Section 9.6, extreme changes in the dynamical behavior of the system may occur for a system of two different configurations, as shown in Figure 30. DICAS geometry G1 may exhibit either a stable PE or a static bifurcation of PE, while geometry G2 may fall into chaotic behavior. The difference in the behavior of such systems can be attributed to a large extent to the presence of the supporting buoys in the system [35].
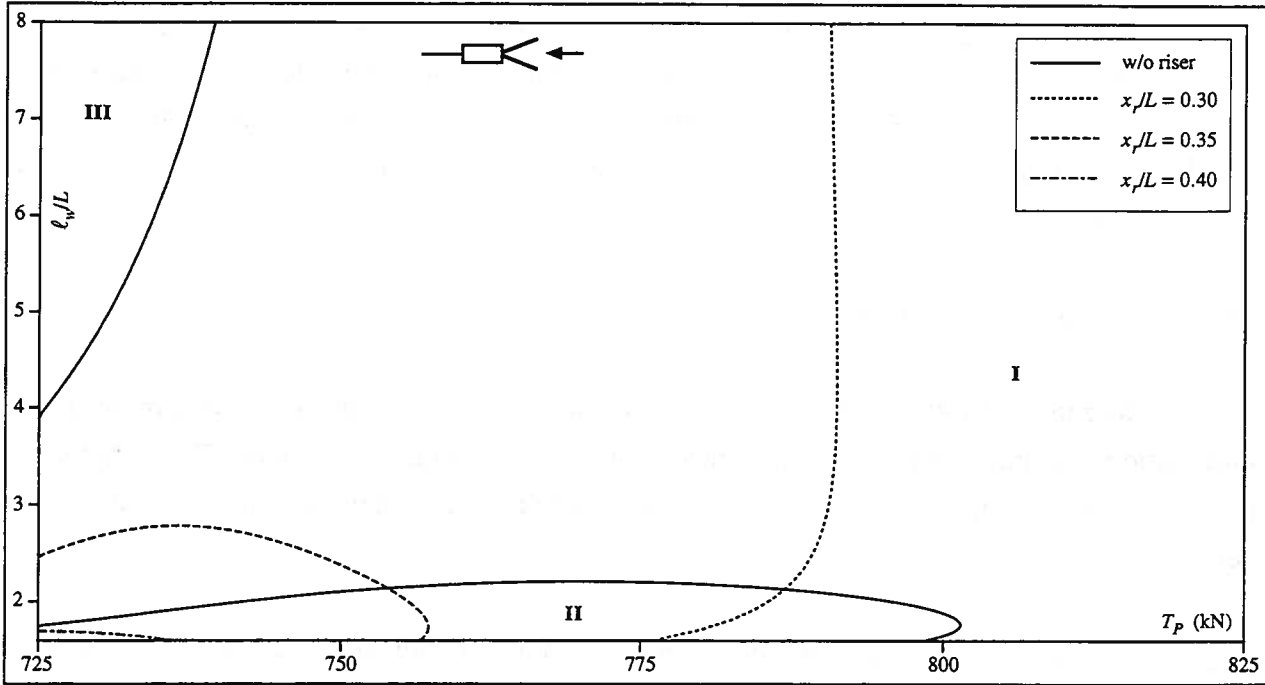
Fig. 29 Effect of riser position on F2A1 Tanker SMS: x_p/L =0.5, y_p/B =0.0, Ω =20°, $\Delta = -0.03\,L_r$, h =450 m, $H_{1/3}$ =3.0 m, $T_{1/3}$ =8.0 s, AC, A-M

Fig. 30 Effect of buoy size, buoy position and water depth for F2A2 DICAS: ℓ_w/L =5.78, $(\,x_p/L\,)_{fwd}$ =0.482, $(\,x_p/L\,)_{aft}$ = −0.5, $(\,y_p/B\,)_{fwd}$ =0.095, $(\,y_p/B\,)_{aft}$ =0.0, $(\,P_{RT}\,)_{fwd}$ =260.57 kN, $(\,P_{RT}\,)_{aft}$ =104.22 kN; BSC, T-M

71

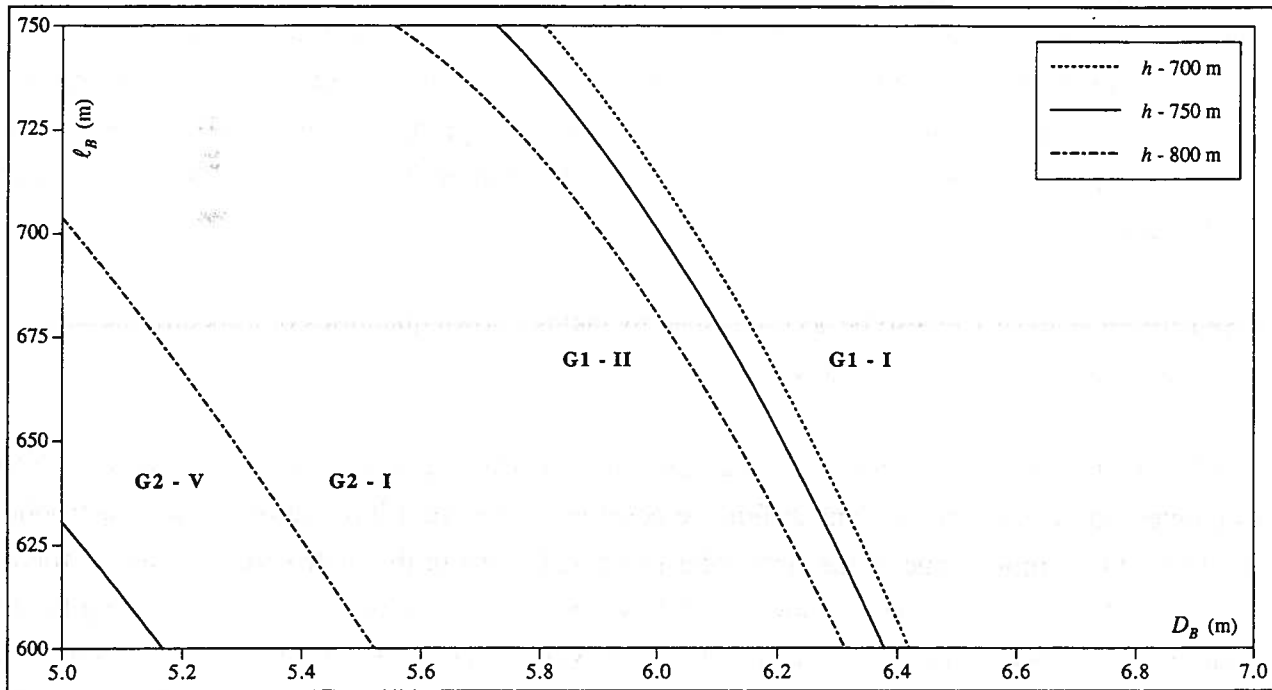Figure 30 also shows the effects of buoy diameter (D_B) and buoy position along the chain with respect to the vessel (ℓ_B) on the system dynamics. For both geometries, the system tends to achieve a stable PE with increasing both D_B and ℓ_B. Practical values for these parameters fall toward the center and the upper right of Figure 30. Therefore, if G1 is selected, PE will be stable only for values of D_B and ℓ_B that fall to the right of BSL.

10.9 Sensitivity Analysis

The catastrophe sets shown in the previous sections provide the designer with important visual information regarding the effects of parameters on specific SMS configurations. These sets also show that the behavior of the system may be affected widely by small changes in the parameters and vice versa.

Systematic variation of four or more values of the system parameters may be difficult to visualize graphically, even if the sets pertain to a single equilibrium position. The relatively small or large changes in the behavior of mooring systems can be explained analytically by determining the sensitivity of the stability criteria and bifurcation boundaries shown in Chapter 6 on the design variables, and thus, the effect of each design variable (or group of variables) on the dynamics of the system. This method consists of taking partial derivatives of the analytical expressions for the bifurcation boundaries with respect to any parameter or group of parameters to determine the sensibility of bifurcations to each parameter. An application of this concept is shown by Garza-Rios Eychenne [26].

Sensitivity analysis can also be accomplished by taking known quantities of a specific parameter and studying its effects, as shown below.

In Figure 11, a major difference between the two maneuvering schools of thought was established, as pointed out in Section 8.1. The difference observed in the Hopf bifurcation in the catastrophe sets in Figure 11, is mostly due to the first order rotational terms in the hydrodynamic lateral force and moment, which are inexistent in O-M and SW-M. Sensitivity analysis consists in setting the linear rotational slow motion derivatives in A-M (Y_r and N_r) and T-M (N_r) to zero and reconstructing the catastrophe sets of Figure 11. Figure 31 [49] shows the changes in the catastrophe sets corresponding to A-M and T-M of Figure 11. The discrepancy in the Hopf bifurcation in Figure 11 is virtually eliminated in Figure 31, thus showing the importance of the values of Y_r and N_r in the maneuvering models.
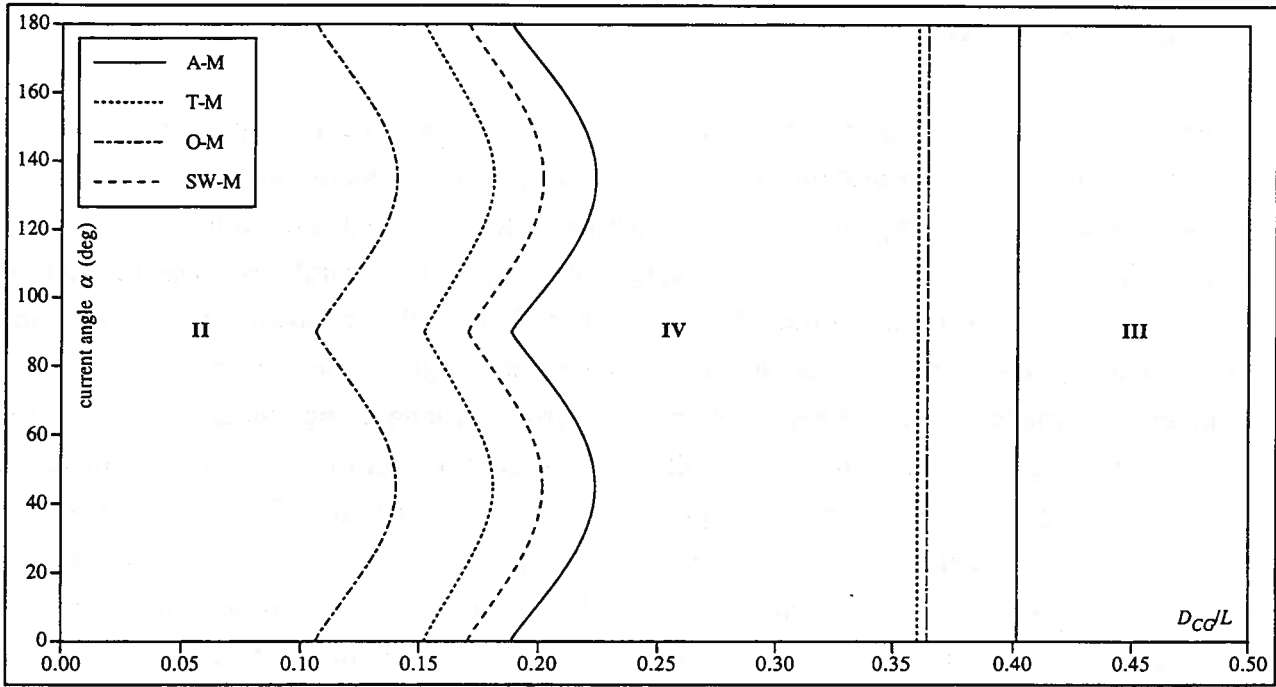
Fig. 31 Effect of turret location and current direction, 4-line TMS: Hydrodynamic derivatives, all hydrodynamic models: $\ell_w/L = 6.0$, $h = 700$ m, $T_P = 1327.8$ kN, AC

CLOSING REMARKS

The methodology developed at the University of Michigan since 1983 has contributed to our understanding of mooring system dynamics and design in two major ways: First, directly, by providing a way of assessing and designing mooring systems; and second, indirectly, by explaining several physical nonlinear phenomena observed during mooring operations. The first and direct contribution consists of providing the designer with a tool for assessing a given mooring configuration, a new design concept, or simply improve the design by changing the value of a parameter. The alternative of trial and error and lengthy nonlinear simulations require extensive experience, can reveal only a small picture of the behavior of a mooring system, and is too time consuming to evaluate new concepts with parameter variation. The second and indirect contribution of this methodology, is summarized in Chapter 2 where several phenomena observed in mooring operations or controversial issues have been explained in the past sixteen years. This methodology does not solve the entire design problem. The fast motions problem must be studied by simulation as a perturbation of the underlying solution to the slow and intermediate frequency scales problem. The problems of first excursion and fatigue failures can be studied using results from both problems.

There are several exciting topics in research and development to pursue based on the UM methodology.

(i) Study a hybrid station-keeping system with both mooring lines and dynamic positioning.

(ii) Couple fast motions to the other two scales presently handled independently in computer software.

(iii) Develop an assessment criterion for mooring systems which is independent of time so that a procedure for optimizing or just improving a design can be established.

(iv) Study theoretically the interaction between slowly-varying drift forces and Hopf bifurcations to explain the phenomena of interaction demonstrated by appropriate selection of simulations in Section 9.5.

BIBLIOGRAPHY

BIBLIOGRAPHY

1. Abkowitz, M.A., Stability and Motion Control of Ocean Vehicles, MIT Press, Cambridge, Massachusetts, 1972.

2. Abkowitz, M.A., "Measurement of Hydrodynamic Characteristics From Ship Maneuvering Trials by System Identification," SNAME Transactions, Vol. 88, 1980, pp. 283-318.

3. API, "Draft Recommended Practice for Design and Analysis of Stationkeeping Systems for Floating Structures," API Recommended Practice, May 1994.

4. Benford, H., "The Control of Yaw in Towed Barges," *International Shipbuilding Progress*, Vol. 2, No. 11, 1955, pp. 269-318.

5. Bernitsas, M.M. and Garza-Rios, L.O., "Effect of Mooring Line Arrangement on the Dynamics of Spread Mooring Systems," *Journal of Offshore Mechanics and Arctic Engineering*, ASME Transactions, Vol. 118, No. 1, February 1996, pp. 7-20.

6. Bernitsas, M.M. and Garza-Rios, L.O., "Mooring Systems Design Based on Analytical Expressions of Catastrophes of Slow Motion Dynamics," *Journal of Offshore Mechanics and Arctic Engineering*, ASME Transactions, Vol. 119, No. 2, May 1997, pp. 86-95.

7. Bernitsas, M.M. and Garza-Rios, L.O., "Turret Mooring Design Based on Analytical Expressions of Catastrophes of Slow Motion Dynamics." *Journal of Offshore Mechanics and Arctic Engineering*, ASME Transactions, Vol. 120, No. 3, August 1998, pp. 154-164.

8. Bernitsas, M.M. and Kekridis, N.S., "Simulation and Stability of Ship Towing," International Shipbuilding Progress, Vol. 32, No. 369, May 1985, pp. 112-123.

9. Bernitsas, M.M. and Kim, B.K., "Effect of Slow Drift Loads on Nonlinear Dynamics of Spread Mooring Systems," *Journal of Offshore Mechanics and Arctic Engineering*, ASME Transactions Vol. 120, No. 4, November 1998, pp. 201-211.

10. Bernitsas, M.M. and Papoulias, F.A., "Stability of Single Point Mooring Systems," Journal of *Applied Ocean Research*, Vol. 8, No. 1, January 1986, pp. 49-58.

11. Bernitsas, M.M. and Papoulias, F.A., "Nonlinear Stability and Maneuvering Simulation of Single Point Mooring Systems," Proceedings of Offshore Station Keeping Symposium, SNAME, Houston, Texas, February 1-2, 1990, pp. 1-19.

12. Bernitsas, M.M., Kokarakis, J.E. and Imron, A., "Large Deformation Three-Dimensional Static Analysis of Deep Water Marine Risers, *Applied Ocean Research*, Vol. 7, No. 4, 1985, pp. 178-187.

13. Brix, J. E., "Lighters and Seagoing Barges and the Design of Yaw Controlling Units," 2nd. International Tug Conference, London, October 1971.

14. Chakrabarti, S., "Deep Water Floating Moored Systems and Their Numerical and Physical Simulation," Proceedings of the JNOC Workshop, OMAE'97, Yokohama, Japan, pp. 147-187

15. Chung, J.S. and Bernitsas, M.M., "Dynamics of Two-Line Ship Towing/ Mooring Systems: Bifurcation, Singularities of Stability Boundaries, Chaos," *Journal of Ship Research*, SNAME, Vol. 36, No. 2, June 1992, pp. 93-105.

16. Chung, J.S. and Bernitsas, M.M., "Hydrodynamic Memory Effect on Stability, Bifurcation, and Chaos of Two Point Mooring Systems," *Journal of Ship Research*, Vol. 41, No. 1, March 1997, pp. 26-44.

17. Clarke, D., Gedling, P. and Hine, G., "The Application of Manoeuvring Criteria in Hull Design Using Linear Theory," Proceedings of the Royal Institute of Naval Architects (RINA), 1983, pp. 45-68.

18. Cummins, W.E., "The Impulse Response Function and Ship Motions," *Schiffstechnik*, Vol. 9, 1962, pp. 101-109.

19. Davison, N.J., Thomas, N.T., Nienhus, V. and Pinkster, J.A., "Application of an Alternative Concept in Dynamic Positioning to a Tanker Floating Production System," Proceedings of the 19th Annual Offshore Technology Conference, OTC Paper No. 5444, Houston, April 1987, pp. 207-223.

20. de Kat, J.O. and Wichers, J.E.W., "Behavior of a Moored Ship in Unsteady Current, Wind, Waves," *Marine Technology,* 1991, pp. 251-264.

21. Dercksen, A. and Wichers, J.E.W., "A Discrete Element Method on Chain Turret Tanker Exposed to Survival Conditions," Proceedings of the Sixth International Conference on the Behaviour of Offshore Structures (BOSS), Vol. 1, London, U.K., 1992, pp. 238-250.

22. Eda, H., "Course Stability, Turning Performance, and Connection Force of Barge Systems in Coastal Seaways," SNAME Transactions, Vol. 80, 1972, pp. 299-328.

23. Faltinsen, O. M., Sea Loads on Ships and Offshore Structures, Cambridge Ocean Technology Series, Cambridge University Press, 1993.

24. Fernandes, A.C. and Aratanha, M., "Classical Assessment to the Single Point Mooring and Turret Dynamics Stability Problems," Proceedings of the 15th International Conference on Offshore Mechanics and Arctic Engineering (OMAE), Vol. I-A, Florence, Italy, June 1996, pp. 423-430.

25. Fossen, T.I., Guidance and Control of Ocean Vehicles, John Wiley and Sons, Ltd., West Sussex, England, 1994.

26. Garza-Rios Eychenne, L.O., *Development of a Design Methodology for Mooring Systems Based on Catastrophe Theory.* Ph.D. Dissertation, Department of Naval Architecture and Marine Engineering, The University of Michigan, Ann Arbor, May 1996.

27. Garza-Rios, L.O. and Bernitsas, M.M., "Analytical Expressions of the Bifurcation Boundaries for Symmetric Spread Mooring Systems," *Applied Ocean Research*, Vol. 17, No. 6, December 1995, pp. 325-341.

28. Garza-Rios, L.O. and Bernitsas, M.M., "Stability Criteria for the Slow Motion Nonlinear Dynamics of Towing and Mooring Systems," Report to the University of Michigan/Sea Grant/Industry Consortium in Offshore Engineering, and Department of Naval Architecture and Marine Engineering, University of Michigan, Ann Arbor, Report No. 332, November 1996.

29. Garza-Rios, L.O. and Bernitsas, M.M., "Analytical Expressions of the Stability and Bifurcation Boundaries for General Spread Mooring Systems," *Journal of Ship Research*, Vol. 40, No. 4, December 1996, pp. 337-350.

30. Garza-Rios, L.O. and Bernitsas, M.M., "Slow Motion Dynamics of Turret Mooring Systems in Deep Water," 8th International Conference on the Behaviour of Offshore Structures (BOSS), Delft, The Netherlands, July 1997, pp. 177-188.

31. Garza-Rios, L.O. and Bernitsas, M.M., "Mathematical Model for the Slow Motion Dynamics of Turret Mooring Systems," Report to the University of Michigan/Industry Consortium in Offshore Engineering and Department of Naval Architecture and Marine Engineering, University of Michigan, Ann Arbor, Report No. 336, February 1998.

32. Garza-Rios, L.O. and Bernitsas, M.M., "Slow Motion Dynamics of Turret Mooring and its Approximation as Single Point Mooring", *Applied Ocean Research*, Vol. 20, No. 6, December 1998.

33. Garza-Rios, L.O. and Bernitsas, M.M., "Analytical Expressions for Stability and Bifurcations of Turret Mooring Systems", *Journal of Ship Research*, Vol. 42, No. 3, September 1998, pp. 216-232.

34. Garza-Rios, L.O. and Bernitsas, M.M., "Slow Motion Dynamics of Mooring Systems in Deep Water with Buoy Supported Catenary Lines," Report to the University of Michigan/Industry Consortium in Offshore Engineering and Department of Naval Architecture and Marine Engineering, University of Michigan, Ann Arbor, Report No. 339, January 1999.

35. Garza-Rios, L.O. and Bernitsas, M.M., "Effect of Size and Position of Supporting Buoys on the Dynamics of Spread Mooring Systems", Proceedings of 18th International Conference on Offshore Mechanics and Arctic Engineering (OMAE '99), St. John, Newfoundland, July 1999.

36. Garza-Rios, L.O., Bernitsas, M.M., and Nishimoto, K., "Catenary Mooring Lines with Nonlinear Drag and Touchdown," Report to the University of Michigan/Sea Grant/Industry Consortium in Offshore Engineering, and Department of Naval Architecture and Marine Engineering, University of Michigan, Ann Arbor, Report No. 333, January 1997.

37. Garza-Rios, L.O., Bernitsas, M.M., and Nishimoto, K., "Slow Motion Dynamics of DICAS Mooring Systems Under Steady Current, Wind, and Mean Drift Excitation," X International Symposium on Offshore Engineering (Brasil Offshore '97), Rio de Janeiro, Brazil, September 1997, pp. 47-62.

38. Garza-Rios, L.O., Bernitsas, M.M., Nishimoto, K. and Masetti, I.Q., "Preliminary Design of Differentiated Compliance Anchoring Systems," *Journal of Offshore Mechanics and Arctic Engineering*, ASME Transactions, Vol. 121. No. 1, February 1999.

39. Gottlieb, O, and Kim, S. C. S., "Nonlinear Oscillations, Bifurcations and Chaos in a Multi-Point Mooring System with a Geometric Nonlinearity," *Journal of Applied Ocean Research*, Vol. 14, 1992, pp. 832-839.

40. Guckenheimer, J., and Holmes, P., Nonlinear Oscillations, Dynamical Systems, and Bifurcations of Vector Fields, Springer-Verlag, New York, Inc., 1983.

41. Hirano, M., Takashina, J., Takaishi, Y. and Saruta, T., "Ship Turning Trajectory in Regular Waves," Transactions of the West Japan Society of Naval Architects, Vol. 60, 1980.

42. International Towing Tank Conference (ITTC), "Report of the Manoeuvrability Committee", Proceedings of the 18th ITTC, The Society of Naval Architects of Japan, Vol. 1, Kobe, Japan, October 1987, pp. 345-400.

43. Kim, B.K. and Bernitsas, M.M., "Effect of Memory on the Stability of Spread Mooring Systems," *Journal of Ship Research* (submitted June 1998).

44. Kim, B.K. and Bernitsas, M.M., "Stability and Simulation of Coupled Spread Mooring and Riser Dynamics," *Applied Ocean Research*, (submitted February 1999).

45. Laures, J.P. and de Boom, W.C., "Analysis of Turret Moored Storage Vessel for the Alba Field," Proceedings of the Sixth International Conference on the Behaviour of Offshore Structures (BOSS), Vol. 1, London, U.K., 1992, pp. 211-223.

46. Leite, A.J.P., Aranha, J.A.P., Umeda, C. and de Conti, M.B., "Current Forces in Tankers and Bifurcation of Equilibrium of Turret Systems: Hydrodynamic Model and Experiments," *Applied Ocean Research*, Vol. 20, 1998, pp. 145-156.

47. Mack, R.C., Gruy, R.H. and Hall, R.A., "Turret Moorings for Extreme Design Conditions," Proceedings of the 27th Offshore Technology Conference, Paper OTC-7696, Vol. II, Houston, TX, 1995, pp. 23-31.

48. Martin, L.L., "Ship Maneuvering and Control in Wind," *SNAME Transactions*, Vol. 88, 1980, pp. 257-281.

49. Matsuura, J.P.J., Nishimoto, K., Bernitsas, M.M., and Garza-Rios, L.O., "Comparative Assessment of Hydrodynamic Models in Slow Motion Mooring Dynamics", Proceedings of 18th International Conference on Offshore Mechanics and Arctic Engineering (OMAE '99), St. John, Newfoundland, July 1999.

50. Mc Kenna, H. A., and Wong, R. K., "Synthetic Fiber Rope, Properties and Calculations Relating to Mooring Systems," *Deepwater Mooring and Drilling*, ASME Transactions, Ocean Engineering Division, Vol. 7, December 1979, pp. 189-203.

51. Newman, J.N., "Second-Order Slowly Varying Forces on Vessels In Irregular Waves," Proceedings, International Symposium on Dynamics of Marine Vehicles and Structures in Waves, London, U.K., 1974, pp. 182-186.

52. Nishimoto, K., Aranha, J.A.P., Matsuura, J.P.J., Kaster, F., Namba, H. and Masetti, I.Q., "Full Scale Decay Test of a Moored Tanker: Measurement Procedure of Surge Damping," Proceedings of the ASME 16th International Conference on Offshore Mechanics and Arctic Engineering (OMAE'97), Vol. I-A, Yokohama, Japan, April 1997, pp. 81-90.

53. Nishimoto, K., Brinati, H.L. and Fucatu, C.H., "Dynamics of Moored Tankers SPM and Turret," Proceedings of the Seventh International Offshore and Polar Engineering Conference (ISOPE), Vol. 1, Honolulu, 1997, pp. 370-378.

54. Obokata, J., "On the Basic Design of Single Point Mooring Systems (1st Report)", *Journal of the Society of Naval Architects of Japan*, Vol. 161, June 1987.

55. Obokata, J., Sasaki, N. and Nagashima, J., "On the Estimation of Current Force Induced on a Ship Hull by Some Model Tests," Kansai Society of Naval Architects of Japan, Vol. 180, 1981, pp. 47-57.

56. Ogilvie, T.F., "Second Order Hydrodynamic Effects on Ocean Platforms," <u>Proceedings</u> of International Workshop on Ship and Platform Motions, 1983, pp. 205-265.

57. Ormberg, H., Fylling, I.J., Larsen, K. and Sødahl, N., "Coupled Analysis of Vessel Motions and Mooring and Riser Dynamics," <u>Proceedings</u> of the ASME 16th International Conference on Offshore Mechanics and Arctic Engineering (OMAE'97), Vol. I-A, Yokohama, Japan, April 1997, pp. 91-100.

58. Papoulias, F. A., and Bernitsas, M. M., "MOORLINE: A Program for Static Analysis of <u>MOOR</u>ing <u>LINE</u>s," Report to the University of Michigan/Sea Grant/Industry Consortium in Offshore Engineering, and Department of Naval Architecture and Marine Engineering, The University of Michigan, Ann Arbor, Publication No. 309, May 1988.

59. Papoulias, F.A. and Bernitsas, M.M., "Autonomous Oscillations, Bifurcations and Chaotic Response of Moored Vessels," *Journal of Ship Research*, Vol. 32, No. 3, September 1988, pp. 220-228.

60. Seydel, R., <u>From Equilibrium to Chaos</u>, Elsevier Science Publishing Co., Inc., New York, 1988.

61. Simos, A.N., Tannuri, E.A. and Pesce, C.P., "Dynamics of a Turret-FPSO System and Hydrodynamic Models", <u>Proceedings</u> of the 17th International Conference on Offshore Mechanics and Arctic Engineering (OMAE), Paper OMAE98-410, Lisbon, Portugal, July 1998.

62. Sharma, S. D., Jiang, T., and Schellin, T. E., "Dynamic Instability and Chaotic Motions of a Single Point Moored Tanker," <u>Proceedings</u> of the 17th ONR Symposium on Naval Hydrodynamics, The Hague, Holland, August 1988, pp. 543-562.

63. Sorheim, H.R., "Analysis of Motion in Single Point Mooring Systems," <u>Modeling Identification and Control</u>, Vol. 1, No. 3, 1980.

64. Strandhagen, A. G., Schoenherr, K. E., and Kobayashi, F. M., "The Stability on Course of Towed Ships," SNAME <u>Transactions</u>, Vol. 58, 1950, pp. 32-66.

65. Takashina, J., "Ship Maneuvering Motion due to Tugboats and its Mathematical Model," *Journal of the Society of Naval Architects of Japan*, Vol. 160, 1986, pp. 93-104.

66. Tanaka, S., "On the Hydrodynamic Forces Acting on a Ship at Large Drift Angles," *Journal of the West Society of Naval Architects of Japan*, Vol. 91, 1995, pp. 81-94.

67. Tick, L. J., "Differential Equations with Frequency Dependent Coefficients," *Journal of Ship Research*, Vol. 3, No. 2, October 1959, pp. 45-46.

68. van Oortmerssen, G., Pinkster, J.A. and van den Boom, H.J.J., "Computer Simulation of Moored Ship Behavior," *Journal of Waterway, Port, Coastal and Ocean Engineering*, Vol. 112, No. 2, 1986, pp. 296-308.

69. Wiggins, S., <u>Introduction to Applied Nonlinear Dynamical Systems and Chaos</u>, Springer-Verlag, New York, Inc., 1990.

University of Michigan
College of Engineering

**Department of Naval Architecture
and Marine Engineering**
NAME Building
2600 Draper Road
Ann Arbor, MI 48109-2145

734-764-6470
734-936-8820 fax
http://www.engin.umich.edu/dept/name/